Design and Detection of Non-Coherent Unitary Constellations for SIMO Systems for Short Packet Communications

A Thesis Submitted
to the College of Graduate and Postdoctoral Studies
in Partial Fulfillment of the Requirements
for the Degree of Master of Science
in the Department of Electrical and Computer Engineering
University of Saskatchewan

by

Thanh Son Duong

Saskatoon, Saskatchewan, Canada

Permission to Use

In presenting this thesis in partial fulfillment of the requirements for a Postgraduate degree from the University of Saskatchewan, it is agreed that the Libraries of this University may make it freely available for inspection. Permission for copying of this thesis in any manner, in whole or in part, for scholarly purposes may be granted by the professors who supervised this thesis work or, in their absence, by the Head of the Department of Electrical and Computer Engineering or the Dean of the College of Graduate Studies and Research at the University of Saskatchewan. Any copying, publication, or use of this thesis, or parts thereof, for financial gain without the written permission of the author is strictly prohibited. Proper recognition shall be given to the author and to the University of Saskatchewan in any scholarly use which may be made of any material in this thesis.

Request for permission to copy or to make any other use of material in this thesis in whole or in part should be addressed to:

Head of the Department of Electrical and Computer Engineering
57 Campus Drive
University of Saskatchewan
Saskatoon, Saskatchewan, Canada
S7N 5A9

OR

Dean of College of Graduate and Postdoctoral Studies
116 Thorvaldson Building, 110 Science Place
University of Saskatchewan
Saskatoon, Saskatchewan, Canada
S7N 5C9

Abstract

Ultra-reliable low-latency communications (URLLC) have been a crucial part of 5G and upcoming 6G networks to cater to mission-critical applications with stringent demands for high reliability and minimal latency. Short packet communications (SPC) have been employed to meet the requirement of low latency. Coherent communications require the transmission of pilot symbols to obtain accurate instantaneous channel state information (CSI), thus suffering from spectral efficiency (SE) loss in SPC. These challenges motivate the use of non-coherent communications, which do not require instantaneous CSI, as an alternative paradigm for coherent communications in SPC.

Among different schemes of non-coherent communications, unitary multi-symbol constellations and multi-level unitary multi-symbol constellations have been investigated to improve the error performance of communication systems. In the literature, there have been two approaches to design and detect unitary constellations and multi-level unitary constellations. The first one is the unstructured constellations with maximum-likelihood (ML) detection, which can achieve optimal error performance but suffer from high complexity in both design and detection. As a result, this approach is not practical for many practical applications. The other approach is the structured unitary constellations with simplified detectors, which can have low complexity in design and detection, therefore being practical. However, the structured constellations sacrifice the optimal error performance of the unstructured constellations. Hence, in this thesis, we focus on the structured unitary and multi-level unitary constellations with low complexity while improving the error performance to meet the reliability requirement of communication systems.

Firstly, we investigate the design of multi-level unitary constellations for block Rayleigh fading channels. By using the Kullback-Leibler (KL) divergence as the design criterion, we formulate a multiple-symbol constellation optimization problem, which turns out to have high computational complexity to construct and detect. We exploit the structure of the formulated problem and decouple the constellation into a Cartesian product of a unitary constellation design and a multi-level design. The proposed multi-level design has low com-

plexity in both construction and detection and is compatible with any type of unitary constellation in the literature. Simulation results show that our multi-level design performs better than traditional pilot-based schemes and other existing low-complexity single-level designs in low SNR regimes.

Secondly, we propose a novel structure of unitary constellations for block Rayleigh fading channels. Our proposed structure involves a Cartesian product of an amplitude vector and a phase-shift keying (PSK) vector, which reduces the design complexity compared to the unstructured unitary constellations. Furthermore, the structure allows iterative detection of amplitude vectors and phase vectors, which reduces the complexity of the ML detector. We adopt the sort-decision-feedback-differential-detection (sort-DFDD) to further reduce the complexity of detecting the PSK vector when compared to the ML detector. Furthermore, we adopt a posterior probability as a reliability criterion to improve the error performance of sort-DFDD, which results in near-optimal error performance in the case of the PSK constellations with equal modulation order. This detector is called Posteriori-based-reliability-sort-DFDD (PR-sort-DFDD) and has polynomial complexity. We also propose an improved detector called improved-PR-sort-DFDD to detect a more generalized PSK structure, i.e., PSK symbols with unequal modulation orders. This detector also approaches the optimal error performance with polynomial complexity. Through simulation, we demonstrate the superiority of our proposed multi-symbol unitary constellation over competing low-complexity unitary constellations and traditional pilot-based schemes.

Acknowledgments

I am deeply grateful to all those who have provided invaluable support during my Master's studies.

First and foremost, I want to express my profound appreciation for the memory of my late supervisor, Professor Ha Nguyen. His exceptional technical knowledge in digital communications and coding theory, coupled with his dedication and professionalism in research, deeply inspired me. His unwavering support and guidance during my initial year at the University of Saskatchewan were instrumental in shaping my academic growth. Although his passing last year was a profound loss to all who knew him, his legacy continues to inspire and guide my work.

I extend my heartfelt thanks to Professor Ebrahim Bedeer Mohamed for his unwavering support throughout my studies. The knowledge I gained from his course in wireless communications during my first year was crucial in establishing my research path. His invaluable support and encouragement as the main supervisor after Professor Ha's passing helped me overcome the challenges, ultimately enabling me to complete my research and chart my academic journey.

I'm also grateful to Professors Eric Salt, Brian Daku, Brian Berscheid, and Rory Gowen for the valuable knowledge in probability theory and digital communications that I acquired through their teaching.

My journey wouldn't have been the same without my peers, from whom I was fortunate to learn during my studies: Khai, Nghia, Thu, Minh, Ali Fazeli, Alireza Maleki, Atefeh, Botao, Aiman, Simin, Fouad, and Porfirio. It was a true pleasure to study and work alongside them.

My deepest love and gratitude go to my family members: my parents, Mom and Dad, and my younger brother Quan, who have supported me through every moment of my life. I would also like to express my gratitude to my aunt Hanh, my cousins Hao and Khoi, and my late uncle, Trung, for their unwavering support during my time in Saskatoon. I'm thankful to the Vietnamese community for the assistance I received during my stay in Canada.

Lastly, I would like to acknowledge the financial support provided by the Cisco grant and the Department of Electrical and Computer Engineering at the University of Saskatchewan, which greatly contributed to my academic journey.

Table of Contents

List of Tables

List of Figures

List of Abbreviations

3GPP	3rd generation partnership project
5G	fifth generation (cellular network)
ARQ	automatic repeat request
BER	bit error rate
BLER	block error rate
CSI	channel state information
DFDD	decision-feedback differential detection
KL	Kullback-Leibler
LOS	line-of-sight
IoT	Internet of Things
IUAP	iterative unitary amplitude-phase (detector)
MCD	minimum chordal distance
MIMO	multiple-input multiple-output
ML	maximum likelihood
MMSE	minimum mean squared error
MRC	maximum ratio combining
MSDD	multi-symbol differential detection
NLOS	non-line-of-sight
PDF	probability density function
PEP	pairwise error probability
PR-sort-DFDD	posteriori-based-reliability-sort-DFDD
PSK	phase-shift keying
QAM	quadrature amplitude modulation
SE	spectral efficiency
SER	symbol error rate
SIMO	single-input multiple-output
SNR	signal-to-noise ratio
SPC	short packet communications

URLLC	ultra-reliable low-latency communications
ZF	zero-forcing

List of Publications

S. T. Duong, H. H. Nguyen, and E. Bedeer, "Multi-level design for multiple-symbol non-coherent unitary constellations for massive SIMO systems," *IEEE Wireless Commun. Lett.*, vol. 12, no. 8, pp. 1349-1353, Aug. 2023.

S. T. Duong, H. H. Nguyen, E. Bedeer, and R. Barton, "Low-complexity design of unitary constellations in non-coherent SIMO systems for 5G NR URLLC applications," to appear in *Proc. IEEE Global Communications Conference 2023 (GLOBECOM)*, 2023.

S. T. Duong, H. H. Nguyen, E. Bedeer, and R. Barton, "Multi-level design for multiple-symbol non-coherent unitary constellations for massive SIMO systems," under review, *IEEE Trans. Wireless Commun.*.

Notations

Matrices, column vectors, and scalar variables are denoted by uppercase bold letters (e.g., $\mathbf{A}$), lowercase bold letters (e.g., $\mathbf{a}$), and lowercase letters (e.g., a), respectively. The notations $(\cdot)^*$, $(\cdot)^T$, and $(\cdot)^H$ represent the conjugate, transpose, and conjugate transpose, respectively. We use $|\cdot|$, $\|\cdot\|$, $\det(\cdot)$, $\mathrm{tr}(\cdot)$, and $\circ$ to denote absolute value, Euclidean norm, determinant, trace, and pairwise product, respectively. The angle of a complex scalar variable a is denoted as $\angle a$. We use $\mathbb{R}_+^{m\times n}$ and $\mathbb{C}^{m\times n}$ to indicate the set of non-negative real matrices and complex matrices with dimension $m \times n$, respectively. The matrix $\mathbf{I}_K$ denotes the $K \times K$ identity matrix, while $\mathbf{1}_K$ and $\mathbf{0}_K$ denote all ones K-dimensional vector and all zeros K-dimensional vector, respectively. The cardinality of the constellation set Ω is represented as $\mathrm{card}\{\Omega\}$, while the exclusion of an element b from the set Ω and the exclusion of a subset $\tilde{\Omega}$ from the set Ω is denoted as $\Omega\backslash b$ and $\Omega\backslash\tilde{\Omega}$, respectively. The Gamma and signum functions are denoted as $\Gamma(.)$ and $\mathrm{sgn}(.)$, respectively. The probability density function (PDF) of a random continuous variable is denoted as $f(.)$, while the probability of an event is denoted as $P(.)$. The circularly symmetric complex Gaussian distribution with mean μ and variance σ^2 is represented as $\mathcal{CN}(\mu, \sigma^2)$, and we use $\mathbb{E}(\cdot)$ to denote the expectation.

1. Introduction

1.1 Motivation

Ultra-reliable low-latency communications (URLLC) have emerged as a revolutionary communications paradigm designed to cater to mission-critical applications that necessitate instantaneous and accurate responses. In the third generation partnership project (3GPP) Release 15 of 5G New Radio, stringent requirements were established for URLLC, enabling packet transmission with a block error rate (BLER) of 10^{-5} and a low latency of 1 ms [1]. These stringent criteria have already addressed the demands of applications such as smart grids, autonomous vehicles, vehicle-to-vehicle (V2V) communications, and industrial Internet of Things (IoT). For instance, in factory automation applications, which involve real-time control of machines and systems in the production line, each component acts as an IoT device, requiring extremely low latency and high reliability to maintain an efficient and smooth automated process. Anticipating the forthcoming 6G wireless communications, URLLC is expected to be integrated further, with even more stringent criteria, including BLER targets below 10^{-6} and latency below 1 ms, enabling the realization of advanced applications such as tactile internet, industrial automation, and augmented reality (AR). The BLER and latency requirements of some mission-critical applications are shown in Table 1.1 [2].

However, achieving high reliability and low latency simultaneously remains a formidable challenge, given the inherent conflict of both objectives. It is possible to enhance reliability by employing automatic repeat request (ARQ) mechanisms or increasing the number of parity check bits of forward error correcting (FEC) coding. The ARQ mechanism relies on the receiver's request for retransmission when errors are detected, while increasing the parity check bits leads to longer messages. Both methods result in higher latency. As a result,

Table 1.1: BLER and latency requirements of some mission-critical applications.

Use case	Latency (ms)	BLER
Smart Grid	3 - 20	$< 10^{-5}$
Professional audio	2	$< 10^{-6}$
Self-driving car	1	$< 10^{-2}$
Industrial automation	0.25 - 10	$< 10^{-9}$
Process automation	50 - 100	$< 10^{-4}$
E-health	30	$< 10^{-5}$
Augmented reality	0.4 - 2	$< 10^{-5}$
V2V communications	5	$< 10^{-5}$
Tactile internet	1	$< 10^{-7}$

designing efficient communication systems that meet both stringent latency and reliability requirements remains a challenge for URLLC.

To address these challenges, short packet communications (SPC) have been employed to achieve the stringent requirement of low latency. By reducing the size of data packets, short packet transmission minimizes the transmission time and processing overhead, leading to significantly lower latency. SPC has been standardized in 5G by 3GPP Release 15, which introduced sub-slot-based transmission where a transmission time interval covers over 2, 4, or 7 symbols [3]. However, the adoption of SPC comes with its own challenges. Firstly, the Shannon capacity theorem only holds true for channel coding with infinite block length. Thus, the limited block length in SPC degrades the error performance of channel coding. Therefore, it is crucial to explore alternative diversity resources to enhance the reliability of SPC. Among these resources, multiple antennas have been extensively investigated in the domain of coherent communications to improve reliability. To facilitate coherent communications, the transmitter needs to transmit a sequence of pilot symbols or training symbols so the receiver can carry out channel estimation to obtain accurate instantaneous channel information (CSI). However, in SPC, the length of the pilot symbols can be comparable to the block length, thus reducing the spectral efficiency (SE) of the communication systems.

In order to facilitate SPC without sacrificing the SE, non-coherent communications have

emerged as potential alternatives for coherent communications. Non-coherent communication systems do not need to acquire accurate instantaneous CSI, thus obviating the need for transmitting training symbols. As a result, non-coherent communication systems can achieve better SE than coherent communication systems. Among different non-coherent communications schemes, multi-symbol unitary constellations, and multi-symbol multi-level unitary constellations are special types of non-coherent constellations that are potential candidates to meet the reliability requirement of URLLC. The unitary constellations have been theoretically proven to be optimal transmission schemes in high signal-to-noise ratio (SNR) regime [4,5], while the multi-level unitary constellations have been shown to further improve the error performance of unitary constellations in low SNR regimes [6]. Unstructured designs for unitary constellations and multi-level unitary constellations with optimal maximum likelihood (ML) detectors have been investigated. These designs are obtained by numerically solving the optimization problem of minimizing the pairwise error probability (PEP) of the ML detector among all pairs of constellation points, hence achieving optimal or near-optimal error performance. However, they have exponential complexity in both design and detection, which results in complex hardware requirements. As a result, they are impractical for some real-life applications. On the other hand, several unitary constellations and multi-level unitary constellations have been proposed with certain structures that can enable lower complexity in both design and detection. However, they sacrifice the error performance and degrade the reliability when compared to the unstructured constellations.

1.2 Research Objectives

Two main objectives for this work are given as follows:

- **Design novel multi-symbol multi-level unitary constellations to further improve the error performance of unitary constellations in low SNR regimes**. To achieve this objective, we formulate an optimization problem of constellation design by using the Kullback-Leibler (KL) divergence as the design criterion. Moreover, we propose a novel structure of multi-level unitary constellations as the Cartesian product of magnitude level and unitary vector and exploit this structure to reduce the

complexity of solving the optimization problem.

- **Design and detect novel multi-symbol unitary constellations that can approach the optimal error performance at reduced computational complexity**. To design the unitary constellations, we formulate an optimization problem of constellation design by using the chordal distance as the design criterion. Furthermore, we propose a novel structure of unitary constellations as the Cartesian product of amplitude vector and phase-shift keying (PSK) vector and exploit the structure to reduce the complexity of solving the optimization problem. We also exploit the proposed structure of unitary constellations to reduce the complexity of the ML detector, which results in novel detectors with polynomial complexity and near-optimal error performance.

1.3 Organization of Thesis

This thesis is organized in a manuscript-based style. Chapter 2 presents the background of wireless communications, including the model of the wireless channel and the overview of coherent and non-coherent communications. The fundamental knowledge and literature survey of the multi-level unitary constellations and unitary constellations are also provided in Chapter 2. The remaining part of the thesis consists of manuscripts that have been accepted or are under review for publication.

Chapter 3 includes a manuscript that investigates the multi-level unitary constellations. Chapter 3 discusses the optimization problem of constellation design to improve the error performance of the multi-level unitary constellations, which have relatively low complexity. Chapter 3 is in the form of a manuscript that has been published in the IEEE Wireless Communications Letters.

Chapter 4 includes a manuscript that investigates the unitary constellations. Chapter 4 discusses the optimization problem of constellation design to improve the error performance of the unitary constellations. The proposed design has relatively low complexity compared to the relevant unitary constellations in the literature. Furthermore, we proposed novel

detectors that can achieve the optimal error performance of the ML detector while having polynomial complexity. Chapter 4 is currently under review for publication in IEEE Transactions on Wireless Communications, while parts of this chapter have been already published in IEEE Global Communications Conference 2023.

Finally, Chapter 5 concludes the thesis and provides potential research directions based on the findings of this thesis.

References

[1] *Study on Scenarios and Requirements for Next Generation Access Technologies.* 3GPP TR38.913 v15.0.0, 2018.

[2] G. J. Sutton, J. Zeng, R. P. Liu, W. Ni, D. N. Nguyen, B. A. Jayawickrama, X. Huang, M. Abolhasan, Z. Zhang, E. Dutkiewicz *et al.*, "Enabling technologies for ultra-reliable and low latency communications: From PHY and MAC layer perspectives," *IEEE Communications Surveys & Tutorials*, vol. 21, no. 3, pp. 2488–2524, 3rd Quart., 2019.

[3] T.-K. Le, U. Salim, and F. Kaltenberger, "An overview of physical layer design for ultra-reliable low-latency communications in 3GPP Releases 15, 16, and 17," *IEEE Access*, vol. 9, pp. 433–444, 2020.

[4] B. M. Hochwald and T. L. Marzetta, "Unitary space-time modulation for multiple-antenna communications in Rayleigh flat fading," *IEEE Trans. Inf. Theory*, vol. 46, no. 2, pp. 543–564, Mar. 2000.

[5] L. Zheng and D. N. C. Tse, "Communication on the Grassmann manifold: A geometric approach to the noncoherent multiple-antenna channel," *IEEE Trans. Inf. Theory*, vol. 48, no. 2, pp. 359–383, Feb. 2002.

[6] M. J. Borran, A. Sabharwal, and B. Aazhang, "On design criteria and construction of noncoherent space-time constellations," *IEEE Trans. Inf. Theory*, vol. 49, no. 10, pp. 2332–2351, Oct. 2003.

2. Background

2.1 Overview of Wireless Communications

2.1.1 Time-varying Linear Model of Wireless Channels

In this subsection, we briefly study a simple multi-path wireless channel, which typically represents the transmission in a highly-scattering environment such as an urban area. A typical wireless communication includes an antenna in the transmitter and another antenna in the receiver. The baseband signal carrying information is converted to the passband frequency by multiplying with the sinusoidal carrier with frequency f_c. The electromagnetic waves carrying the passband signal are emitted by the transmitting antenna, propagate through the environment, and then intercepted by the receiving antenna. During the propagation, the signal power attenuates due to absorption, reflection, scattering, and diffraction. Furthermore, the interaction with different objects results in multipath signal components arriving in the receiver. Ideally, the propagation of the electromagnetic waves can be accurately modeled by solving the system of Maxwell's equations. However, there are many unknown variables, and this model is too complex to solve; hence, simpler models are typically used to evaluate and simulate the propagation of electromagnetic waves. In the following, the linear-time model is used to describe and evaluate the propagation of the signal.

Let us consider a multi-path channel where the received signal is the sum of the line-of-sight (LOS) component and N non-light-of-sight (NLOS) components. Let us denote $s(t) \in \mathbb{C}$ and $r(t) \in \mathbb{C}$ as the baseband signal at the transmitting antenna and the passband signal at the receiving antenna, respectively. The signal bandwidth is denoted as B_s. Then, the relation between the transmitted signal and received signal can be described as follows [1,

Eq. (3.2)]:

$$r(t) = \mathrm{Re}\left\{\sum_{n=0}^{N} a_n(t)s(t-\tau_n(t))e^{j2\pi f_c(t-\tau_n(t))+\phi_{D_n}(t)}\right\}, \tag{2.1}$$

where n is the index of the multipath component with $n = 0$ corresponding to LOS path, $\tau_n(t)$, $\phi_{D_n}(t)$ and $\alpha_n(t)$ corresponds to the delay, Doppler phase shift, and amplitude gain of the n-th component. The amplitude gain $\alpha_n(t)$ corresponds to the path loss and shadowing of the n-th component. The phase change caused by the signal propagating over a distance $d_n(t)$ is $e^{j2\pi f_c\tau_n(t)}$ where $\tau_n(t) = d_n(t)/c$. The Doppler phase shift caused by the mobility of the environment is $e^{j2\pi f_c\phi_{D_n}(t)}$. By combining all the phase changes into one component, we can obtain the received signal as follows:

$$r(t) = \mathrm{Re}\left\{\sum_{n=0}^{N} a_n(t)s(t-\tau_n(t))e^{j(2\pi f_c t-\phi_n(t))}\right\}, \tag{2.2}$$

where $\phi_n(t) = 2\pi f_c\tau_n(t) - \phi_{D_n}(t)$ is the total phase change of the signal. Based on the representation in (2.2), we can obtain the received baseband signal $y(t)$, which satisfies $r(t) = \mathrm{Re}\{y(t)e^{j2\pi f_c t}\}$. The received baseband signal $y(t)$ is equal to the convolution of the equivalent baseband time-varying channel impulse response $h(t,\tau)$ and baseband transmitted signal $s(t)$, and is given by:

$$y(t) = h(\tau, t) * s(t), \tag{2.3}$$

where $(*)$ is the convolution operator and $h(\tau, t)$ is given as follows [1, Eq. (3.6)]:

$$h(\tau, t) = \sum_{n=0}^{N} a_n(t)\delta(t-\tau_n(t))e^{-j\phi_n(t)}. \tag{2.4}$$

2.1.2 Categorization of Wireless Channels

The signal power attenuates when the signal propagates through the wireless environment. This phenomenon is called *fading* and can be characterized into two main types: *large-scale fading* and *small-scale fading*. The *large-scale fading* is due to the path loss, which is caused by the dissipation of the power radiated into the free-space environment, and shadowing, which is caused by the obstacles between the transmitter and receiver. The

variation in the large-scale fading only occurs when the distance of propagation of the signal changes by a long distance (typically tens to thousands of meters). The *small-scale fading* comes from the constructive and destructive addition of multi-path signal components, which are caused by the interaction of the signals with different objects during the propagation. Unlike the *large-scale fading*, the variation in the *small-scale fading* occurs over a very small distance, which is usually in the order of the wavelength of the propagating waves. As a result, the variation caused by the *small-scale fading* occurs much faster than the variation caused by the *large-scale fading*.

Another approach to categorizing the wireless channel is based on the comparison of the duration and bandwidth of the baseband signal with the coherence bandwidth and the coherence time of the wireless channel. This results in the categorization of the wireless channel into *slow fading* or *fast fading* channel, or *flat fading* or *frequency-selective fading* channel.

2.1.2.1 Slow Fading versus Fast Fading Channels

The coherence time T_c is defined as the time duration in which the channel complex coefficient $h(t)$ remains constant. The coherence time is associated with the Doppler frequency, which corresponds to the mobility of the environment. In general, the coherence time decreases when the mobility of the environment increases, which is equivalent to an increase in the Doppler frequency. This phenomenon can be represented by the reciprocal relationship between the coherence time and Doppler frequency, which can be described as follows [2, Eq. (4)]:

$$T_D \propto \frac{1}{f_D}. \tag{2.5}$$

Please note that to know the exact scale of the relation in (2.5), we have to define how small change of channel is considered to be constant. For example, it is well known in the literature that if the time correlation of the channel complex coefficient $h(t)$ at different times is smaller than 0.5, the channel can be considered to be constant. Hence, the coherence time can be

found by using Clarke's model as follows [2, Eq. (2.62)]:

$$T_D = \frac{J_0^{-1}(0.5)}{\pi f_D} = \frac{0.423}{f_D}. \tag{2.6}$$

where $J(.)$ is the Bessel function of the zeroth order.

Based on the comparison between the coherence time and time duration, we can categorize the wireless channel into the *slow fading* and *fast fading*. The *slow fading* channel occurs when the coherence time is significantly larger than the symbol durations, which is typically in the orders of time duration of symbols. If the coherence time is small compared to the symbol durations, then the channel is considered *fast fading*. Furthermore, if the coherence time covers a number of symbol durations, the channel is called *block fading* channel over such durations.

2.1.2.2 Flat Fading versus Frequency-Selective Channels

The coherence bandwidth B_c is defined as the bandwidth in which the frequency response of channel impulse remains constant. If the bandwidth B_s of the transmitted signal is smaller than the coherence bandwidth B_c, then the wireless channel is considered *flat fading*. In contrast, if $B_s \gg B_c$, then the signal suffers from distortion due to the variation at different frequencies. This results in *frequency-selective fading* channel. One can estimate the coherence bandwidth by using the reciprocal relation between the bandwidth coherence and the time delay of multipath components. Let us denote $T_m = \max_n |\tau_0 - \tau_n|$ as the delay spread of the channel. Then, the coherence bandwidth B_c can be given by [2, Eq. (2.48)]:

$$B_c = \frac{1}{2T_m}. \tag{2.7}$$

Furthermore, in *flat-fading* channel, the delay spread T_m is much less than the symbol duration T_s; hence, all the multipath components arrive at the same symbol duration. In this case, only a single-tap channel is required to model the wireless channel. In contrast, multipath components arrive at different symbol durations in *frequency-selective fading* channel; thus, the wireless channel can be represented by multiple taps.

2.1.3 Statistical Model of Narrowband Wireless Channels

In this subsection, we introduce the statistical model of the wireless channel. For simplicity, we assume the statistical model of the flat fading channel, which corresponds to a one-tap wireless channel. Let us rewrite the baseband equivalence of the signal model in (2.2) as follows:

$$y(t) = \sum_{n=0}^{N} a_n(t) s(t - \tau_n(t)) e^{-j\phi_n(t)}. \tag{2.8}$$

Because the difference between $\tau_n(t)$ for different n is relatively small compared to the symbol duration, $s(t - \tau_n(t))$ is relatively the same for every n. Without loss of generality, we can assume that $s(t - \tau_n(t)) = s(t)$ for every n-th component. As a result, the signal model in (2.8) can be simplified as follows:

$$\begin{aligned} y(t) &= \sum_{n=0}^{N} a_n(t) s(t) e^{-j\phi_n(t)} \\ &= \left[\sum_{n=0}^{N} a_n(t) e^{-j\phi_n(t)} \right] s(t) \\ &= h(t) s(t), \end{aligned} \tag{2.9}$$

where $h(t)$ can be given as follows:

$$h(t) = \sum_{n=0}^{N} a_n(t) e^{-j\phi_n(t)}, \tag{2.10}$$

Because the continuous signal is sampled to discrete signal in the receiver, the continuous-time model in (2.9) can be converted to the discrete-time signal model given by:

$$y[k] = h[k] s[k], \tag{2.11}$$

where k corresponds to k-th symbol duration and $h[k]$ is given by:

$$h[k] = \sum_{n=0}^{N} a_n[k] e^{-j\phi_n[k]}. \tag{2.12}$$

Since N is usually very large, the channel complex coefficient $h[k]$ as a sum of multiple paths can be modeled as a Gaussian distribution by using the Central Limit Theorem. There are two main assumptions regarding the distribution of the multiple paths:

- NLOS transmission: In this case, no paths have dominant amplitude, and the phase delay of all paths is uniformly distributed over $[0, 2\pi]$. Since the channel complex coefficient h is the sum of many independent circular symmetric random variables, h can be modeled as zero-mean Gaussian random variable [2]. As a result, the channel complex coefficient h can be modeled as Gaussian distribution with zero means, i.e., $h \in \mathcal{CN}(0, \sigma_h^2)$ where σ_h^2 is the variance and the power of the channel complex coefficient h. This channel is also called the Rayleigh fading channel.

- LOS transmission: Since the LOS path tends to have the highest power, it is less likely to be canceled by other paths. Therefore, the sum of multiple paths will be dominated by the LOS path. Therefore, the channel complex coefficient h can be modeled as Gaussian distribution with non-zero means, i.e., $h \in \mathcal{CN}(\mu, \sigma_h^2)$ where μ is the path gain of LOS path and σ_h^2 is the variance of the channel complex coefficient h [2]. This channel is called the Rician fading channel.

2.2 Overview of Coherent Communications

2.2.1 Coherent Detection in Perfect Channel State Information

First, let us consider a MIMO system including a M_t-antenna transmitter and a M-antenna receiver. Let s_i be the transmitted signal at the i-th antenna in the transmitter. Let us denote $h_{i,j}$ be the channel complex coefficient between the i-th antenna in the transmitter and the j-th antenna in the receiver. Then, the received signal y_j in the j-the antenna of the receiver can be given by:

$$y_j = \sum_{i}^{M_t} h_{i,j} s_i + n_j, \tag{2.13}$$

where n_j be the Gaussian noise in the j-th antenna at the receiver. Let $\mathbf{y} = [y_1, \ldots, y_M]^T \in \mathbb{C}^{M\times 1}$, $\mathbf{n} = [n_1, \ldots, n_M] \in \mathbb{C}^{M\times 1}$ be the vector of the received signal and additive noise, respectively. Let $\mathbf{H} \in \mathbb{C}^{M\times M_t}$ be the matrix of channel complex coefficient whose i, j-th element is $h_{i,j}$. Then, we can vectorize the signal model in (2.13) as follows:

$$\mathbf{y} = \mathbf{H}\mathbf{s} + \mathbf{n}. \tag{2.14}$$

In this part, the receiver is assumed to know the exact channel information. Given perfect channel information, the transmitted signal s can be estimated by using linear processing schemes. In specific, the estimated transmitted signal $\tilde{\mathbf{s}}$ can be obtained by multiplying the received signal with a combining vector $\mathbf{A} \in \mathbb{C}^{M \times M_t}$ given as follows [3, Eq. (4.15)]:

$$\tilde{\mathbf{s}} = \mathbf{A}^H \mathbf{y}. \tag{2.15}$$

Then, we can detect the signal $\mathbf{s}$ by quantizing the estimated signal $\tilde{\mathbf{s}}$.

We can use the Maximum Ratio Combining (MR) or Zero-Forcing (ZF) to obtain the combining matrix. The MR combining aims to maximize the power of the receiving signal and has good performance in a low SNR regime. Meanwhile, the ZF combining aims to cancel out the interference between different antennas and has good performance in a high SNR regime. The combining vector of MR and ZF can be given by [3, Eq. (4.16)]:

$$\mathbf{A}_{\text{MR}} = \mathbf{H}, \tag{2.16}$$

$$\mathbf{A}_{\text{ZF}} = \mathbf{H}(\mathbf{H}^H \mathbf{H})^{-1}. \tag{2.17}$$

It can be seen that to obtain the combining vector $\mathbf{A}$, the receiver must know the exact value of the matrix of channel complex coefficient $\mathbf{H}$. The process of obtaining the matrix of channel complex coefficient $\mathbf{H}$ is also known as channel estimation. In the following subsection, we introduce channel estimation and discuss the difficulties and challenges of channel estimation.

2.2.2 Channel Estimation and its Challenges

First, let us assume a flat and block fading channel where the channel coefficients $\mathbf{H}$ remain constant over a block of consecutive K symbols and then change to an independent realization in the coming block. Thus, the channel estimation must be carried out in every period of coherence time.

Let us assume that $\sqrt{K_p \rho_p}\mathbf{\Phi}_i$ be the pilot sequence of the i-th transmit antenna where K_p be the length of the pilot sequence, ρ_p is the signal power of each pilot symbol, and $\mathbf{\Phi}_i = [\phi_{i,1}, \ldots, \phi_{i,K_p}]^T \in \mathbb{C}^{K_p \times 1}$ denotes the orthonormal vector. Please note that to maintain

the orthogonality of all the pilot sequences, K_p must be greater than M_t. Let $\mathbf{Y}_p \in \mathbb{C}^{M\times K_p}$ be the matrix of the received signal, whose i,j-th element corresponds to the received signal in the i-th antenna of the j-th transmitted symbols. Let $\mathbf{N}_p \in \mathbb{C}^{M\times K_p}$ be the matrix of corresponding additive noise in the receiver. Let $\mathbf{h}_i \in \mathbb{C}^{M\times 1}$ be the vector of channel complex coefficient between the i-th antennas and M antennas in the receiver. Then the received signal $\mathbf{Y}_p$ corresponding to the pilot sequence can be given as follows [3, Eq. (4.4)]:

$$\mathbf{Y}_p = \sqrt{K_p\rho_p}\sum_{i}^{M_t}\mathbf{h}_i\mathbf{\Phi}_i^T + \mathbf{N}_p. \tag{2.18}$$

Given a known pilot sequence, the receiver can estimate the channel vector $\tilde{\mathbf{h}}$ by using minimum mean squared error (MMSE). The estimated vector of channel complex coefficient $\tilde{\mathbf{h}}_i$ can be given by [3, Eq. (4.6)]:

$$\tilde{\mathbf{h}}_i = \frac{\sqrt{K_p\rho_p}\sigma_h^2}{K_p\rho_p\sum_{i'=1}^{M_t}\sigma_h^2|\mathbf{\Phi}_{i'}^H\mathbf{\Phi}_i|^2+\sigma^2}\mathbf{Y}_p\mathbf{s}_p^*, \tag{2.19}$$

where σ_h^2 is the channel power of $\mathbf{h}_i$. Please note that due to the effect of additive noise, the estimated vector of channel complex coefficient $\tilde{\mathbf{h}}_i$ may not be exactly equal to the actual channel complex coefficient $\mathbf{h}_i$. The inaccuracy of the channel estimation can be evaluated by calculating the squared mean error of channel estimation, i.e., $\|\mathbf{h}_i - \tilde{\mathbf{h}}_i\|^2$. The channel estimation becomes more accurate when the squared mean error decreases. The mean squared error of the channel estimation can be given by [3, Eq. (4.13)]:

$$\mathbb{E}(\|\tilde{\mathbf{h}}_i - \mathbf{h}_i\|^2) = \frac{K_p\rho_p\sum_{i'=1,i'\neq i}^{M_t}\sigma_h^4|\mathbf{\Phi}_{i'}^H\mathbf{\Phi}_i|^2+\sigma_h^2\sigma^2}{K_p\rho_p\sum_{i'=1}^{M_t}\sigma_h^2|\mathbf{\Phi}_{i'}^H\mathbf{\Phi}_i|^2+\sigma^2}. \tag{2.20}$$

Because the pilot sequences between different transmitting antennas are orthogonal, i.e., $\mathbf{\Phi}_{i'}^H\mathbf{\Phi}_i = 0$ for $i^{'} \neq i$. Then the squared mean error of the channel estimation can be rewritten as follows:

$$\mathbb{E}(\|\tilde{\mathbf{h}}_i - \mathbf{h}_i\|^2) = \frac{\sigma_h^2\sigma^2}{K_p\rho_p\sigma_h^2+\sigma_h^2\sigma^2} = \frac{\sigma_h^2}{K_p\rho_p\sigma_h^2/\sigma^2+1} = \frac{\sigma_h^2}{K_pSNR_p+1}. \tag{2.21}$$

where $\mathrm{SNR}_p = \rho_p\sigma_h^2/\sigma^2$ is the SNR level of the received signal corresponding to the pilot symbols.

It can be seen that coherent communications suffer from two main problems from channel estimation:

- **Spectral efficiency loss**: For a MIMO scheme with K_p transmit antennas, the pilot sequence must be at least K_p symbols to maintain the orthogonality. If the pilot symbols are retransmitted in every coherence time of K symbols, the coherent communications suffer from SE loss of K_p/K. The SE loss becomes more problematic in SPC when K can be small and K_p is comparable to K.

- **Channel estimation error**: As seen in (2.21), the accuracy of channel estimation depends on the length of pilot symbols, i.e., K_p, and the SNR level of the pilot sequence. For realistic scenarios of SPC where the length of the pilot is small, and the SNR level can be limited, the coherent communications suffer from significant channel estimation error, which degrades the performance of coherent detection. The effect of channel estimation error has been investigated in [4,5], which showed that the coherent detection with imperfect channel information can have up to 2.5 dB performance loss compared to the coherent detection with perfect channel information. Furthermore, it is not always beneficial to increase the length of the pilot sequence to improve the accuracy of channel estimation since it can also reduce SE.

Because coherent communications suffer from SE loss caused by the pilot symbols and channel estimation error degrade the performance of coherent detection, it is important to investigate other communications schemes that do not require pilot symbols for obtaining accurate CSI. Such a scheme is called non-coherent communications and will be discussed in the following sections.

2.3 Overview of Non-Coherent Communications

Non-coherent communications have been well-investigated in the literature to improve the SE of the communications system. Specifically, non-coherent communications use the statistical CSI instead of accurate instantaneous CSI, thus do not need to transmit the pilot symbols for channel estimation. Because the pilot symbols greatly reduce the SE of coherent communications in SPC, the non-coherent communications can achieve better SE compared to the coherent scheme. In the following, we provide an overview of non-coherent communications in wireless communications.

2.3.1 Statistical Knowledge of Wireless Channels

The statistical CSI can include the following information:

- **Type of fading distribution**: such as Rayleigh fading or Rician fading.
- **Moments of distribution of channel complex coefficient**: Given the distribution $f(h)$ of the channel complex coefficient h, the n-th moments of the distribution of channel complex coefficient h is given by [6, Eq. (5-67)]:

$$\mathbf{E}[h^n] = \int h^n f(h) dh. \tag{2.22}$$

  Please note that the first-order moments and the second-order moments of the channel complex coefficient can be associated with the expected value μ and the variance σ_h^2 of the channel complex coefficient.

- **Spatial correlation**: The spatial correlation refers to the correlation between different antennas; hence, is applied to the MIMO transmission. Given the matrix of channel complex coefficient, i.e., $\mathbf{H}$, the spatial correlation can be represented by the channel covariance matrix $\mathbf{R}$ given as follows:

$$\mathbf{R} = \mathbb{E}(\text{Vec}(\mathbf{H})^H \text{Vec}(\mathbf{H})), \tag{2.23}$$

  where $\text{Vec}(\mathbf{H})$ be the vectorization of the matrix $\mathbf{H}$. If $\mathbf{R}$ is a diagonal matrix, then the channel complex coefficients between different antennas are independently distributed. Otherwise, the channel is named as spatial correlated fading in the literature. Please note that the Rayleigh fading with independently distributed antennas is typically referred to IID Rayleigh fading channel.

2.3.2 Assumptions of Channel State Information

In non-coherent communications, we have important assumptions related to the availability the CSI:

No Instantaneous CSI: It is typically assumed that both transmitter and receiver **do not know** the instantaneous CSI.

Availability of Statistical CSI: There are several assumptions of channel information regarding the availability of statistical CSI:

- **Perfect Statistical CSI**: The transmitter and receiver know perfectly the type of fading channel and other parameters characterizing the fading channel, such as the mean value or channel variance. In this case, the receiver can use the optimal maximum-likelihood (ML) detector to detect the transmitted signal with optimal error performance.

- **Partial Statistical CSI**: The transmitter and receiver do not fully know the statistical CSI. A typical assumption of partially known statistical CSI is that the transmitter and receiver do not fully know the type of fading but know some first-order moments, such as the expected value and channel variance. Without full statistical knowledge, the receiver can exploit the channel hardening properties, i.e., transforming the fading multi-antenna channel into an almost deterministic scalar channel via the Central Limit Theorem. The channel hardening has been well-investigated to detect the transmitted signal non-coherently in [7–9].

In this thesis, we assume that the **perfect statistical CSI** is known by the receiver. The channel is known to be IID Rayleigh fading, and the receiver knows perfectly the variance of the channel. The assumption of Rayleigh fading is well-justified in rich-scattering environments such as urban environments because the number of scatters is large enough to invoke the central limit theorem. Furthermore, it is easy to estimate the channel variance without resulting in SE loss. This is because the channel variance is associated with the *large-scale fading* coefficients, which change at a significantly lower rate when compared to the coherence time. The problem of finding the channel variance has been well-studied in the literature, e.g., in [10, 11].

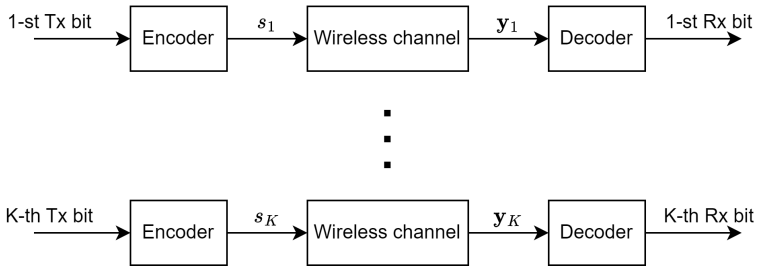

(a) Single-symbol encoding and decoding. Please note that all the encoders and decoders are the same ones in different symbol durations.

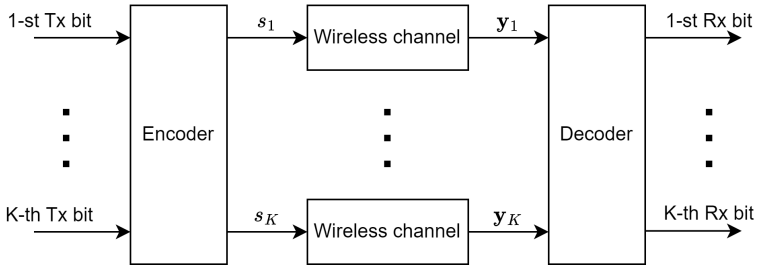

(b) Multiple-symbol encoding and decoding.

Figure 2.1: Comparison between single-symbol and multi-symbol encoding/decoding.

2.3.3 Categorization of Non-coherent Communications in Single-Input Multiple-Output Systems

For the scope of this thesis, we focus on the single-input multiple-output (SIMO) system. This system is suitable for IoT applications where each IoT device only contains one antenna for simple hardware. In general, non-coherent communications in the SIMO systems can be divided into two following schemes:

Single-Symbol Encoding and Decoding Each symbol is encoded and decoded independently from other symbols, as shown in Fig. 2.1a. Unlike single-symbol encoding and decoding in coherent communications, single-symbol encoding and decoding only convey the amplitude information and do not convey phase information. This is because the transmitted signal's phase is expected to distribute uniformly in the receiver; hence, it is not possible to detect the signal's phase without knowing the phase of the channel. On the other hand, the amplitude of the channel complex coefficient is partially known thanks to the knowledge of the channel variance. Furthermore, the amplitude of the channel complex coefficient be-

comes more deterministic as the number of antennas increases, which is known as channel hardening. Because only the amplitude information is conveyed, the single-symbol encoding and decoding is also considered as energy-encoding and decoding in the literature [9, 12, 13]. The advantage of single-symbol encoding and decoding is that this transmission scheme can work efficiently in the fast-fading channel where the coherence time is less than one symbol. Moreover, because only amplitude (or energy) information is processed in both transmitter and receiver, no phase synchronization is required, resulting in low hardware complexity. However, the single-symbol encoding and decoding suffer from SE loss because no phase information is transmitted.

Multiple-Symbol Encoding and Decoding: In multiple-symbol encoding and decoding, the transmitter jointly encodes input bits into multiple symbols, and the received signal of the multiple symbols is jointly decoded to retrieve the information bits, as shown in Fig. 2.1b. The multi-symbol encoding and decoding can be categorized further into the following schemes:

- Non-coherent detection of conventional symbols such as QAM and PSK.
- Unitary constellations.
- Multi-level unitary constellations.

By encoding information into multi-symbol and decoding multi-symbol at once, information can be encoded into the phase difference between different transmitted symbols and retrieved by estimating the phase difference between different received symbols, thus improving the SE compared to the single-symbol encoding and decoding. A notable example of this is differential phase-shift keying (DPSK)[1], where the information is encoded into the phase difference between two consecutive symbols and decoded by differential detection (DD) in the receiver. In general, the DPSK encodes and decodes phase information into a block of two symbols, and no amplitude information is transmitted because the amplitude remains constant. On the other hand, the unitary constellation can be considered to be a more

[1]DPSK can be seen as a special case of non-coherent detection of conventional symbols.

generalized version of DPSK where the information is encoded and decoded into a block of K symbols where K can be greater than two. The term "unitary" refers to the fact that the energy of all transmitted symbols within a block of K symbols are the same. Finally, multi-level unitary constellations are a more generalized version of unitary constellations, where the energy of multi-symbol transmitted signals can have different energy levels. Each level of multi-level unitary constellations contains signal points with the same energy, thus each level can be considered to be a unitary constellation.

In the scope of this thesis, we investigate multi-symbol encoding and decoding to improve the SE of the non-coherent communication system. We focus on two types of multi-symbol encoding and decoding, i.e., unitary constellations and multi-level unitary constellations, which will be discussed in the following sections.

2.4 Multi-level Unitary Constellations

In this section, we introduce multi-level unitary constellations in SIMO systems. First, we start with the overall system model of multi-level encoding and decoding, using the multi-level unitary representation for the multi-symbol signal to characterize the multi-level unitary constellations.

2.4.1 System Model

Let us assume a block Rayleigh fading channel where the channel complex coefficient remains constant over K symbols. Let $\mathbf{h} \in \mathbb{C}^{M\times 1}$ be the channel complex coefficient between one transmit antenna and M receiving antennas, which are unknown to both the transmitter and receiver. The transmitter encodes information into multiple symbols within a coherence time of K symbols. Let s_k be the k-th transmitted symbol, and $\mathbf{y}_k$ and $\mathbf{n}_k$ be the corresponding received signal and noise vector of the k-th transmitted symbol, respectively. Then, we

have the channel model of each k-th symbol as follows:

$$\begin{aligned}
\mathbf{y}_0 &= \mathbf{h}s_0 + \mathbf{n}_0, \\
\mathbf{y}_1 &= \mathbf{h}s_1 + \mathbf{n}_1, \\
&\dots \\
\mathbf{y}_{K-1} &= \mathbf{h}s_{K-1} + \mathbf{n}_{K-1}.
\end{aligned} \tag{2.24}$$

Please note that the noise vector $\mathbf{n}_k$ are independent zero-mean circular Gaussian random variables with variance σ^2. Let us assume $\mathbf{s} = [s_0, \dots, s_{K-1}]$ be the transmitted signal consisting of K transmitted symbols, and $\mathbf{Y} = [\mathbf{y}_0, \dots, \mathbf{y}_{K-1}]$ and $\mathbf{N} = [\mathbf{n}_0, \dots, \mathbf{n}_{K-1}]$ be the corresponding matrix of received signals and noise vectors. Then, we combine the signal model in (2.24) and simplify it as follows:

$$\mathbf{Y} = \mathbf{h}\mathbf{s}^T + \mathbf{N}. \tag{2.25}$$

Now, we represent the multi-symbol signal $\mathbf{s}$ as the product of a magnitude and a unitary vector. Mathematically, $\mathbf{s}$ can be given by:

$$\mathbf{s} = \alpha\mathbf{v}, \tag{2.26}$$

where α and $\mathbf{v}$ are the magnitude and unitary vector defined as:

- **Magnitude** $\alpha = \|\mathbf{s}\|$: denotes the energy of the transmitted signal $\mathbf{s}$.
- **Unitary vector** $\mathbf{v} = \frac{\mathbf{s}}{\|\mathbf{s}\|}$: represents the direction of $\mathbf{s}$ in $\mathcal{C}^{K\times 1}$. By definition, $\|\mathbf{v}\| = 1$, and $\mathbf{v}$ is called a unitary vector.

The magnitude α and unitary vector $\mathbf{v}$ in the case of a 2-symbol signal can be illustrated in Fig. 2.2. We choose the real value for the unitary vector $\mathbf{v}$ for simplification of illustration.

2.4.2 Detection of Multi-level Unitary Constellations

Given that **perfect statistical CSI is known by the receiver**, one can detect the transmitted signal with optimal error performance by using the maximum-likelihood (ML)

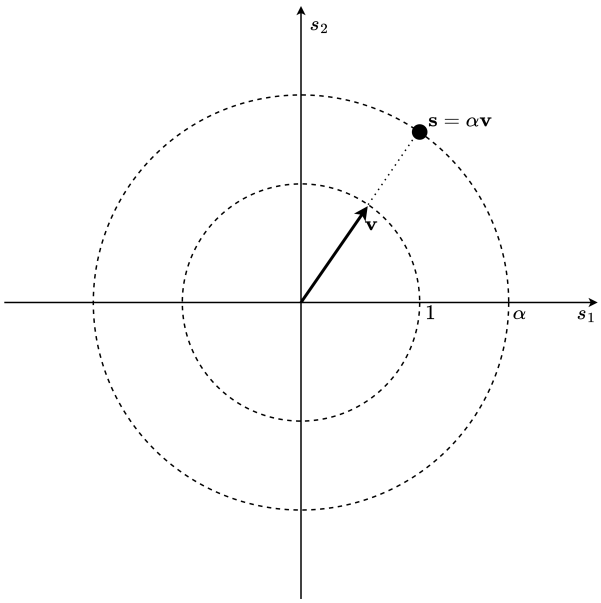

Figure 2.2: Illustration of multi-level unitary representation of 2-symbol real-valued signal $\mathbf{s} = [s_1, s_2]$.

detector. First, given the independent Rayleigh fading, let us assume that $\mathbf{h}$ has an independent Gaussian distribution as $\mathbf{h} \sim \mathcal{CN}(\mathbf{0}_M, \sigma_h^2 \mathbf{I}_M)$ where σ_h^2 is the channel power. Please note that because $\mathbf{N}$ and $\mathbf{h}$ follow multivariate zero-mean Gaussian distribution, the received signal $\mathbf{Y}$ also follows the zero-mean multivariate Gaussian distribution. Given the known channel variance σ_h^2 and noise variance σ^2, the receiver can obtain the probability density function (PDF) of the received signal $\mathbf{Y}$ given transmitted signal $\mathbf{s}$, which is multivariate Gaussian distribution and given as follows [14]:

$$f(\mathbf{Y}|\mathbf{s}) = \frac{\exp\left(-\mathrm{tr}(\mathbf{Y}\left(\mathbb{E}(\mathbf{Y}^H\mathbf{Y}|\mathbf{s})\right)^{-1}\mathbf{Y}^H\right)}{\pi^{KM}\det^M\left(\mathbb{E}(\mathbf{Y}^H\mathbf{Y}|\mathbf{s})\right)}, \tag{2.27}$$

where $\mathbb{E}(\mathbf{Y}^H\mathbf{Y}|\mathbf{s})$ is the expected value of covariance matrix of received signal $\mathbf{Y}$ given the transmitted sequence $\mathbf{s}$. It is easy to obtain the covariance matrix as follows:

$$\mathbb{E}(\mathbf{Y}^H\mathbf{Y}|\mathbf{s}) = \sigma_h^2\mathbf{s}^*\mathbf{s}^T + \sigma^2 I_K. \tag{2.28}$$

Without loss of generality, let us assume that $\sigma_h^2 = 1$. By using the Sherman–Morrison formula to calculate $(\mathbf{s}^*\mathbf{s}^T + \sigma^2 I_K)^{-1}$, we can reformulate the PDF function as follows:

$$f(\mathbf{Y}|\mathbf{s}) = \frac{\exp\left(-\frac{1}{\sigma^2}\mathrm{tr}(\mathbf{Y}^H\mathbf{Y}) + \frac{1}{\sigma^2(\sigma^2+\|\mathbf{s}\|^2)}\mathrm{tr}\left(\mathbf{Y}^H\mathbf{Y}\ \mathbf{s}^*\mathbf{s}^T\right)\right)}{\pi^{KM}\left[(\sigma^2+\|\mathbf{s}\|^2)\sigma^{2K-2}\right]^M}. \tag{2.29}$$

Let Ω_s be the constellations of the multi-symbol $\mathbf{s}$ and l_s be the number of bits allocated to $\mathbf{s}$. It is important to recognize that the size of the constellation Ω_s is 2^{l_s}. Given the PDF function, we can derive the optimal ML detector given as follows:

$$\mathbf{s}_{\mathrm{ML}} = \underset{\mathbf{s}\in\Omega_s}{\operatorname{argmax}} \left(\frac{\mathrm{tr}\left(\mathbf{Y}^H\mathbf{Y}\ \mathbf{s}^*\mathbf{s}^T\right)}{\sigma^2(\sigma^2+\|\mathbf{s}\|^2)} - M\ln(\sigma^2+\|\mathbf{s}\|^2) \right), \tag{2.30}$$

By replacing $\mathbf{s} = \alpha\mathbf{v}$, the joint detector of multi symbols in $\mathbf{s}$ becomes the joint detector of α and unitary vector $\mathbf{v}$ given as follows:

$$\{\alpha_{\mathrm{ML}}, \mathbf{v}_{\mathrm{ML}}\} = \underset{(\alpha,\mathbf{v})}{\operatorname{argmax}} \left(\frac{\alpha^2\mathrm{tr}\left(\mathbf{Y}^H\mathbf{Y}\mathbf{v}^*\mathbf{v}^T\right)}{\sigma^2(\sigma^2+\alpha^2)} - M\ln(\sigma^2+\alpha^2) \right). \tag{2.31}$$

The optimal error performance of the ML detector in (2.31) can be achieved by using an exhaustive search. However, the complexity of the exhaustive search method is proportionate with the size of the constellation Ω_s, which is also exponential in the number of bits l_s. As a result, the ML detector with exhaustive search has high complexity and is not suitable for large l_s. It is also potential to reduce the complexity of the ML detector if the constellations of α and $\mathbf{v}$ have a certain structure that can be effectively exploited to reduce the search space. Many of the low-complexity enabling structures are complicated; hence for the scope of this thesis, we will not investigate those structures in detail and only discuss them in the literature review in Section 2.6. It is also worth noting that if the constellations of α and $\mathbf{v}$ have no structures or have random structures, the high-complexity exhaustive search is still required to solve the ML detector in (2.31).

2.4.3 Design of Multi-level Unitary Constellations

2.4.3.1 Design Criterion

First, we introduce the design criterion of the multi-level unitary constellations. In general, the objective of the constellation design is to reduce the error probability of the ML detector in (3.7). This can be done by minimizing the pairwise error probability (PEP) between any two transmitted signals $\mathbf{s}_a$ and $\mathbf{s}_b$, which is defined as follows:

$$\Pr(\mathbf{s}_a \to \mathbf{s}_b) = \Pr(\text{Decision} = \mathbf{s}_b | \text{Transmit } \mathbf{s}_a). \tag{2.32}$$

If the closed-form expression of PEP is derived, we can formulate an optimization problem to minimize the PEP, thus decreasing the error probability of the constellations. However, to the best of our knowledge, such closed-form expressions of PEP for the multi-level unitary constellations are not known. As a result, using approximated values or boundaries of the PEP as a design criterion is a more practical approach. In this thesis, we use the KL divergence between the PDF of $\mathbf{s}_a$ and the PDF of $\mathbf{s}_b$ as a design criterion because it was theoretically proven to be an upper bound for the error exponent of the PEP [14]. To be specific, let us write the KL divergence between the PDF function of $\mathbf{s}_a$ and the PDF function of $\mathbf{s}_b$ is given by:

$$D_{KL}\left(f(\mathbf{Y}|\mathbf{s}_a)||f(\mathbf{Y}|\mathbf{s}_b)\right) = \mathbb{E}_{f(\mathbf{Y}|\mathbf{s}_a)}\left\{\log\left(\frac{f(\mathbf{Y}|\mathbf{s}_a)}{f(\mathbf{Y}|\mathbf{s}_b)}\right)\right\}. \tag{2.33}$$

The authors in [14] theoretically proved that the relation between KL divergence and the upper bound of PEP between $\mathbf{s}_a$ and $\mathbf{s}_b$, which are given as follows:

$$\lim_{\epsilon \longrightarrow 0} \lim_{M \longrightarrow \infty} \frac{1}{M} \ln \Pr(\mathbf{s}_b \rightarrow \mathbf{s}_a) = -D_{KL}\left(f(\mathbf{Y}|\mathbf{s}_a)||f(\mathbf{Y}|\mathbf{s}_b)\right), \tag{2.34}$$

where ϵ is the upper bound of $\Pr(\mathbf{s}_a \rightarrow \mathbf{s}_b)$, i.e., $\Pr(\mathbf{s}_a \rightarrow \mathbf{s}_b) < \epsilon$ and M is the number of antennas. In other words, the best achievable error exponent for $\Pr(\mathbf{s}_b \rightarrow \mathbf{s}_a)$ when M is large enough and $\Pr(\mathbf{s}_a \rightarrow \mathbf{s}_b)$ is sufficiently small. In this case, the PEP between $\mathbf{s}_a$ and $\mathbf{s}_b$ can be given by:

$$\Pr(\mathbf{s}_b \rightarrow \mathbf{s}_a) \approx \exp\left(-M D_{KL}\left(f(\mathbf{Y}|\mathbf{s}_a)||f(\mathbf{Y}|\mathbf{s}_b)\right)\right). \tag{2.35}$$

2.4.3.2 Design Formulation

Let Ω_s be a multi-symbol constellation of $\mathbf{s}$. As seen in (2.35), the PEP between $\mathbf{s}_b$ and $\mathbf{s}_a$ decreases when the KL divergence between $\mathbf{s}_b$ and $\mathbf{s}_a$ increases. As a result, the optimization problem of minimizing the PEP of all possible pairs $\mathbf{s}_a$ and $\mathbf{s}_b$ is equivalent to the optimization problem of maximizing the KL divergence of all possible pairs $\mathbf{s}_a$ and $\mathbf{s}_b$. Furthermore, the problem of maximizing all possible pairs $\mathbf{s}_a$ and $\mathbf{s}_b$ can be formulated as the following max-min optimization:

$$\max_{\Omega_s} \min_{\mathbf{s}_i, \mathbf{s}_k \in \Omega_s, \mathbf{s}_i \neq \mathbf{s}_k} D_{\mathrm{KL}}\left(\mathbf{s}_i, \mathbf{s}_k\right). \tag{2.36}$$

In the following, we formulate the closed-form expression of KL divergence for the multi-level unitary constellations and exploit the expression of KL divergence to reduce the design complexity. First, the KL divergence for the general cases of the multi-symbol signal $\mathbf{s}$ in the block fading channel can be given by [14, Eq. 34]:

$$\begin{aligned} D_{\mathrm{KL}}\left(f(\mathbf{Y}|\mathbf{s}_i), f(\mathbf{Y}|\mathbf{s}_k)\right) &= \frac{1}{M}\mathbb{E}_{f(\mathbf{Y}|\mathbf{s}_i)}\left(\ln\left(\frac{f(\mathbf{Y}|\mathbf{s}_i)}{f(\mathbf{Y}|\mathbf{s}_k)}\right)\right), \\ &= \left(\frac{\|\mathbf{s}_k\|^2\|\mathbf{s}_i\|^2 - \|\mathbf{s}_k^T\mathbf{s}_i^*\|^2}{\sigma^2(\sigma^2+\|\mathbf{s}_k\|^2)}\right) + \left(\frac{\sigma^2+\|\mathbf{s}_i\|^2}{\sigma^2+\|\mathbf{s}_k\|^2} - \ln\left(\frac{\sigma^2+\|\mathbf{s}_i\|^2}{\sigma^2+\|\mathbf{s}_k\|^2}\right) - 1\right). \end{aligned} \tag{2.37}$$

By using the multi-level unitary representation of $\mathbf{s}$ in (2.26), we can reformulate the KL divergence in (2.37) as follows:

$$D_{\mathrm{KL}}\left(\alpha_k, \mathbf{v}_k, \alpha_i, \mathbf{v}_i\right) = \frac{\alpha_k^2\alpha_i^2\left(1-|\mathbf{v}_k^T\mathbf{v}_i^*|^2\right)}{\sigma^2(\sigma^2+\alpha_k^2)} + \left(\frac{\sigma^2+\alpha_i^2}{\sigma^2+\alpha_k^2} - \ln\left(\frac{\sigma^2+\alpha_i^2}{\sigma^2+\alpha_k^2}\right) - 1\right). \tag{2.38}$$

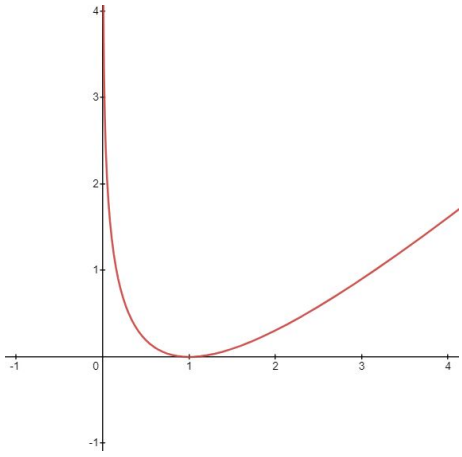

Figure 2.3: Function $x - \log(x) - 1$.

It is interesting to investigate the geometrical interpretation of the KL divergence in (2.38). It can be seen in (2.38) that the KL divergence consists of two following terms:

- **Inter-level distance**: The inter-level distance is caused by the difference between energy levels α_k and α_i, and can be represented by the second term of (2.38) as follows:

$$D_{\mathrm{inter}}\left(\alpha_k, \alpha_i\right) = \left(\frac{\sigma^2+\alpha_i^2}{\sigma^2+\alpha_k^2} - \ln\left(\frac{\sigma^2+\alpha_i^2}{\sigma^2+\alpha_k^2}\right) - 1\right). \tag{2.39}$$

  D_{inter} can be rewritten as $x - \log(x) - 1$, where $x = (\sigma^2+\alpha_i^2)/(\sigma^2+\alpha_k^2)$ represents the difference between energy levels $\alpha_i^2+\sigma^2$ and $\alpha_k^2+\sigma^2$. As shown in Fig. 2.3, the

function $x - \log(x) + 1$ increases when the distance between x and one increases and is equal to zero when $x = 1$. Hence, $D_{\text{inter}}(\alpha_k, \alpha_i)$ is equal to zero when $\alpha_i = \alpha_j$ and increases as the difference between $\alpha_i^2 + \sigma^2$ and $\alpha_k^2 + \sigma^2$ increases.

- **Intra-level distance**: The intra-level distance is caused by the difference between two unitary vectors $\mathbf{v}_i$ and $\mathbf{v}_k$ and scaled by the energy levels α_i^2 and α_k^2. The intra-level distance can be represented by the first term of (2.38) as follows:

$$D_{\text{intra}}(\alpha_k, \mathbf{v}_k, \alpha_i, \mathbf{v}_i) = \frac{\alpha_k^2 \alpha_i^2}{\sigma^2(\sigma^2 + \alpha_k^2)} D_v^2(\mathbf{v}_k, \mathbf{v}_i), \tag{2.40}$$

where $D_v(\mathbf{v}_k, \mathbf{v}_i)$ is the chordal distance[2] between unitary vectors $\mathbf{v}_i$ and $\mathbf{v}_k$, and is given by:

$$D_v(\mathbf{v}_k, \mathbf{v}_i) = \sqrt{1 - |\mathbf{v}_k^T \mathbf{v}_i^*|^2} = \sin\left(\angle(\mathbf{v}_i, \mathbf{v}_k)\right). \tag{2.41}$$

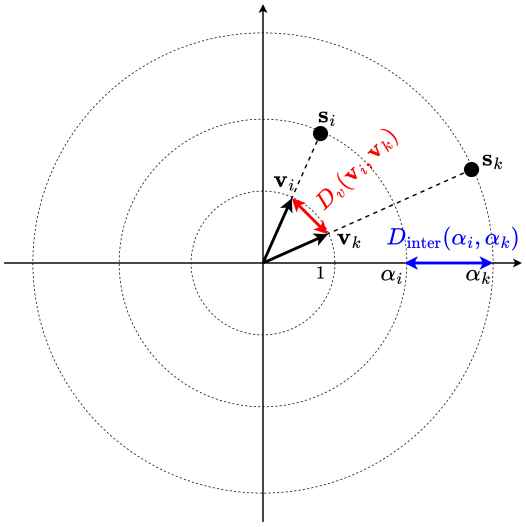

Figure 2.4: Illustrations of inter-level distance and intra-level distance between two transmitted signal $\mathbf{s}_i = \alpha_i \mathbf{v}_i$ and $\mathbf{s}_k = \alpha_k \mathbf{v}_k$. *Please note that the two axes represent the direction of unitary vectors and are not equivalent to the in-phase and quadrature components.*

The geometrical interpretation of the inter-level distance and intra-level distance can be shown in Fig. 2.4. Based on this representation, a **design approach** was proposed in [14]. In that design approach, the multi-level unitary constellations are divided into different sub-constellations. Each sub-constellation contains signals with the same energy level; thus, each

[2]The chordal distance also represents the angle between two unitary vectors.

sub-constellation is considered to be a unitary constellation. This division helps to simplify the design process by decoupling the design process into two small distinct design problems:

- **Multi-level design**: This problem includes two smaller problems. The first one is to choose the best way of dividing the multi-level unitary constellations, as shown in Fig. 2.5a. Secondly, given a fixed division of the multi-level unitary constellations, one maximizes $D_{\text{inter}}(\alpha_k, \alpha_i)$ between different sub-constellations by designing the energy level α^2, as shown in Fig. 2.5b.

- **Unitary design**: This problem is to maximize $D_{\text{intra}}(\alpha_k, \mathbf{v}_k, \alpha_i, \mathbf{v}_i)$ of all signals within the unitary sub-constellation, as shown in Fig. 2.5c. Please note that because $\alpha_k = \alpha_i$ for all signal in the unitary sub-constellations, the $D_{\text{intra}}(\alpha_k, \mathbf{v}_k, \alpha_i, \mathbf{v}_i)$ is only determined by the chordal distance $D_v(\mathbf{v}_k, \mathbf{v}_i)$. As a result, the problem is equivalent to designing the unitary vectors $\mathbf{v}$ to maximize the chordal distance between them.

By decoupling the design of the multi-level unitary constellation into the multi-level design and unitary design, the complexity of the multi-level unitary constellation is reduced to the complexity of the multi-level design and the complexity of the unitary design. Please note that both the complexity of multi-level design and unitary design depend on their corresponding structures. The complexity of the design of some multi-level structures will be discussed in the literature review in Section 2.6.1, while the design complexity of the unitary constellations will be discussed in the literature review in Section 2.6.2.

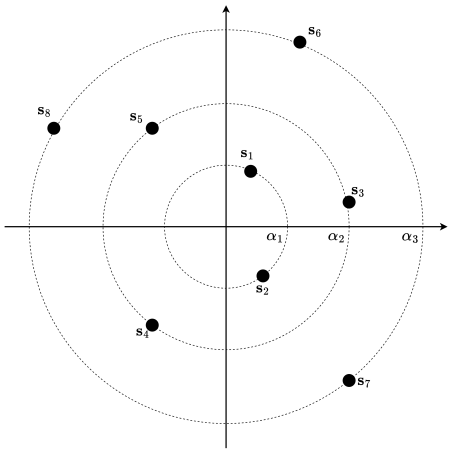

(a) Multi-level design: Dividing constellations into three sub-constellations whose size are $\{2, 3, 3\}$.

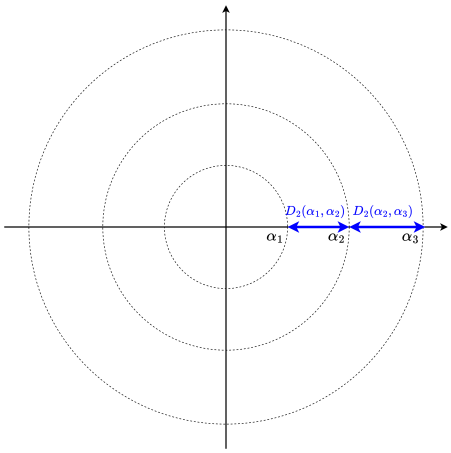

(b) Multi-level design: Design of energy level α^2 to maximize D_{inter} (marked with blue lines) between different sub-constellations.

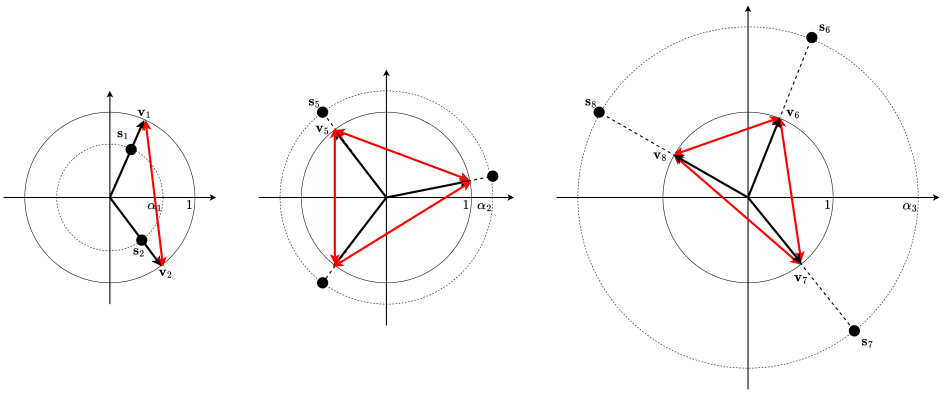

(c) Unitary design: Design of unitary vector $\mathbf{v}$ to maximize D_{intra} (marked with red lines) within each sub-constellation.

Figure 2.5: Design process of multi-level unitary constellations.

2.5 Unitary Constellations

The definition of unitary constellations was originally provided in the context of the MIMO system in [15]. Let us assume general MIMO communications where $\mathbf{V} \in \mathbb{C}^{K \times M_t}$ is a matrix of the transmitted signal with K being the number of transmitted symbol and M_t being the number of transmit antenna. The transmitted signal $\mathbf{V}$ belongs to the unitary constellations when $\mathbf{V}$ satisfies the following conditions [15]:

$$\mathbf{V}^H \mathbf{V} = \mathbf{I}_{M_t}. \tag{2.42}$$

Please note that in the SIMO system where the transmitted signal $\mathbf{V}$ can be represented as a vector $\mathbf{v}$, the condition in (2.42) is simplified to the following conditions:

$$\mathbf{v}^H\mathbf{v} = \|\mathbf{v}\|^2 = 1. \tag{2.43}$$

In other words, in the SIMO systems, the constellations are considered to be unitary when the energy of all transmit signals is equal to one.

Unitary constellations play a crucial role in MIMO communication because they are proven theoretically to be an optimal non-coherent MIMO transmission scheme in a high SNR regime [15, 16]. In the following, we introduce the design and detection of unitary constellations, investigate the literature on unitary constellations, and point out the challenges in designing and detecting unitary constellations.

2.5.1 Detection of Unitary Constellations

Let Ω_v be the unitary constellation of unitary signal $\mathbf{V}$. Because the energy level α^2 is fixed in the unitary constellations, we can obtain the non-coherent ML detector for unitary constellations from the ML detector in (2.31) as follows:

$$\mathbf{v}_{\text{ML}} = \underset{\mathbf{v}\in\Omega_v}{\text{argmax}}\ \text{tr}\left(\mathbf{Y}^H\mathbf{Y}\ \mathbf{v}^*\mathbf{v}^T\right) = \underset{\mathbf{v}\in\Omega_v}{\text{argmax}}\,\|\mathbf{Y}\mathbf{v}^*\|^2. \tag{2.44}$$

Please note that the ML detector in (2.44) is also named the generalized likelihood ratio test (GLRT) detector in the literature of unitary constellations. One advantage of the ML/GLRT detector in (2.44) for unitary constellations over the ML detector in (2.31) for the multi-level unitary constellations is that it does not require the statistical knowledge of the fading channel; thus, being beneficial in situations where the statistical knowledge is not available to the receiver.

The complexity of the ML detector in (2.44) depends on the structure of unitary constellations. In general, if unitary constellations have no structure or have random structure, solving (2.44) still requires an exhaustive search over the constellation set Ω_v, each search involves the calculation of the argument in (2.44) with a complexity of $\mathcal{O}(K^2)$. If l_v is the number of bits allocated to Ω_v, then the size of constellations Ω_v is 2^{l_v}. As a result, if the

unitary constellations are unstructured, the complexity of the ML detector in (2.44) is given by:

$$\mathcal{O}(2^{l_v}K^2). \tag{2.45}$$

The complexity of solving (2.44) can be reduced if $\mathbf{v}$ has a specific structure that allows low complexity in detection. Different structures of unitary constellations have been proposed with different detection complexities, which will be investigated in the literature review.

2.5.2 Design of Unitary Constellations

2.5.2.1 Design Criterion

The objective of the unitary constellation design is to minimize the error probability of the ML detector in (2.44), which can achieved by minimizing the PEP between any two transmitted unitary signal $\mathbf{v}_a$ and $\mathbf{v}_b$. Because it is difficult to derive the exact expression of PEP for unitary constellations, other simplified expressions of PEP can be used as design criteria such as the high-SNR asymptotic expression of PEP [17] and the Chernoff bound of PEP [18]. Among different design criteria, the Chernoff bound of PEP has been the most widely investigated design criterion in the literature. The Chernoff bound of the PEP of the ML detector is first proposed for general MIMO communications [15]. Let $\mathbf{V} \in \mathbb{C}^{K\times M_t}$ be the transmitted signal, then the Chernoff bound of the PEP between two transmitted signals $\mathbf{V}_a$ and $\mathbf{V}_b$ can be derived as follows [15]:

$$\Pr(\mathbf{V}_a \to \mathbf{V}_b) \leq \frac{1}{2}\prod_{m=1}^{M_t}\left[1+\frac{1-d_m^2}{4\sigma^2(1+\sigma^2)}\right]^{-M}. \tag{2.46}$$

where d_m is the m-th singular value of the matrix $(\mathbf{V}_a^H\mathbf{V}_b) \in \mathbb{C}^{M\times M}$. In general, by minimizing all the singular values d_m, one can reduce the Chernoff bound; hence, reducing the PEP. Based on the Chernoff bound in [15], different design criteria for unitary constellations in the MIMO system have been proposed:

- Minimizing exact expression of the Chernoff bound in (2.46) [18].
- Maximizing the high-SNR asymptotic expression of the Chernoff bound in (2.46), which is equivalent to maximizing $\prod_{m=1}^{M_t}(1-d_m^2)$ [19].

- Minimizing the largest component of the Chernoff bound in (2.46), which is equivalent to minimizing the largest singular value [15].
- Minimizing $\sum_{m=1}^{M_t} d_m^2$, which is equivalent to maximizing the chordal distance $D_v(\mathbf{V}_a, \mathbf{V}_b) = \sqrt{\sum_{m=1}^{M_t}(1 - d_m^2)}$ [19].
- Minimizing $\prod_{m=1}^{M_t} d_m^2$ [20].

In the scope of this thesis, we focus on SIMO systems. Interestingly, for the SIMO system, all the above-mentioned design criteria are equivalent to maximizing the chordal distance. Then, the Chernoff bound of PEP in the SIMO system can be also rewritten as a function of the chordal distance as follows:

$$\Pr(\mathbf{v}_a \to \mathbf{v}_b) \leq \frac{1}{2}\left[1 + \frac{D_v^2(\mathbf{v}_a, \mathbf{v}_b)}{4\sigma^2(1+\sigma^2)}\right]^{-M}. \tag{2.47}$$

Because the $D_v(\mathbf{v}_a, \mathbf{v}_b)$ determines the upper bound of the PEP, maximizing the $D_v(\mathbf{v}_a, \mathbf{v}_b)$ is equivalent to minimizing the worst-case of PEP, therefore reducing the error probability of the detector. It is also worth noting that if we use the KL divergence as the design criterion, then the problem of maximizing the KL divergence is also reduced to the problem of maximizing the chordal distance, as seen in Section 2.3.

2.5.2.2 Design Formulation

The main objective of constellation design is to minimize the PEP between any pair of constellation points. Please note that this objective is equivalent to minimizing the worst-case of PEP. Hence, we can formulate the optimization problem as follows:

$$\hat{\Omega}_v = \underset{\Omega_v}{\operatorname{argmin}} \left\{ \max_{\substack{\mathbf{v}_a \neq \mathbf{v}_b \\ \mathbf{v}_a, \mathbf{v}_b \in \Omega_v}} \Pr(\mathbf{v}_a \to \mathbf{v}_b) \right\}, \tag{2.48a}$$

$$\text{s.t. } \|\mathbf{v}\| = 1, \ \forall \mathbf{v} \in \Omega_v, \tag{2.48b}$$

$$\text{card}\{\Omega_v\} = 2^{l_v}. \tag{2.48c}$$

It is important to investigate the complexity of solving the unitary constellation design problem in (2.48). It is not possible to estimate and formulate the design complexity based

on the number of basic arithmetic operations because the design of many constellations in the literature requires solving optimization problems, which can have different complexity depending on the toolboxes and optimization techniques. As a result, to evaluate the complexity of the optimization problems, a more general way is to estimate the number of variables involved in the optimization problems.

Based on the structure of unitary constellations, we can divide the unitary constellations into unstructured unitary constellations and structured unitary constellations:

- **Unstructured unitary constellations**: The unstructured unitary constellation can be obtained by numerically solving the optimization problem in (2.48). This is because the problem in (2.48) has no constraints that impose the constellation into a specific structure (the constraint $\|\mathbf{v}\| = 1$ only confine the constellation into unitary constellation). For l_v be the number of bits allocated to the unitary constellation Ω_v, there are 2^{l_v} constellation points $\mathbf{v}$ in Ω_v and $2^{l_v}(2^{l_v} - 1)/2$ different pairs of constellation points. As a result, solving the optimization problem in (2.48) requires exponential complexity in l_v, which is impractical to transmit a large number of bits.

- **Structured unitary constellations**: In this case, the unitary constellations have a certain structure. This structure allows the structured unitary constellations to be characterized by fewer parameters compared to the unstructured unitary constellations; hence, reducing the complexity in design. However, please note that the structure can also act as a constraint that reduces the degree of freedom of the problem of constellation design, thus degrading the PEP performance compared to unstructured unitary constellations.

2.6 Literature Review

2.6.1 Multi-level Unitary Constellations

To the best of our knowledge, few studies have studied the design and detection of multi-level unitary constellations. The design and detection of the multi-level unitary constellations were first proposed and investigated in [14], in which the authors in [14] prove theoretically

that the KL divergence can be used as an effective design criterion for the multi-level unitary constellations. Furthermore, they proposed a method for the multi-level design, which can be considered to be unstructured. For multi-level unitary constellations Ω_s with 2^{l_s} constellation points where l_s is the number of transmitted bits, the multi-level design method in [14] can be summarized as follows:

1. Find all possible ways to divide the multi-level constellations.
2. For each possible way of dividing the multi-level constellation, solving the multi-level design.

While their method can result in optimal PEP performance, it suffers from high complexity in design because the number of ways to divide the multi-level constellations increases exponentially with the size of the constellations.

Low-complexity design and detection for the multi-level unitary constellations have been proposed in [21]. In this paper, the authors proposed a specific structure of the multi-level unitary constellations, which is given by:

$$\mathbf{s} = \alpha[\cos(\theta), \sin(\theta)e^{j\phi}]^T, \tag{2.49}$$

where θ and ϕ belongs to PSK constellations. The design complexity in [21] is reduced to the complexity of solving closed-form equations in [21, Proposition 1]. The number of searches in the ML detector of [21] is to $(2^{l_\alpha}+2^{l_\theta}+2^{l_\phi})$ where l_α, l_θ and l_ϕ are the number of bits allocated to α, θ and ϕ. Since $l_\alpha + l_\theta + l_\phi = l_s$, the detection complexity in [21] is much lower than the ML detector with exhaustive search over 2^{l_s} constellation points. A similar structure for the multi-level unitary constellations was proposed for the general fading channel in [22]. However, the proposed detector and design criterion based on Riemann distance in [22] is not optimal for the Rayleigh fading channel; hence, this method in [22] suffers from significant performance loss compared to [21] and error floor in high SNR regime. Please note that both designs for proposed multi-level unitary constellations in [22] and [21] are only applicable to $K = 2$ and, therefore, not applicable to the general case of K.

As a result, the low-complexity design and detection of multi-level unitary constellations for the general case of multi-symbol (K can be anywhere for $K \geq 3$) has not been investigated. It is worth noting that a low-complexity design and detection of multi-level unitary constellations with good error performance is also desirable.

2.6.2 Unitary Constellations

The unstructured unitary constellation can be obtained by numerically solving the optimization problem of minimizing the PEP between any pairs of constellation points. The closed-form expression for the Chernoff bound of PEP was first proposed by Hochwald and Mazetta in [15]. Then, based on the Chernoff bound, the authors in [15] proposed the design of unstructured unitary constellations by using the largest singular value as the design criterion. The unstructured unitary constellations with other design criteria have been proposed such as the high-SNR asymptomatic expression [17], the Chernoff bound [18], and the product of singular values [20]. The main advantage of unstructured unitary constellations is that they have optimal or near-optimal PEP performance; hence, they have excellent error performance. However, they suffer from the following disadvantages:

- *High complexity in design*: This is because designing unstructured unitary constellations requires optimizing all possible pairs of constellation points in the unitary constellations. For l_v be the number of bits allocated to the unitary constellation Ω_v, there are 2^{l_v} constellation points $\mathbf{v}$ in Ω_v and $2^{l_v}(2^{l_v}-1)/2$ different pairs of constellation points. As a result, maximizing all possible pairs of constellation points requires exponential complexity in l_v, which is impractical to transmit a large number of bits.

- *High complexity in detection*: The unstructured unitary constellation requires the ML detector in (2.44) with an exhaustive search over 2^{l_v} constellation points. Thus, the complexity of detecting unstructured unitary constellations grows exponentially in l_v, which is impractical to transmit a large number of bits.

- *High complexity in storage* $\mathcal{O}(2^{l_v})$: All constellation points of unstructured unitary constellations must be stored. As a result, the storage complexity is equal to the size

of unitary constellations, which grows exponentially with the number of transmitted bits l_v,

There has been research to reduce the complexity of unstructured unitary constellations. However, none of them completely resolves the high complexity of unstructured unitary constellations. In [23], the iterative collision-based packing algorithm was proposed to construct the unstructured unitary constellations with lower complexity. However, the complexity is still exponential in the number of transmitted bits. The quasi-ML detector was proposed in [20] to reduce the detection complexity of the ML detector. In [20], the authors presented a low-complexity unitary constellation based on the rotation method and a low-complexity receiver called a reduced-search quasi-ML detection algorithm. While this technique was shown to reduce the complexity of the ML detection, the complexity is still comparable to the ML detection, especially in the low and medium SNR regimes. Furthermore, it requires the storage of constellation points and distances between constellation points and reference points, which is not suitable for large constellations.

On the other hand, certain structures can be imposed into the structured unitary constellations to reduce the design complexity. In many cases, the predetermined structure allows lower complexity in design compared to unstructured unitary constellations. For example, Hochwald proposed structured unitary constellations where the set of constellations is taken from a Discrete Fourier Transform (DFT) matrix in [19]. The unitary constellation design problem of the Fourier-based method [19] is equivalent to a problem of optimizing the frequency response in a filter design problem. The co-prime PSK constellations in [24] can be represented as $[x, y, z]^T$ where z is the optimization variable, x and y belong to a M_x-PSK constellation and M_y-PSK constellation, with M_x and M_y being co-prime numbers, respectively. In [25], from parent unitary constellations, new constellation points are generated by moving from the original unitary constellations along a geodesic direction. All the structured constellations in [19], [24], and [25] have relatively low complexity in design. However, they still require the ML detector with an exhaustive search like unstructured unitary constellations, thus still being impractical for a large number of transmitted bits.

To overcome this problem, in addition to low complexity in design, more strict structures for unitary constellations have been proposed to reduce low complexity in detection. Usually, these structures are variants of already-known structures such as PSK or QAM constellations; hence allowing low complexity in detection. Although achieving low complexity in design and detection, they sacrifice the optimal error performance of the unstructured unitary constellations. This is because the structure can act as additional constraints that reduce the degree of freedom, which results in error performance loss. Furthermore, some structures of unitary constellations are only applicable for certain cases of a transmitted number of bits or the coherence time. Therefore, they can not be applied to a more general case of unitary constellations. To understand the problem, let us examine some structured unitary constellations with low complexity in both detection and design in the literature [21, 26–28]. Based on Welch's code, the unitary constellations in [27] have both low complexities in construction and detection. However, the structured unitary constellations in [27] are only applicable for K being a power of two. Furthermore, the method in [27] is only able to construct unitary constellations with a small size and SE smaller than one. In [22], a unitary constellation structure based on the PSK constellations was proposed. Although this constellation has both low complexities in construction and detection and achieves relatively good performance, it is only applicable to the case of $K = 2$. In [26], the authors proposed an exponential constellation, which maps QAM symbols into a non-coherent unitary sequence. The unitary constellations in [26] do not require numerical optimization in design, and reduce the detection complexity to the detection of QAM symbols. However, the structured unitary constellations have mediocre error performance compared to the unstructured unitary constellations. In [28], the authors introduced a novel structure of unitary constellations for SIMO systems called a cube-split constellation. Such a constellation is obtained by dividing the Grassmannian surface into bent cubes and then mapping QAM symbols in the Euclidean space of these cubes. The cube-split constellation has low complexity equally to the exponential constellations in [26]. However, they are only applicable for K being a power of two and only have good performance for some specific constellation sizes.

A special case of structured unitary constellations is PSK constellations with equal mod-

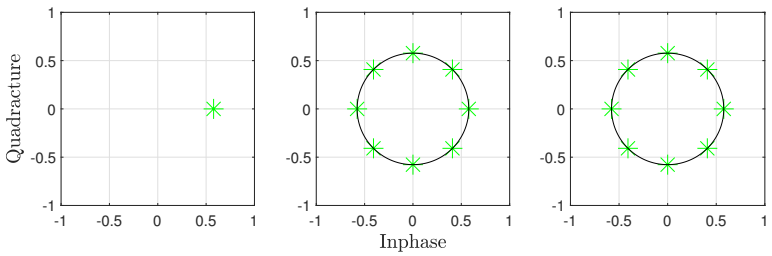

Figure 2.6: A sequence of PSK symbols with constant amplitude.

ulation orders and constant amplitude, as shown in Fig. 2.6. The non-coherent detection of this specific structure, i.e., the PSK sequence, can be classified into two major groups: (i) multi-symbol differential detection (MSDD) [29–31] and (ii) decision-feedback differential detection (DFDD) [32–34]. The MSDD algorithm has optimal error performance because it is based on the ML detector in (2.44) and is given by:

$$\mathbf{v}_{\mathrm{ML}} = \underset{\mathbf{v}\in\Omega_v}{\operatorname{argmax}}\ \operatorname{tr}\left(\mathbf{Y}^H\mathbf{Y}\ \mathbf{v}^*\mathbf{v}^T\right) = \underset{\mathbf{v}\in\Omega_v}{\operatorname{argmax}}\ \operatorname{tr}\left(\mathbf{Z}\ \mathbf{V}\right), \tag{2.50}$$

where $\mathbf{Z}$ and $\mathbf{V}$ is defined as follows:

$$\mathbf{Z} = \mathbf{Y}^H\mathbf{Y} = \begin{bmatrix} \mathbf{y}_0^H\mathbf{y}_0 & \cdots & \mathbf{y}_0^H\mathbf{y}_{K-1} \\ \vdots & \ddots & \vdots \\ \mathbf{y}_{K-1}^H\mathbf{y}_0 & \cdots & \mathbf{y}_{K-1}^H\mathbf{y}_{K-1}. \end{bmatrix},\ \mathbf{V} = \mathbf{v}^*\mathbf{v}^T = \begin{bmatrix} v_0^*v_0 & \cdots & v_0^*v_{K-1} \\ \vdots & \ddots & \vdots \\ v_{K-1}^*v_0 & \cdots & v_{K-1}^*v_{K-1} \end{bmatrix}. \tag{2.51}$$

Please note that *differential detection* refers to the detection based on the phase difference between received signals, which is reflected by the fact that $\mathbf{y}_i^H\mathbf{y}_j$ is associated with the phase difference between the received signals of the i-th transmitted symbol and j-th transmitted signal. *Multi-symbol* refers to joint detection of multiple symbols in (2.50), i.e., $\mathbf{v} = [v_0, v_1, \ldots, v_{K-1}]^T$. Despite the optimal error performance, the MSDD suffers from the exponential complexity as a result of multi-symbol detection. Hence, the MSDD is not suitable for practical applications.

The DFDD addresses the high complexity of the MSDD by only detecting one symbol at a time. The detection of that symbol is aided by the previously detected symbols as shown in Fig. 2.7a. The DFDD algorithm can be explained as follows:

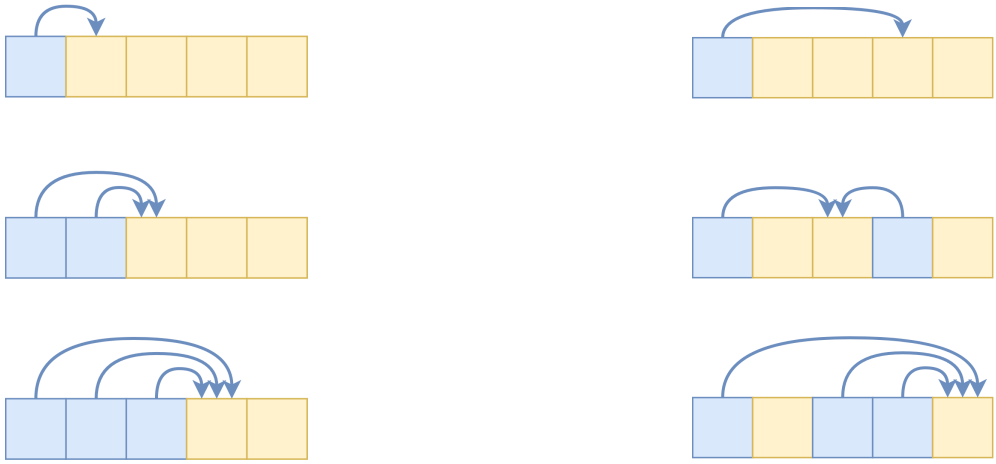

(a) (unsort) DFDD (sorting order: 1, 2, 3). (b) Sort-DFDD (sorting order: 3, 2, 4).

Figure 2.7: Mechanism of conventional (unsort) DFDD and sort-DFDD algorithms. Blue and yellow boxes indicate the detected and undetected PSK symbols, respectively. The arrow indicates the information from detected PSK symbols to detect an unknown PSK symbol.

- We assume that the symbol v_0 is known by the receiver; hence, we denote $\bar{v}_0$[3].
- Given known symbol $\bar{v}_0$, v_1 can be found by solving a simplified MSDD in (2.50), which only involves the 0-th and 1-st rows and columns of (2.51) as follows:

$$\bar{v}_1 = \underset{v_1}{\text{argmax}} \ \text{tr}\left(\begin{bmatrix} \mathbf{y}_0^H \mathbf{y}_0 & \mathbf{y}_0^H \mathbf{y}_1 \\ \mathbf{y}_1^H \mathbf{y}_0 & \mathbf{y}_1^H \mathbf{y}_1 \end{bmatrix} \begin{bmatrix} \bar{v}_0^* \bar{v}_0 & \bar{v}_0^* v_1 \\ v_1^* \bar{v}_0 & v_1^* v_1 \end{bmatrix} \right). \tag{2.52}$$

- Given known symbol $\bar{v}_0$ and $\bar{v}_1$, v_2 can be found by solving a simplified MSDD in (2.50), which only involves the 0-th, 1-st, and 2-nd rows and columns of (2.51) as follows:

$$\bar{v}_2 = \underset{v_2}{\text{argmax}} \ \text{tr}\left(\begin{bmatrix} \mathbf{y}_0^H \mathbf{y}_0 & \mathbf{y}_0^H \mathbf{y}_1 & \mathbf{y}_0^H \mathbf{y}_2 \\ \mathbf{y}_1^H \mathbf{y}_0 & \mathbf{y}_1^H \mathbf{y}_1 & \mathbf{y}_1^H \mathbf{y}_2 \\ \mathbf{y}_2^H \mathbf{y}_0 & \mathbf{y}_2^H \mathbf{y}_1 & \mathbf{y}_2^H \mathbf{y}_2 \end{bmatrix} \begin{bmatrix} \bar{v}_0^* \bar{v}_0 & \bar{v}_0^* \bar{v}_1 & \bar{v}_0^* v_2 \\ \bar{v}_1^* \bar{v}_0 & \bar{v}_1^* \bar{v}_1 & \bar{v}_1^* v_2 \\ v_2^* \bar{v}_0 & v_2^* \bar{v}_1 & v_2^* v_2 \end{bmatrix} \right). \tag{2.53}$$

- The process continues until all symbols are detected.

Please note that the mentioned decision rules can be simplified further. Let us assume that $\bar{v}_0, \bar{v}_1, \ldots, \bar{v}_{n-1}$ are known symbols, then the simplified MSDD algorithm to detect v_n can be

[3]We denote a known variable x as $\bar{x}$.

given by:

$$\bar{v}_n = \underset{v_n}{\text{argmax}} \ \text{tr}\left(\begin{bmatrix} \mathbf{y}_0^H\mathbf{y}_0 & \cdots & \mathbf{y}_0^H\mathbf{y}_{n-1} & \mathbf{y}_0^H\mathbf{y}_n \\ \vdots & \ddots & \vdots & \vdots \\ \mathbf{y}_{n-1}^H\mathbf{y}_0 & \cdots & \mathbf{y}_{n-1}^H\mathbf{y}_{n-1} & \mathbf{y}_{n-1}^H\mathbf{y}_n \\ \mathbf{y}_n^H\mathbf{y}_0 & \cdots & \mathbf{y}_n^H\mathbf{y}_{n-1} & \mathbf{y}_n^H\mathbf{y}_n \end{bmatrix} \begin{bmatrix} \bar{v}_0^*\bar{v}_0 & \cdots & \bar{v}_0^*\bar{v}_{n-1} & \bar{v}_0^*v_n \\ \vdots & \ddots & \vdots & \vdots \\ \bar{v}_{n-1}^*\bar{v}_0 & \cdots & \bar{v}_{n-1}^*\bar{v}_{n-1} & \bar{v}_{n-1}^*v_n \\ v_n^*\bar{v}_0 & \cdots & v_n^*\bar{v}_{n-1} & v_n^*v_n \end{bmatrix} \right). \tag{2.54}$$

Since all variables except for v_n are known in (2.54), the decision rule in (2.54) can be simplified as follows:

$$\bar{v}_n = \underset{v_n}{\text{argmax}} \ \text{Re}\left\{ \left(\sum_{i=0}^{n-1} \mathbf{y}_i^H\mathbf{y}_n\bar{v}_i \right) v_n \right\}. \tag{2.55}$$

The detector in (2.55) has low complexity and can be implemented by a few delay and multiplication components, as shown in [34, Fig. 2]. However, it suffers from significant performance loss compared to the MSDD. This is because if a PSK symbol is detected incorrectly, this incorrect decision is still used as feedback for the detection of upcoming PSK symbols, thus degrading the detection of the next PSK symbols due to error propagation.

In [35], the sort-DFDD algorithm partially resolves the error propagation issue by detecting PSK symbols with the highest reliability first and then using them as feedback to detect the remaining undetected PSK symbols. This results in the detection not following a sequential order, as shown in Fig. 2.7b. Because reliable symbols are less likely to cause errors, the sort-DFDD algorithm reduces the effect of error propagation, thus improving error performance compared to the original DFDD algorithm. The decision rule of the sort-DFDD algorithm is similar to the decision rule of the original (unsort) DFDD, except that the row and column of $\mathbf{Z}$ and $\mathbf{V}$ of the sort-DFDD is reordered according to the new sorting order. To obtain the optimal sorting order for the sort-DFDD algorithm, the authors proposed the quantization error as the reliability criterion for the sort-DFDD algorithm. However, there is still a considerable performance gap between the sort-DFDD algorithm and the optimal MSDD algorithm.

In conclusion, the design and detection of unitary constellations suffer from a performance-complexity trade-off. On the one hand, optimal error performance can be achieved by de-

signing unstructured unitary constellations with the optimal ML detector with an exhaustive search. However, this approach requires optimal exponential complexity in design and detection, thus being impractical for practical applications. On the other hand, we can impose a special structure on unitary constellations and exploit that structure to reduce complexity in design. Different techniques have been investigated to reduce the complexity of the ML detector. However, this approach usually may result in performance loss. As a result, developing unitary constellations with low complexity in both design and detection while suffering minimal performance loss compared to unstructured unitary constellations remains a challenging problem.

References

[1] A. Goldsmith, *Wireless communications*. Cambridge university press, 2005.

[2] D. Tse and P. Viswanath, *Fundamentals of wireless communication*. Cambridge university press, 2005.

[3] X. Lin and N. Lee, "5G and Beyond," *Cham, Switzerland: Springer Nature Switzerland AG*, 2021.

[4] X. Tang, M.-S. Alouini, and A. J. Goldsmith, "Effect of channel estimation error on M-QAM BER performance in Rayleigh fading," *IEEE Trans. Commun.*, vol. 47, no. 12, pp. 1856–1864, Dec. 1999.

[5] B. Xia and J. Wang, "Effect of channel-estimation error on QAM systems with antenna diversity," *IEEE Trans. Commun.*, vol. 53, no. 3, pp. 481–488, Mar. 2005.

[6] F. Edition, A. Papoulis, and S. U. Pillai, "Probability, random variables, and stochastic processes," 2002.

[7] M. Chowdhury, A. Manolakos, and A. J. Goldsmith, "Design and performance of noncoherent massive SIMO systems," in *Proc. IEEE Annu. Conf. Inf. Sci. Syst. (CISS)*, Mar. 2014, pp. 1–6.

[8] M. Chowdhury, A. Manolakos, and A. Goldsmith, "Scaling laws for noncoherent energy-based communications in the SIMO MAC," *IEEE Trans. Inf. Theory*, vol. 62, no. 4, pp. 1980–1992, Feb. 2016.

[9] H. Xie, W. Xu, H. Q. Ngo, and B. Li, "Non-coherent massive MIMO systems: A constellation design approach," *IEEE Trans. Wireless Commun.*, vol. 19, no. 6, pp. 3812–3825, Mar. 2020.

[10] D. Neumann, M. Joham, and W. Utschick, "Covariance matrix estimation in massive MIMO," *IEEE Signal Process. Lett.*, vol. 25, no. 6, pp. 863–867, Apr. 2018.

[11] K. Upadhya and S. A. Vorobyov, "Covariance matrix estimation for massive MIMO," *IEEE Signal Process. Lett.*, vol. 25, no. 4, pp. 546–550, Feb. 2018.

[12] A. Manolakos, M. Chowdhury, and A. J. Goldsmith, "Constellation design in noncoherent massive SIMO systems," in *Proc. IEEE Glob. Commun. Conf. (GLOBECOM)*, Mar. 2014, pp. 3690–3695.

[13] A. Manolakos, M. Chowdhury, and A. Goldsmith, "Energy-based modulation for noncoherent massive SIMO systems," *IEEE Trans. Wireless Commun.*, vol. 15, no. 11, pp. 7831–7846, Sep. 2016.

[14] M. J. Borran, A. Sabharwal, and B. Aazhang, "On design criteria and construction of noncoherent space-time constellations," *IEEE Trans. Inf. Theory*, vol. 49, no. 10, pp. 2332–2351, Oct. 2003.

[15] B. M. Hochwald and T. L. Marzetta, "Unitary space-time modulation for multiple-antenna communications in Rayleigh flat fading," *IEEE Trans. Inf. Theory*, vol. 46, no. 2, pp. 543–564, Mar. 2000.

[16] L. Zheng and D. N. C. Tse, "Communication on the Grassmann manifold: A geometric approach to the noncoherent multiple-antenna channel," *IEEE Trans. Inf. Theory*, vol. 48, no. 2, pp. 359–383, Feb. 2002.

[17] D. Cuevas, J. Álvarez-Vizoso, C. Beltrán, I. Santamaria, V. Tuček, and G. Peters, "Union bound minimization approach for designing Grassmannian constellations," *IEEE Trans. Commun.*, vol. 71, no. 4, pp. 1940–1952, Feb. 2023.

[18] Y. Wu, K. Ruotsalainen, and M. Juntti, "Unitary space–time constellation design based on the Chernoff bound of the pairwise error probability," *IEEE Trans. Inf. Theory*, vol. 54, no. 8, pp. 3842–3850, Jul. 2008.

[19] B. M. Hochwald, T. L. Marzetta, T. J. Richardson, W. Sweldens, and R. Urbanke, "Systematic design of unitary space-time constellations," *IEEE Trans. Inf. Theory*, vol. 46, no. 6, pp. 1962–1973, Sep. 2000.

[20] R. H. Gohary and T. N. Davidson, "Noncoherent MIMO communication: Grassmannian constellations and efficient detection," *IEEE Trans. Inf. Theory*, vol. 55, no. 3, pp. 1176–1205, Feb. 2009.

[21] S. Li, Z. Dong, H. Chen, and X. Guo, "Constellation Design for Noncoherent Massive SIMO Systems in URLLC Applications," *IEEE Trans. Commun.*, vol. 69, no. 7, pp. 4387–4401, Apr. 2021.

[22] S. Li, J.-K. Zhang, and X. Mu, "Design of optimal noncoherent constellations for SIMO systems," *IEEE Trans. Commun.*, vol. 67, no. 8, pp. 5706–5720, Apr. 2019.

[23] B. Tahir, S. Schwarz, and M. Rupp, "Constructing Grassmannian frames by an iterative collision-based packing," *IEEE Signal Process. Lett.*, vol. 26, no. 7, pp. 1056–1060, May. 2019.

[24] J.-K. Zhang, F. Huang, and S. Ma, "Full diversity blind space-time block codes," *IEEE Trans. Inf. Theory*, vol. 57, no. 9, pp. 6109–6133, Aug. 2011.

[25] K. M. Attiah, K. Seddik, R. H. Gohary, and H. Yanikomeroglu, "A systematic design approach for non-coherent grassmannian constellations," in *Proc. IEEE Int. Symp. Inf. Theory (ISIT)*, Jul. 2016, pp. 2948–2952.

[26] I. Kammoun, A. M. Cipriano, and J.-C. Belfiore, "Non-coherent codes over the Grassmannian," *IEEE Trans. Wireless Commun.*, vol. 6, no. 10, pp. 3657–3667, Oct. 2007.

[27] J. Kim, K. Cheun, and S. Choi, "Unitary space-time constellations based on quasi-orthogonal sequences," *IEEE Trans. Commun.*, vol. 58, no. 1, pp. 35–39, Jan. 2010.

[28] K.-H. Ngo, A. Decurninge, M. Guillaud, and S. Yang, "Cube-split: A structured Grassmannian constellation for non-coherent SIMO communications," *IEEE Trans. Wireless Commun.*, vol. 19, no. 3, pp. 1948–1964, Dec. 2019.

[29] P. Ho and D. Fung, "Error performance of multiple-symbol differential detection of PSK signals transmitted over correlated Rayleigh fading channels," *IEEE Trans. Commun.*, vol. 40, no. 10, pp. 1566–1569, Oct. 1992.

[30] D. Divsalar and M. K. Simon, "Maximum-likelihood differential detection of uncoded and trellis coded amplitude phase modulation over AWGN and fading channels-metrics and performance," *IEEE Trans. Commun.*, vol. 42, no. 1, pp. 76–89, Jan. 1994.

[31] D. S. Papailiopoulos, G. Abou Elkheir, and G. N. Karystinos, "Maximum-likelihood noncoherent PAM detection," *IEEE Trans. Commun.*, vol. 61, no. 3, pp. 1152–1159, Jan. 2013.

[32] F. Adachi and M. Sawahashi, "Decision feedback differential phase detection of M-ary DPSK signals," *IEEE Trans. Veh. Technol.*, vol. 44, no. 2, pp. 203–210, May. 1995.

[33] ——, "Decision feedback differential detection of differentially encoded 16APSK signals," *IEEE Trans. Commun.*, vol. 44, no. 4, pp. 416–418, Apr. 1996.

[34] R. Schober, W. H. Gerstacker, and J. B. Huber, "Decision-feedback differential detection of MDPSK for flat Rayleigh fading channels," *IEEE Trans. Commun.*, vol. 47, no. 7, pp. 1025–1035, Jul. 1999.

[35] A. Schenk and R. F. Fischer, "Noncoherent detection in massive MIMO systems," in *Proc. VDE Int. ITG Workshop Smart Antennas (WSA)*, Mar. 2013, pp. 1–8.

3. Multi-level Design for Multiple-Symbol Non-Coherent Unitary Constellations for Massive SIMO Systems

Published as:

S. T. Duong, H. H. Nguyen, and E. Bedeer, "Multi-level design for multiple-symbol non-coherent unitary constellations for massive SIMO systems," *IEEE Wireless Commun. Lett.*, vol. 12, no. 8, pp. 1349-1353, Aug. 2023.

The design approach for multi-level unitary constellations with the KL divergence as the design criterion is provided in Section 2.4.3. The multi-level design provided in [1] is impractical for large constellations as the number of choices for dividing multi-level unitary constellations grows exponentially with the size of constellations. A low-complexity multi-level design was proposed in [2], but only applicable to $K = 2$, hence restricting its application. Motivated by these challenges, we proposed a structure of the multi-level unitary constellations based on the Cartesian product of magnitude and unitary vectors. Furthermore, we propose and solve an optimization problem to improve the error performance of our proposed constellations. This method has low complexity and can be applied to more general cases of K. Simulation results show the merits of the proposed multi-level design in terms of error performance, as it can outperform unitary constellations in low SNR regimes.

Multi-level Design for Multiple-Symbol Non-Coherent Unitary Constellations for Massive SIMO Systems

Son T. Duong, Ha H. Nguyen, and Ebrahim Bedeer

Abstract

This paper investigates non-coherent detection of single-input multiple-output (SIMO) systems over block Rayleigh fading channels. Using the Kullback-Leibler divergence as the design criterion, we formulate a multiple-symbol constellation optimization problem, which turns out to have high computational complexity to construct and detect. We exploit the structure of the formulated problem and decouple it into a unitary constellation design and a multi-level design. The proposed multi-level design has low complexity in both construction and detection. Simulation results show that our multi-level design has better performance than traditional pilot-based schemes and other existing low-complexity multi-level designs.

3.1 Introduction

Ultra-reliable low-latency communication (URLLC) has been introduced as one of the pillars of the fifth generation (5G) and beyond cellular networks. Short packet communications (SPCs) with packets length of tens of bytes have been widely adopted to achieve low latency, while massive multiple-antenna systems with coherent detection have been well-studied as a diversity resource to achieve the stringent BLER requirement. However, to enable coherent detection, the transmitter must acquire accurate channel state information by sending a long sequence of training symbols, which decreases the spectral efficiency (SE) of SPCs. Thus, it is important to investigate the non-coherent detection of SPCs.

The design of non-coherent constellations with encoding and decoding of one symbol at a time has been well-studied in massive single-input multiple-output (SIMO) systems [3, 4]. However, the scheme suffers from loss of the SE since only the amplitude of the signal carries information. That said, to improve the SE and error performance, we aim to design non-coherent constellations that carry information in both amplitude and phase and are encoded and decoded over several symbols duration.

For SPCs, traditional non-coherent communications based on differential encoding and decoding, e.g., [5], may suffer from SE loss due to the insertion of pilots every coherence time, especially in the case of transmitting a few symbols. That said, there is a need to have other design objectives for non-coherent communications for SPCs. The Kullback-Leibler (KL) divergence is recognized as an effective design criterion for non-coherent communications [1]. In particular, the authors in [1] proved that the pairwise error probability (PEP) performance achieved by the maximum likelihood (ML) detector of any two signals is bounded by the KL divergence. This means that by maximizing the KL divergence between any two signals, one also maximizes the symbol error rate (SER) performance of the constellation. By utilizing the KL divergence as a constellation design criterion, the authors in [1] divided the constellation into different energy levels, where each level contains constellation points with the same energy. The optimization of the energy levels is called multi-level design while designing the constellation points within the same energy level is called unitary constellation design.

While researchers had focused on designing unitary constellations, e.g., see [6–8] and the references therein, the multi-level design over several symbols has attracted little attention [1, 2, 9]. For instance, the authors in [1] found the optimal multi-level design using an exhaustive search, and the ML detection of the optimal multi-level design was also obtained through an exhaustive search which limits its application to only a small number of symbols. In [2, 9], the authors provided a low-complexity multi-level design over only two symbols. However, both the designs in [2,9] applies only to a specific unitary constellation and cannot be generalized to other structures or to other numbers of symbols.

To the best of our knowledge, a low-complexity multi-level design over any number of symbols for non-coherent detection of SPCs has not been considered in the literature. That said, we design a multi-level scheme based on the KL divergence to improve the SER performance of existing non-coherent unitary constellations designs. The proposed multi-level constellation has low complexity in both its construction and detection to meet the latency requirement of URLLC systems. Simulation results show that our multi-level design significantly improves the SER performance of existing unitary constellations and outperforms other low-complexity non-coherent schemes.

Notation: Matrices, column vectors, and scalar variables are denoted by uppercase bold letters (e.g., $\mathbf{A}$), lowercase bold letters (e.g., $\mathbf{a}$) and lowercase letters (e.g., a), respectively. We use $(\cdot)^*$, $(\cdot)^T$, and $(\cdot)^H$ to denote the conjugate, transpose, and conjugate transpose, respectively. We use $|\cdot|$, $\|\cdot\|$, $\det(\cdot)$, and $\mathrm{tr}(\cdot)$ to denote absolute value, Euclidean norm, determinant, and trace operations, respectively. We use $\mathbb{R}^{m\times n}$ and $\mathbb{C}^{m\times n}$ to indicate the set of real and complex matrices with dimension $m \times n$, respectively. $\mathbf{I}_K$ denotes the $K \times K$ identity matrix and $\mathrm{card}\{\Omega\}$ represents the cardinality of the set Ω. The circularly symmetric complex Gaussian distribution with mean μ and variance σ^2 is represented as $\mathcal{CN}(\mu, \sigma^2)$, and we use $\mathbb{E}(\cdot)$ to denote the expectation of a random variable.

The remainder of the paper is organized as follows. The system model is presented in Section 3.2. We overview the design method based on KL divergence and propose our multi-level structure in Section 3.3. The optimization formulation of our proposed multi-level structure is provided in Section 3.4. Simulation results and related discussion are given in Section 3.5. Section 3.6 concludes the paper.

3.2 System Model

Consider the uplink transmission of a SIMO system in which a single-antenna transmitter communicates with an M-antenna base station. Let $\mathbf{h} \sim \mathcal{CN}(0, \mathbf{I}_M)$ be the vector of independent Rayleigh fading channel coefficients between the transmitter and the receiver, and it is unknown to both of them. We assume a block fading channel where the channel coefficients stay constant over a block of consecutive K symbols and then change to an independent realization in the coming block. Please note that each block of K different transmit symbols $\{s_0, s_1, \ldots, s_{K-1}\}$ represents one constellation point $\mathbf{s} = [s_0, s_1, \ldots, s_{K-1}]^T \in \mathbb{C}^{K\times 1}$ in our proposed multiple-symbol constellation. The received signal $\mathbf{Y} \in \mathbb{C}^{M\times K}$ at the receiver can be formulated as:

$$\mathbf{Y} = \mathbf{h}\mathbf{s}^T + \mathbf{N}, \tag{3.1}$$

where $\mathbf{N} \in \mathbb{C}^{M\times K}$ is the noise matrix, whose elements are independent zero-mean circular Gaussian random variables with variance σ^2. The transmitted sequence is assumed to satisfy the power constraint $\mathbb{E}(\|\mathbf{s}\|^2) = 1$. Thus, the average SNR at each receiving antenna is given

as $\text{SNR} = 1/(K\sigma^2)$.

Given the transmit signal $\mathbf{s}$, the probability density function of the received signal $\mathbf{Y}$ can be written as follows [1], [2]:

$$f(\mathbf{Y}|\mathbf{s}) = \frac{\exp\left(-\frac{\text{tr}(\mathbf{Y}^H\mathbf{Y})}{\sigma^2} + \frac{\text{tr}\left(\mathbf{Y}^H\mathbf{Y}\ \mathbf{s}^*\mathbf{s}^T\right)}{\sigma^2(\sigma^2+\|\mathbf{s}\|^2)}\right)}{\pi^{KM}\left[(\sigma^2+\|\mathbf{s}\|^2)\sigma^{2K-2}\right]^M}. \tag{3.2}$$

Given a known constellation of $\mathbf{s}$, i.e., Ω_s, the ML detector to detect the transmit signal $\mathbf{s}$ is [2]:

$$\mathbf{s}_{\text{ML}} = \underset{\mathbf{s}\in\Omega_s}{\text{argmax}} \left(\frac{\text{tr}\left(\mathbf{Y}^H\mathbf{Y}\ \mathbf{s}^*\mathbf{s}^T\right)}{\sigma^2(\sigma^2+\|\mathbf{s}\|^2)} - M\ln(\sigma^2+\|\mathbf{s}\|^2)\right). \tag{3.3}$$

Please note that the KL distance depends on the channel fading model. For Rayleigh fading channels, the KL distance between two transmit signals $\mathbf{s}_i$ and $\mathbf{s}_k$ is defined as the average KL divergence of their two conditional probability density functions per antenna, which is given by [1, Eq. (38)]:

$$\begin{aligned} &D_{\text{KL}}\left(f(\mathbf{Y}|\mathbf{s}_i), f(\mathbf{Y}|\mathbf{s}_k)\right) = \frac{1}{M}\mathbb{E}_{f(\mathbf{Y}|\mathbf{s}_i)}\left(\ln\left(\frac{f(\mathbf{Y}|\mathbf{s}_i)}{f(\mathbf{Y}|\mathbf{s}_k)}\right)\right), \\ &= \left(\frac{\|\mathbf{s}_k\|^2\|\mathbf{s}_i\|^2 - \|\mathbf{s}_k^T\mathbf{s}_i^*\|^2}{\sigma^2(\sigma^2+\|\mathbf{s}_k\|^2)}\right) + \left(\frac{\sigma^2+\|\mathbf{s}_i\|^2}{\sigma^2+\|\mathbf{s}_k\|^2} - \ln\left(\frac{\sigma^2+\|\mathbf{s}_i\|^2}{\sigma^2+\|\mathbf{s}_k\|^2}\right) - 1\right). \end{aligned} \tag{3.4}$$

3.3 KL-Based Multi-Level Constellation Design

As pointed out in [1], the KL distance between any two transmit sequences $\mathbf{s}_i$ and $\mathbf{s}_k$ determines the pairwise symbol error probability between them. For this reason, the pair with the smallest KL distance will produce the highest error probability and contribute the most to the error rate of the whole constellation set. That said, we aim to design a constellation set Ω_s that maximizes the minimum KL distance, which can be formally expressed as follows:

$$\max_{\Omega_s} \min_{\mathbf{s}_i,\mathbf{s}_k\in\Omega_s,\mathbf{s}_i\neq\mathbf{s}_k} D_{\text{KL}}\left(\mathbf{s}_i,\mathbf{s}_k\right). \tag{3.5}$$

Since any sequence $\mathbf{s}$ is a $(K\times 1)$-dimensional complex vector, it can be characterized by its magnitude $\alpha\in\mathbb{R}$ and its direction vector $\mathbf{v}\in\mathbf{C}^{K\times 1}$, which are defined as follows:

$$\alpha = \|\mathbf{s}\|,\ \mathbf{v} = \frac{\mathbf{s}}{\|\mathbf{s}\|}. \tag{3.6}$$

Mathematically, $\mathbf{v}$ is a unitary vector obtained by normalizing the original vector $\mathbf{s}$ such that any two sequences $\mathbf{s}_i$ and $\mathbf{s}_k$ with the same direction will have the same unitary vector $\mathbf{v}$.

The maximum likelihood detector in (3.3) can be rewritten in terms of α and $\mathbf{v}$ as follows:

$$\{\alpha_{\mathrm{ML}}, \mathbf{v}_{\mathrm{ML}}\} = \underset{(\alpha,\mathbf{v})}{\operatorname{argmax}} \left(\frac{\alpha^2 \mathrm{tr}\left(\mathbf{Y}^H \mathbf{Y} \mathbf{v}^* \mathbf{v}^T\right)}{\sigma^2(\sigma^2+\alpha^2)} - M\ln(\sigma^2+\alpha^2) \right). \tag{3.7}$$

Similarly, the KL divergence in (3.4) is also rewritten in terms of α and $\mathbf{v}$ as follow:

$$\begin{aligned} &D_{\mathrm{KL}}\left(\alpha_k, \mathbf{v}_k, \alpha_i, \mathbf{v}_i\right) = D_1\left(\alpha_k, \mathbf{v}_k, \alpha_i, \mathbf{v}_i\right) + D_2\left(\alpha_k, \alpha_i\right) \\ &= \frac{\alpha_k^2 \alpha_i^2 \left(1 - |\mathbf{v}_k^T \mathbf{v}_i^*|^2\right)}{\sigma^2(\sigma^2+\alpha_k^2)} + \left(\frac{\sigma^2+\alpha_i^2}{\sigma^2+\alpha_k^2} - \ln\left(\frac{\sigma^2+\alpha_i^2}{\sigma^2+\alpha_k^2}\right) - 1 \right). \end{aligned} \tag{3.8}$$

As can be seen from (3.8), the KL distance between two constellation points $\mathbf{s}_i$ and $\mathbf{s}_k$ consists of two terms D_1 and D_2. The first term D_1 is due to the difference of direction vectors $\mathbf{v}_i$ and $\mathbf{v}_k$, and it is scaled by the energy levels α_i^2 and α_k^2 of the two points. On the other hand, the second term D_2 is mainly due to the difference between the energy levels of the two points.

Equation (3.8) indicates that designing the optimal Ω_s based on the KL distance requires a joint optimization over both α and $\mathbf{v}$, which is an extremely complex process. One can observe that the KL distance in (3.8) reduces to D_2, i.e., $D_1 = 0$, when the two constellation points have the same direction $\mathbf{v}$ but different energies; and reduces to D_1, i.e., $D_2 = 0$, when the two constellation points have the same energy levels. That said, to strike a balance between the SER performance and complexity, we split the constellation set Ω_s into different subsets $\mathcal{W}_n$, $n = 0, ..., N-1$, where each subset $\mathcal{W}_n$ comprises of w_n points with the same energy level α_n^2. By doing so, we transform the constellation design problem in (3.8) into optimizing the KL distance between constellation points inside a given subset $D_{\mathrm{intra}}(\mathcal{W}_n)$ (which only contains D_1) and optimizing the KL distance between different subsets $D_{\mathrm{inter}}(\mathcal{W}_{n_1}, \mathcal{W}_{n_2})$. Please note that both $D_{\mathrm{intra}}(\mathcal{W}_n)$ and $D_{\mathrm{inter}}(\mathcal{W}_{n_1}, \mathcal{W}_{n_2})$ will be formally defined in Section 3.4.

For l_s bits allocated to this constellation set Ω_s, the number of points of all subsets $\mathcal{W}_n$, $n = 0, ..., N-1$, must be summed up to 2^{l_s}, i.e., $\sum_{n=0}^{N-1} w_n = 2^{l_s}$. To find the optimal

combination of $\{w_0, w_1, ..., w_{N-1}\}$, an exhaustive search algorithm can be used [1]; however, its computational complexity prohibits its practical implementation, especially for a higher number of bits per constellation. To overcome such a high computational complexity, we propose a constellation structure with subset $\mathcal{W}_n$, $n = 0, 1, ..., N-1$, defined as

$$\mathcal{W}_n = \{\alpha_n \mathbf{v}_0, \alpha_n \mathbf{v}_1, ..., \alpha_n \mathbf{v}_{2^{l_v}-1}\}, \quad n = 0, 1, ..., N-1, \tag{3.9}$$

where $N = 2^{l_\alpha}$. We define the set $\Omega_\alpha = \{\alpha_0, \alpha_1, \ldots, \alpha_{2^{l_\alpha}-1}\}$ as the set of α that satisfies $\alpha_0 < \alpha_1 < \cdots < \alpha_{2^{l_\alpha}-1}$, and we define the set $\Omega_v = \{\mathbf{v}_0, \ldots, \mathbf{v}_{2^{l_v}-1}\}$ as the set containing all possible unitary vectors $\mathbf{v}$, with l_α and l_v be the number of bits allocated to Ω_α and Ω_v, respectively.

One can observe that the set Ω_s can be seen as the Cartesian product of Ω_α and Ω_v, and such an observation serves two purposes: the low-complexity construction and detection of our proposed multi-level constellation design as discussed below.

Low-complexity construction of the multi-level constellation The number of possible choices for w_n for our proposed structure in (3.9) is only $l_s + 1$. In contrast, the method in [1] requires an exhaustive search with exponential complexity. Furthermore, [1] requires the construction of unitary constellations Ω_v of any sizes that are not necessarily a power of two. Instead, our method only requires unitary constellations whose cardinality range is the power of two, which are readily available in the literature.

Low-complexity ML detection of the multi-level constellation Instead of searching over all possible $\mathbf{s} = \alpha\mathbf{v}$, as shown in (3.7), we only need to search over α and $\mathbf{v}$ separately, which is represented as follows:

$$\mathbf{v}_{\mathrm{ML}} = \underset{\mathbf{v}\in\Omega_v}{\operatorname{argmax}} \ \operatorname{tr}\left(\mathbf{Y}^H \mathbf{Y} \mathbf{v}^* \mathbf{v}^T\right). \tag{3.10}$$

$$\alpha_{\mathrm{ML}} = \underset{\alpha\in\Omega_\alpha}{\operatorname{argmax}} \left(\frac{\alpha^2 \operatorname{tr}\left(\mathbf{Y}^H \mathbf{Y} \mathbf{v}_{\mathrm{ML}}^* \mathbf{v}_{\mathrm{ML}}^T\right)}{\sigma^2(\sigma^2 + \alpha^2)} - M \ln(\sigma^2 + \alpha^2) \right). \tag{3.11}$$

By doing this, the ML decoding complexity of the whole constellation can be reduced from $\mathcal{O}(2^{l_\alpha + l_v})$ to $\mathcal{O}(2^{l_\alpha}) + \mathcal{O}(2^{l_v})$, where $\mathcal{O}(2^{l_\alpha})$ and $\mathcal{O}(2^{l_v})$ are the complexities of detecting α and $\mathbf{v}$, respectively. The decoding complexities can be further reduced if we embed special unitary constellations with low decoding complexity.

3.4 Optimization of Multi-level Constellations Under Fixed Bit Allocation

In this section, we optimize the multi-level constellation given fixed l_α and l_v. Given the proposed structure in (3.9), $D_{\text{intra}}(\mathcal{W}_n)$ and $D_{\text{inter}}(\mathcal{W}_{n_1}, \mathcal{W}_{n_2})$ can be written as follows:

$$D_{\text{intra}}(\mathcal{W}_n) = \frac{\alpha_n^4}{\sigma^2(\sigma^2+\alpha_n^2)} \min_{\mathbf{v}_k \neq \mathbf{v}_i} (1 - |\mathbf{v}_k^T \mathbf{v}_i^*|^2), \tag{3.12}$$

$$D_{\text{inter}}(\mathcal{W}_{n_1}, \mathcal{W}_{n_2}) = \frac{\sigma^2+\alpha_{n_1}^2}{\sigma^2+\alpha_{n_2}^2} - \ln\left(\frac{\sigma^2+\alpha_{n_1}^2}{\sigma^2+\alpha_{n_2}^2}\right) - 1. \tag{3.13}$$

For a given l_α and l_v, our problem in (3.5) can be reformulated as follows:

$$\{\Omega_\alpha, \Omega_v\} = \underset{\Omega_\alpha, \Omega_v}{\text{argmax}}$$

$$\left(\min \left[\min_{\mathcal{W}_n \subseteq \Omega_s} D_{\text{intra}}(\mathcal{W}_n), \min_{\substack{n_1 \neq n_2 \\ \mathcal{W}_{n_1}, \mathcal{W}_{n_2} \subseteq \Omega_s}} D_{\text{inter}}(\mathcal{W}_{n_1}, \mathcal{W}_{n_2}) \right] \right), \tag{3.14a}$$

$$\text{s.t. } \|\mathbf{v}_i\| = 1, \ \forall \mathbf{v}_i \in \Omega_v, \ \text{card}\{\Omega_v\} = 2^{l_v}, \tag{3.14b}$$

$$\frac{1}{2^{l_\alpha}} \sum_{\alpha_i \in \Omega_\alpha} \alpha_i^2 = 1, \ \text{card}\{\Omega_\alpha\} = 2^{l_\alpha}, \tag{3.14c}$$

Since $\alpha_n^4/(\sigma^2(\sigma^2+\alpha_n^2))$ is an increasing function of α_n for $\alpha_n \geq 0$, $D_{\text{intra}}(\mathcal{W}_n)$ is minimized when α_n is minimized, i.e., $\alpha_n = \alpha_0$. Since $1/x - \ln(1/x) - 1 < x - \ln(x) - 1$ for $x > 1$, $D_{\text{inter}}(\mathcal{W}_{n_1}, \mathcal{W}_{n_2}) < D_{\text{inter}}(\mathcal{W}_{n_2}, \mathcal{W}_{n_1})$ for $n_1 < n_2$. Thus, the minimum inter distance must be in the cases of $D_{\text{inter}}(\mathcal{W}_{n_1}, \mathcal{W}_{n_2})$ where $n_1 < n_2$. Also, since D_{inter} increases when the energy difference between two subsets increases, the minimum inter distance must be the cases of two consecutive subsets. As a result, we simplify our problem in (3.14) as follows:

$$\{\Omega_\alpha, \Omega_v\} = \underset{\Omega_\alpha, \Omega_v}{\text{argmax}} \left\{ \min \left(D_{\text{intra}}(\mathcal{W}_0), \ D_{\text{inter}}(\mathcal{W}_n, \mathcal{W}_{n+1}) \right) \right\}, \tag{3.15a}$$

$$\text{s.t. (3.14b) and (3.14c).}$$

We can see that the distance $D_{\text{intra}}(\mathcal{W}_0)$ contains the variable $\mathbf{v}$ in the form of $\min_{\mathbf{v}_k \neq \mathbf{v}_i}(1 - |\mathbf{v}_k^T \mathbf{v}_i^*|^2)$, and this optimization problem of $\mathbf{v}$ is not affected by α. Thus, we can decouple our problem into two separate optimization problems, i.e., unitary set optimization and

multi-level optimization. The unitary set optimization is given by:

$$\Omega_v = \underset{\Omega_v}{\operatorname{argmax}} \left\{ \min_{\mathbf{v}_k \neq \mathbf{v}_i} (1 - |\mathbf{v}_k^T \mathbf{v}_i^*|^2) \right\}, \tag{3.16a}$$

$$\text{s.t. (3.14b)},$$

which is a classic problem called sphere packing on Grassmannian manifolds and has been well-studied in the literature [6–8]. Thus, we can use any available unitary set Ω_v from the literature and focus on multi-level optimization. Given Ω_v, let $T_v = \min_{\mathbf{v}_k \neq \mathbf{v}_i}(1 - |\mathbf{v}_k^T \mathbf{v}_i^*|^2)$ be the minimum distance of the unitary constellation Ω_v. The multi-level optimization problem for a given T_v can be written as follows:

$$\Omega_\alpha = \underset{\Omega_\alpha}{\operatorname{argmax}} \left\{ \min_{\substack{\alpha_0 \\ r_0,\ldots,r_{N-2}}} \left(\frac{\alpha_0^4 T_v}{\sigma^2(\sigma^2+\alpha_0^2)}, \frac{1}{r_n} - \ln\left(\frac{1}{r_n}\right) - 1 \right) \right\}, \tag{3.17a}$$

$$\text{s.t. (3.14c)}.$$

with $r_n = (\sigma^2 + \alpha_{n+1}^2)/(\sigma^2 + \alpha_n^2)$. The optimal $\{\bar{\alpha}_0, \bar{r}_0, \ldots, \bar{r}_{N-2}\}$ must satisfy the conditions:

$$\bar{r}_0 = \bar{r}_1 = \cdots = \bar{r}_{N-2}, \tag{3.18a}$$

$$\frac{\bar{\alpha}_0^4\ T_v}{\sigma^2(\sigma^2+\bar{\alpha}_0^2)} = \frac{1}{\bar{r}_0} - \ln\left(\frac{1}{\bar{r}_0}\right) - 1. \tag{3.18b}$$

The proof is presented in the Appendix. Now we proceed to construct the optimal set $\Omega_{\bar{\alpha}} = \{\bar{\alpha}_0, \ldots, \bar{\alpha}_{N-1}\}$ given the two conditions in (3.18). From (3.18a), it is easy to prove that $\sigma^2 + \bar{\alpha}_i^2 = (\sigma^2 + \bar{\alpha}_0^2)(\bar{r}_0)^i$. Thus,

$$\begin{aligned} 2^{l_\alpha}(\sigma^2+1) &= \sum_{i=0}^{2^{l_\alpha}-1} (\sigma^2 + \bar{\alpha}_i^2) = (\sigma^2 + \bar{\alpha}_0^2) \sum_{i=0}^{2^{l_\alpha}-1} (\bar{r}_0)^i \\ &= (\sigma^2 + \bar{\alpha}_0^2) \left(\frac{(\bar{r}_0)^{2^{l_\alpha}} - 1}{\bar{r}_0 - 1} \right). \end{aligned} \tag{3.19}$$

The solution of (3.18b) and (3.19) can be obtained by conventional methods such as bisection or Newton method. Finally, after obtaining all the multi-level constellations for all possible bit allocation, i.e., $(l_\alpha, l_v) \in \{(0, l_s), (1, l_s - 1), \ldots, (l_s, 0)\}$, we choose the bit allocation l_α and l_v and its corresponding constellation with the highest KL distance.

3.5 Simulation Result

In this section, we evaluate the SER performance of our proposed multi-level constellation and compare it to other constellations from the literature. Since already-optimized unitary constellations are prerequisites for our method, we evaluate our proposed multi-level constellations with two types of unitary constellations: the general unitary constellations obtained by numerically solving the optimization problem in (3.16) and the cube-split constellations in [8]. While the general unitary constellations have the best SER performance among all unitary constellations, the cube-split constellations have low decoding complexity while still attaining acceptable performance compared to other non-coherent schemes.

3.5.1 Optimal Bit Allocation to Ω_α

First, we plot the number of bits allocated to Ω_α, i.e., l_α. Since our scheme is SNR-adaptive, given a collection of unitary constellations Ω_v, l_α and l_v will only depend on the SNR level. In general, if l_α is greater than zero, it means our multi-level design achieved higher KL distance than unitary constellations. In contrast, if l_α is equal to zero, our multi-level design simply converges to unitary constellations, and no performance gain is achieved from our multi-level design. Figure 3.1 shows that l_α tends to decrease when the SNR increases and converges to 1-level design (unitary constellations) in the high SNR regime. This is in line with the statement of optimality of unitary constellations in the high SNR regime in [1]. It can also be seen from Fig. 3.1 that for higher K, our multi-level design still has advantages over unitary constellations, though less frequently than the case of $K = 2$.

3.5.2 SER Performance Evaluation

In this sub-section, we evaluate the SER performance gain achieved by our multi-level design (combined with unitary constellations) when compared to only unitary constellations without multi-level design. We also use two non-coherent schemes as baselines for comparisons: non-coherent detection of pilot-based QAM, which includes a pilot symbol and a sequence of QAM symbols, and the multi-level constellations from [9] and [2]. Fig. 3.2 shows that multi-level design improves the SER performance in both general unitary con-

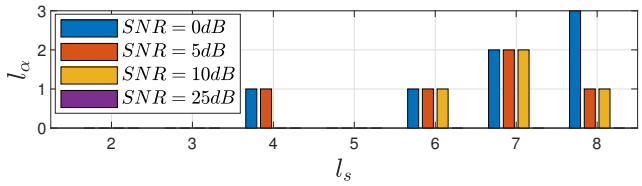

(a) $K = 2$, Multi-level design with cube-split constellations.

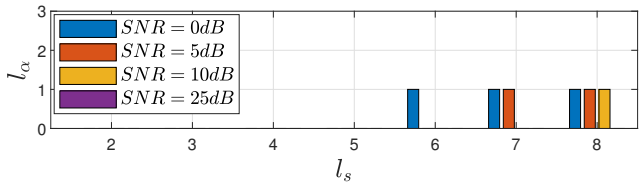

(b) $K = 2$, Multi-level design with general unitary constellations.

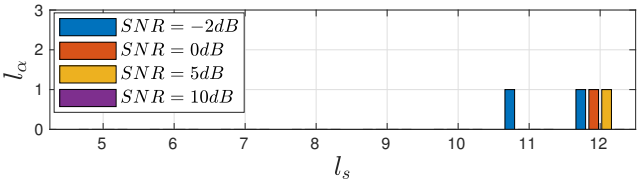

(c) $K = 3$, Multi-level design with general unitary constellations.

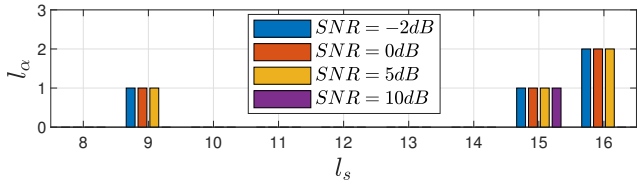

(d) $K = 4$, Multi-level design with cube-split constellations.

Figure 3.1: Number of bits allocated to Ω_α for optimal multi-level design.

stellations and cube-split constellations for both low and high SNR regimes. By embedding our multi-level design into cube-split constellations, the cube-split design achieves a significant improvement in SER performance and outperforms the conventional pilot-based QAM scheme. Additionally, the proposed multi-level design improves the performance of general unitary constellations and also outperforms both of the reference schemes. Please note that the multi-level design will converge to the 1-level design when SNR further increases, as discussed in Fig. 3.1.

In Fig. 3.3, we evaluate the SER performance versus different numbers of antennas M, i.e., $\{8, 16, 32, 64, 128, 128, 256\}$, given two fixed SNR levels: 3 dB and 8 dB. In general, the SER performance of all the schemes decreases exponentially, which is in line with the fact

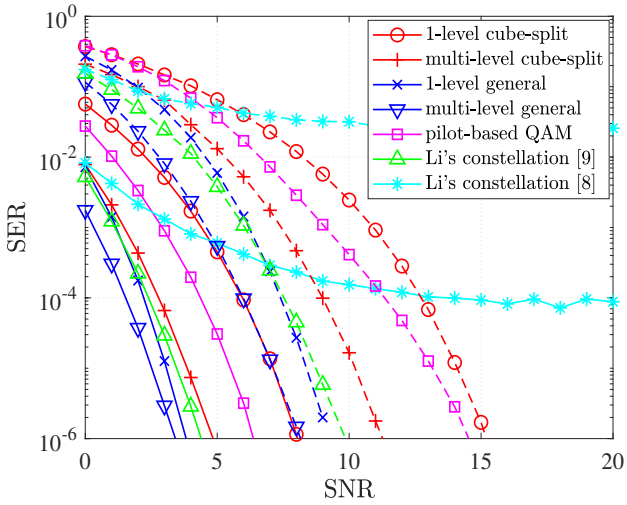

Figure 3.2: SER comparison between the proposed multi-level design, 1-level design, and other non-coherent schemes in case of $K = 2$ and $M = 256$. Solid line: $l_s = 6$. Dashed line: $l_s = 8$.

that for sufficiently large M, the PEP of the ML detector (3.3) decreases exponentially as M increases [1]. In the case of SNR = 3 dB, both the multi-level design of the general unitary constellations and the cube-split constellations outperform that of 1-level design when M is large enough. However, in the case of SNR = 8 dB, there is no performance gain in the multi-level design of the general constellations compared to the 1-level design because the multi-level design of the general constellations converges to the 1-level design in that SNR level. Also, for large values of M, the multi-level design of the general constellations outperforms that of [2] and pilot-based QAM. In that scenario, the multi-level design of the cube-split constellations has similar or slightly lower performance than [2] and better performance than pilot-based QAM.

Since our method can be applied to any number of time slots K, we also evaluate the SER performance among different values of K given the same SE of 4 bits/s/Hz. In the case of $K = 1$, energy encoding and detection in [4], which is also a specific case of our multi-level design for $K = 1$, will be used as a reference. Firstly, Fig. 3.4 shows that our multi-level design also improves the performance of the cube-split constellation for $K = 4$ and general unitary constellation for $K = 3$. In general, since the overall performance of non-coherent constellations improves when K increases, it is reasonable to apply our multi-level design to enhance the performance of unitary constellations in a higher number of time slots. In

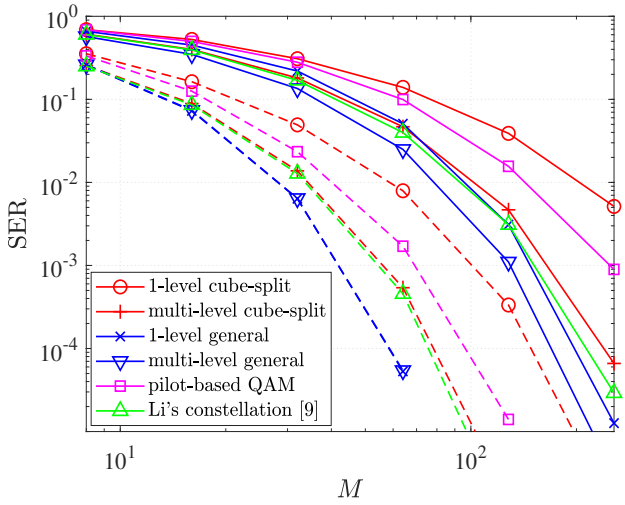

Figure 3.3: SER comparison between the proposed multi-level design, 1-level design, and other non-coherent schemes in case of $K = 2$, $l_s = 6$. Solid lines: SNR = 3 dB and dashed lines: SNR = 8 dB.

contrast, the multi-level designs in [2,9] (which is only designed for $K = 2$) and [1] (which has high complexity and therefore cannot be applied for large K) cannot achieve performance gain by increasing the number of time slots.

3.6 Conclusion

In this paper, we proposed a low-complexity design for multi-level constellations based on KL divergence. Our multi-level design is shown to improve the SER performance of non-coherent schemes based on unitary constellations as well as outperforms other non-coherent schemes while having low complexity in construction and detection.

3.7 Appendix

We prove the set $\Omega_{\bar{\alpha}}$ is the optimal solution of (3.18) by contradiction. In this case, the objective value corresponding to $\Omega_{\bar{\alpha}}$ is $\frac{\bar{\alpha}_0^4\ T(k_\alpha)}{\sigma^2(\sigma^2+\bar{\alpha}_0^2)}$ or $\frac{1}{\bar{r}_0} - \ln\left(\frac{1}{\bar{r}_0}\right) - 1$. Now, assume that $\Omega_{\bar{\alpha}}$ is not the optimal solution, then there exists at least one other set $\Omega_{\hat{\alpha}} = \{\hat{\alpha}_0, ..., \hat{\alpha}_{N-1}\}$ and

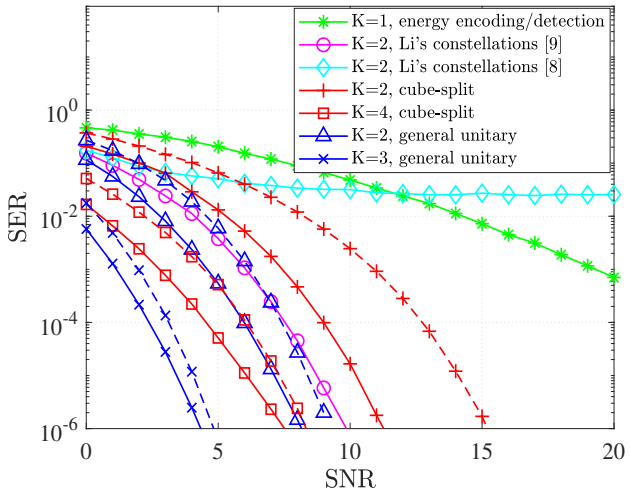

Figure 3.4: SER comparison between the proposed multi-level design, 1-level design, and other non-coherent schemes for $M = 256$. All schemes have the same spectral efficiency, i.e., 4 bits/s/Hz. Solid lines: multi-level design. Dash lines: 1-level design.

its corresponding $\{\hat{r}_0, \ldots, \hat{r}_{N-2}\}$ that has higher objective value. This is equivalent to:

$$\frac{\hat{\alpha}_0^4\, T_v}{\sigma^2(\sigma^2+\hat{\alpha}_0^2)} > \frac{\bar{\alpha}_0^4\, T_v}{\sigma^2(\sigma^2+\bar{\alpha}_0^2)}, \tag{3.20}$$

$$\frac{1}{\hat{r}_n} - \ln\left(\frac{1}{\hat{r}_n}\right) - 1 > \frac{1}{\bar{r}_n} - \ln\left(\frac{1}{\bar{r}_n}\right) - 1,\ \forall n \in \{0, \ldots, N-2\}. \tag{3.21}$$

Since $\frac{\alpha_0^4}{\sigma^2(\sigma^2+\alpha_0^2)}$ is an increasing function of $\alpha_0 > 0$ and $1/r - \ln(1/r) - 1$ is an increasing function of $r > 1$, (3.20) and (3.21) are equivalent to $\hat{\alpha}_0 > \bar{\alpha_0}$ and $\hat{r}_n > \bar{r}_n$, respectively. Thus,

$$\sigma^2 + \hat{\alpha}_n^2 = (\sigma^2 + \hat{\alpha}_0^2) \prod_{i=0}^{n-1} \hat{r}_i > (\sigma^2 + \bar{\alpha}_0^2) \prod_{i=0}^{n-1} \bar{r}_i = \sigma^2 + \bar{\alpha}_n^2. \tag{3.22}$$

$\Omega_{\hat{\alpha}}$ clearly does not satisfy the power constraints because:

$$\frac{1}{2^{k_\alpha}} \sum_{i=0}^{2^{k_\alpha}-1} \hat{\alpha}_i^2 > \frac{1}{2^{k_\alpha}} \sum_{i=0}^{2^{k_\alpha}-1} \bar{\alpha}_i^2 = 1, \tag{3.23}$$

which concludes the proof. ■

References

[1] M. J. Borran, A. Sabharwal, and B. Aazhang, "On design criteria and construction of noncoherent space-time constellations," *IEEE Trans. Inf. Theory*, vol. 49, no. 10, pp. 2332–2351, Oct. 2003.

[2] S. Li, Z. Dong, H. Chen, and X. Guo, "Constellation Design for Noncoherent Massive SIMO Systems in URLLC Applications," *IEEE Trans. Commun.*, vol. 69, no. 7, pp. 4387–4401, Apr. 2021.

[3] M. Chowdhury, A. Manolakos, and A. Goldsmith, "Scaling laws for noncoherent energy-based communications in the SIMO MAC," *IEEE Trans. Inf. Theory*, vol. 62, no. 4, pp. 1980–1992, Feb. 2016.

[4] W. Han, Z. Dong, H. Chen, and X. Gao, "Constellation design for energy-based noncoherent massive SIMO systems over correlated channels," *IEEE Wireless Commun. Lett.*, vol. 11, no. 10, pp. 2165–2169, Oct. 2022.

[5] V. M. Baeza and A. G. Armada, "Analysis of the performance of a non-coherent large scale SIMO system based on M-DPSK under rician fading," in *Proc. IEEE Eur. Signal Process. Conf. (EUSIPCO)*, Aug. 2017, pp. 618–622.

[6] R. H. Gohary and T. N. Davidson, "Noncoherent MIMO communication: Grassmannian constellations and efficient detection," *IEEE Trans. Inf. Theory*, vol. 55, no. 3, pp. 1176–1205, Feb. 2009.

[7] J.-K. Zhang, F. Huang, and S. Ma, "Full diversity blind space-time block codes," *IEEE Trans. Inf. Theory*, vol. 57, no. 9, pp. 6109–6133, Aug. 2011.

[8] K.-H. Ngo, A. Decurninge, M. Guillaud, and S. Yang, "Cube-split: A structured Grassmannian constellation for non-coherent SIMO communications," *IEEE Trans. Wireless Commun.*, vol. 19, no. 3, pp. 1948–1964, Dec. 2019.

[9] S. Li, J.-K. Zhang, and X. Mu, "Design of optimal noncoherent constellations for SIMO systems," *IEEE Trans. Commun.*, vol. 67, no. 8, pp. 5706–5720, Apr. 2019.

4. Design and Detection of Unitary Constellations in Non-Coherent SIMO Systems for Short Packet Communications

Chapter 4 is submitted as:

S. T. Duong, H. H. Nguyen, E. Bedeer, and R. Barton, "Design and Detection of Unitary Constellations in Non-Coherent SIMO Systems for Short Packet Communications," under review, *IEEE Trans. Wireless Commun.*, 2023.

One part of chapter 4 regarding the design of unitary constellations is accepted as:

S. T. Duong, H. H. Nguyen, E. Bedeer, and R. Barton, "Low-complexity design of unitary constellations in non-coherent SIMO systems for 5G NR URLLC applications," to appear in *Proc. IEEE Global Communications Conference 2023 (GLOBECOM)*, 2023.

In Chapter 2, several designs of unitary constellations have been provided with different complexity and performance. In general, the unstructured designs of unitary constellations have excellent error performance but suffer from high complexity. In contrast, structured unitary constellations can have low complexity in design and detection but sacrifice the excellent error performance of unstructured unitary constellations.

In this chapter, we propose a novel structure of unitary constellations. We exploit the proposed structure to formulate and solve an optimization problem to improve the chordal distance as the design criterion. Furthermore, our design method to optimize the constellations has lower complexity than the unstructured unitary constellations. In addition, we proposed novel detectors that can approach the optimal error performance of the ML de-

tectors with polynomial complexity. Simulation results show the merits of our proposed constellations in terms of error performance when compared to the relevant schemes in the literature.

Design and Detection of Unitary Constellations in Non-Coherent SIMO Systems for Short Packet Communications

Son T. Duong, Ha H. Nguyen, Ebrahim Bedeer, and Robert Barton

Abstract

This paper proposes a novel design of multi-symbol unitary constellation for non-coherent single-input multiple-output (SIMO) communications over block Rayleigh fading channels. To facilitate the design and the detection of large unitary constellations at reduced complexity, the proposed constellations are constructed as the Cartesian product of independent amplitude and phase-shift-keying (PSK) vectors, and hence, can be iteratively detected. The amplitude vector is detected by exhaustive search, whose complexity is sufficiently low in short packet transmission scenarios. To detect the PSK vector, we use the posterior probability as a reliability criterion in the sorted decision-feedback differential detection (sort-DFDD), which results in near-optimal error performance for PSK symbols with equal modulation orders. This detector is called posteriori-based-reliability-sort-DFDD (PR-sort-DFDD) and has polynomial complexity. We also propose an improved detector called improved-PR-sort-DFDD to detect a more generalized PSK structure, i.e., PSK symbols with unequal modulation orders. This detector also approaches the optimal error performance with polynomial complexity. Simulation results show the merits of our proposed multi-symbol unitary constellation when compared to competing low-complexity unitary constellations.

4.1 Introduction

Ultra-reliable low-latency communication (URLLC) is one of the services of the 5G New Radio (5G NR) to support the newly emerging applications such as telesurgery, intelligent transportation, and industrial automation [1]. These emerging applications require a block error rate (BLER) from 10^{-5} to 10^{-9} and a latency from 1 ms to 10 ms for the transmission of short messages, i.e., several tens of bytes. Such requirements pose a challenge in designing efficient communication systems with limited power and bandwidth resources since latency and reliability are usually conflicting objectives.

To meet the stringent latency requirements of URLLC, a variety of technologies, which cover different layers of communication networks, have been proposed and standardized for 5G [2]. At the physical layer, low latency is achieved with the transmission of short packets. However, since short packet transmission does not support powerful channel coding, exploiting different diversity resources to provide high reliability is needed for URLLC. Among different diversity schemes, the use of multiple antennas in the form of single-input multiple-output (SIMO) or multiple-input multiple-output (MIMO) systems with coherent detection has been extensively investigated in recent years [3–5]. Many Internet of Things (IoT) transmission scenarios can be seen as SIMO systems as end devices are equipped with a single antenna while a typical base station or a gateway can be equipped with multiple antennas. The performance of coherent detection of multiple-antenna systems is strongly affected by the accuracy of the estimated channel state information (CSI) [6]. In order to obtain accurate instantaneous CSI at the receiver, the transmitter has to send a sequence of training symbols or pilots, whose length can be comparable to the number of symbols in the short packet. Hence, using a long sequence of training symbols to estimate the CSI in short packet communications (SPCs) decreases the spectral efficiency (SE).

Non-coherent communication schemes, which do not require pilot symbols for channel estimation, can reduce the SE loss caused by using the pilot symbols in SPCs [7]. Among different non-coherent communications, energy-based encoding and decoding have been well-investigated in massive SIMO systems for fast fading channels where the coherence time is less than the duration of one information symbol [8–11]. In particular, the channel hardening property resulting from using a large number of receiving antennas is exploited to decode the signal. However, non-coherent energy-based schemes suffer from loss of the SE since only the amplitude of the signal carries information. For wireless channels having coherence time covering multiple symbol durations, non-coherent multi-symbol encoding and decoding have been investigated to transmit additional information in the phase, thus improving the SE. In differential phase-shift keying (DPSK), the information is encoded into the phase difference between two consecutive symbols, and differential detection is carried out to estimate the phase difference at the receiver [12]. Another widely investigated multi-symbol encoding and

decoding scheme in the literature is unitary constellations. In unitary constellations, all the transmitted multiple-symbol signals have the same energy level, and the received signal can be decoded by using a non-coherent multi-symbol maximum likelihood (ML) detector [13]. Multi-level unitary constellations can be considered to be generalized schemes of unitary constellations, where information is encoded into constellations of energy levels and unitary constellations. The design of energy levels has been only investigated in [14, 15], however, both papers do not study the design of unitary constellations.

In this paper, we focus on the design and detection of unitary constellations. The investigation of unitary constellations is justified as it is proven to be the optimal non-coherent transmission scheme in high SNR regimes [13, 16]. Different designs of unitary constellations have been proposed in the literature, and they can be classified into two main groups: structured unitary constellations and unstructured unitary constellations. Unstructured unitary constellations are typically obtained by numerically solving optimization problems of minimizing pairwise error probability (PEP). For MIMO communications, different design criteria have been investigated such as high-SNR asymptotic expression of PEP [17], the Chernoff bound of PEP [18], singular values of two signal's correlation [13, 19], and chordal distance [19]. Please note in the SIMO system, the design criteria based on singular values in [13, 19] are simplified to the chordal distance. While the unstructured unitary constellations can achieve optimal PEP performance, they have exponential complexity in design and therefore are only feasible for small constellation sizes. On the other hand, structured unitary constellations have a pre-determined structure mainly to reduce the complexity of the design process, thus allowing the design of larger unitary constellations [19–25]. As expected, structured unitary constellations have inferior PEP performance when compared to unstructured unitary constellations. Additionally, some structures of unitary constellations are restricted to some specific cases of blocklength and constellation size. For example, the structure in [25] is restricted to a blocklength of only two symbols, while the structures in [23] and [24] are restricted to a blocklength of power of two.

The optimal ML detector of unitary constellations is complex for both unstructured and structured unitary constellations with large constellation sizes [24]. Therefore, various

approaches have been proposed to reduce the detection complexity of the unitary constellations [22, 24–26]. Quasi-ML detection was proposed in [26] to reduce the complexity of solving the ML detection. However, the quasi-ML detection requires the storage of all possible constellation points, which makes it still impractical for large constellations. Another approach is to design the structure of unitary constellations in a way that allows lower complexity in detection (in addition to low complexity in design). Please note that this approach is not applicable to unstructured unitary constellations and many structured unitary constellations, such as, the Fourier-based method [19], geometric motion [20], and the co-prime PSK constellations [21]. In [25], a unitary constellation based on phase-shift keying (PSK) was proposed that reduces the complexity of the ML detector into the complexity of detecting PSK symbols. In [22] and [24], exponential mapping and cube-split mapping were proposed to map QAM symbols into a non-coherent unitary sequence, respectively, thus reducing the complexity of encoding and decoding the unitary constellation to the complexity of encoding and decoding QAM symbols.

A special case of structured unitary constellations is a sequence of PSK symbols. The non-coherent detection of this structure can be classified into two major groups: (i) multi-symbol differential detection (MSDD) [27–29] and (ii) decision-feedback differential detection (DFDD) [30–32]. The MSDD algorithm is equivalent to the ML detector and therefore has optimal error performance at the cost of exponential complexity. In the DFDD algorithm, the decisions of detected PSK symbols are used as feedback to detect the next PSK symbol in sequential order. The DFDD algorithm has low complexity but suffers from performance loss due to the error propagation because if a PSK symbol is detected incorrectly, this incorrect decision is still used as feedback to detect the next PSK symbol. The sort-DFDD algorithms in [33,34] resolve the error propagation issue by detecting the most reliable PSK symbols first and then using them as feedback. Because reliable symbols are less likely to cause errors, the sort-DFDD algorithm reduces the effect of error propagation. The reliability criterion was defined as the quantization error in [33] and the log-likelihood ratio (LLR) in [34]. Please note that the sort-DFDD algorithm in [33] was only designed for PSK sequence with equal modulation orders and equal amplitude; while the sort-DFDD algorithm in [34] was further

restricted to 4-PSK constellations.

In this paper[1], we propose a novel multi-symbol unitary constellation with low complexity in both the design and detection in the non-coherent SIMO system for SPCs. The main contributions of this paper are summarized as follows:

1. We propose a novel unitary constellation based on two design rules. In design rule 1, we confine the unitary constellations into the pairwise product of amplitude vector and phase vector, and the amplitude vector and the phase vector are independent of each other, i.e., they belong to independent constellation sets. In design rule 2, we restrict the symbols of the phase vector to belong to a set of PSK constellations, which can have either equal modulation orders or unequal modulation orders.

2. We formulate an optimization problem to maximize the minimum chordal distance (MCD) between any two vectors of the proposed unitary constellations. We exploit the proposed structure, imposed by the two design rules, to solve the unitary constellation design problem at reduced computation complexity when compared to general unstructured unitary constellations in [13].

3. We exploit the first design rule and propose a novel detector, named, iterative unitary amplitude-phase detector (IUAP), to decouple the joint detection of the amplitude and phase vectors of the ML detector into independent amplitude vector detection and phase vector detection.

4. For the phase vector detection, we exploit the second design rule and propose two modified versions of the sort-DFDD algorithm. Inspired by [34], we consider the posterior probability as the reliability criterion and propose the PR-sort-DFDD algorithm when the phase vector has equal modulation orders. For the case that the phase vector has unequal modulation orders, we use the information from undetected PSK symbols with low modulation order to assist with the detection of PSK symbols with high modulation orders. This is what we call the proposed improved-PR-sort-DFDD algorithm.

[1]In [35], we presented only the design of the proposed unitary constellation. In the current paper, we additionally present low-complexity detectors of the proposed unitary constellation.

5. Simulation results show that our proposed unitary constellations have a larger MCD than other low-complexity unitary constellations from the literature. Our proposed detectors achieve near error performance of the optimal ML detector while having lower complexity. Additionally, our proposed unitary constellation with the proposed detectors achieves a better error performance when compared to the low-complexity unitary constellations and pilot-based QAM and PSK schemes.

Notation: Matrices, column vectors, and scalar variables are denoted by uppercase bold letters (e.g., $\mathbf{A}$), lowercase bold letters (e.g., $\mathbf{a}$), and lowercase letters (e.g., a), respectively. The notations $(\cdot)^*$, $(\cdot)^T$, and $(\cdot)^H$ represent the conjugate, transpose, and conjugate transpose, respectively. We use $|\cdot|$, $\|\cdot\|$, $\det(\cdot)$, $\mathrm{tr}(\cdot)$, and $\circ$ to denote absolute value, Euclidean norm, determinant, trace, and pairwise product, respectively. The angle of a complex scalar variable a is denoted as $\angle a$. We use $\mathbb{R}_+^{m\times n}$ and $\mathbb{C}^{m\times n}$ to indicate the set of non-negative real matrices and complex matrices with dimension $m \times n$, respectively. The matrix $\mathbf{I}_K$ denotes the $K \times K$ identity matrix, while $\mathbf{1}_K$ and $\mathbf{0}_K$ denote all ones K-dimensional vector and all zeros K-dimensional vector, respectively. The cardinality of the constellation set Ω is represented as $\mathrm{card}\{\Omega\}$, while the exclusion of an element b from the set Ω and the exclusion of a subset $\tilde{\Omega}$ from the set Ω is denoted as $\Omega\backslash b$ and $\Omega\backslash\tilde{\Omega}$, respectively. The Gamma and signum functions are denoted as $\Gamma(.)$ and $\mathrm{sgn}(.)$, respectively. The probability density function (PDF) of a random continuous variable is denoted as $f(.)$, while the probability of an event is denoted as $P(.)$. The circularly symmetric complex Gaussian distribution with mean μ and variance σ^2 is represented as $\mathcal{CN}(\mu, \sigma^2)$, and we use $\mathbb{E}(\cdot)$ to denote the expectation.

The remainder of the paper is organized as follows. The system model and overview of unitary constellations are presented in Section 4.2. We propose our structure of the proposed unitary constellations and its design method in Section 4.3. The detection of the proposed unitary constellation is presented in Section 4.4. Simulation results and related discussion are given in Section 4.5. Finally, Section 4.6 concludes the paper.

4.2 System Model

We consider the uplink transmission of a SIMO system in which a single antenna transmitter communicates with an M-antenna base station. Let us denote $\mathbf{h} \in \mathbb{C}^{M\times 1}$ as the vector representing the channel coefficients between the transmitter and the receiver. We assume that the channel is unknown to both of the transmitter and receiver and distributed as $\mathbf{h} \sim \mathcal{CN}(\mathbf{0}_M, \mathbf{I}_M)$. We additionally assume block fading where the channel coefficients remain constant over a block of consecutive K symbols, then change to an independent realization in the coming block of consecutive K symbols. Let $\mathbf{v} \in \mathbb{C}^{K\times 1}$ be a sequence of K transmit symbols drawn from a unitary constellation set Ω_v that satisfies the constraint $\|\mathbf{v}\|^2 = 1$. The received signal $\mathbf{Y} \in \mathbb{C}^{M\times K}$ can be written as:

$$\mathbf{Y} = \mathbf{h}\mathbf{v}^T + \mathbf{N}, \tag{4.1}$$

where $\mathbf{N} \in \mathbb{C}^{M\times K}$ is the matrix of the additive noise. The elements of $\mathbf{N}$ are independent zero-mean circular Gaussian random variables with variance σ^2. In the following two subsections, we provide the unitary constellation design and detection criteria, respectively.

4.2.1 Unitary Constellation Design Criterion: Minimum Chordal Distance (MCD)

Hochwald and Marzetta in [13] proved that the Chernoff bound of the PEP between two unitary signals $\mathbf{v}_a$ and $\mathbf{v}_b$ when using the ML detector is given by:

$$\Pr(\mathbf{v}_a \to \mathbf{v}_b) \leq \frac{1}{2}\left[1 + \frac{D_v^2(\mathbf{v}_a, \mathbf{v}_b)}{4\sigma^2(1+\sigma^2)}\right]^{-M}, \tag{4.2}$$

where $D_v(\mathbf{v}_a, \mathbf{v}_b)$ is the chordal distance between $\mathbf{v}_a$ and $\mathbf{v}_b$:

$$D_v(\mathbf{v}_a, \mathbf{v}_b) = \sqrt{1 - |\mathbf{v}_a^H \mathbf{v}_b|^2}. \tag{4.3}$$

One can see that the PEP between $\mathbf{v}_a$ and $\mathbf{v}_b$ increases as $D_v(\mathbf{v}_a, \mathbf{v}_b)$ decreases. Hence, the unitary constellation Ω_v can be designed by maximizing the minimum chordal distance

(MCD) between all vectors $\mathbf{v}$ in the unitary constellation Ω_v, which is given by:

$$\hat{\Omega}_v = \underset{\Omega_v}{\operatorname{argmax}} \left\{ \min_{\substack{\mathbf{v}_a \neq \mathbf{v}_b \\ \mathbf{v}_a, \mathbf{v}_b \in \Omega_v}} D_v(\mathbf{v}_a, \mathbf{v}_b) \right\}, \tag{4.4a}$$

$$\text{s.t. } \|\mathbf{v}\| = 1, \ \forall \mathbf{v} \in \Omega_v, \ \text{card}\{\Omega_v\} = 2^{l_v}, \tag{4.4b}$$

where l_v is the number of bits allocated to Ω_v. The problem in (4.4) requires the optimization of 2^{l_v} constellation points; hence, its complexity grows exponentially with l_v.

By directly solving (4.4) using numerical techniques, we obtain the general unitary constellation [13]. The general unitary constellation is unstructured because there are no constraints in (4.4) that confine the constellations into a specific unitary structure. In other words, adding any constraints to reduce the design or detection complexity results in what is called structured unitary constellations. While the general unitary constellation outperforms structured unitary constellations in terms of the MCD and error performance, its exponential complexity in design and detection makes it impractical for many applications. Thus, designing structured unitary constellations that can achieve good MCD and error probability performance with low complexity in design and/or detection, when compared to the general unitary constellations, is crucial. Such low complexity design of the proposed structured unitary constellation is what will be discussed in Section 4.3.

4.2.2 Unitary Constellation Detection Criterion: Maximum Likelihood (ML) Detection

For the general case of $\mathbf{v}$, the probability density function (PDF) of the received signal $\mathbf{Y}$ given the sequence of the K transmit symbols $\mathbf{v}$ can be written as follows [13]:

$$f(\mathbf{Y}|\mathbf{v}) = \frac{\exp\left(-\frac{\text{tr}(\mathbf{Y}^H\mathbf{Y})}{\sigma^2} + \frac{\text{tr}\left(\mathbf{Y}^H\mathbf{Y}\ \mathbf{v}^*\mathbf{v}^T\right)}{\sigma^2(\sigma^2+\|\mathbf{v}\|^2)} \right)}{\pi^{KM}\left[(\sigma^2+\|\mathbf{v}\|^2)\sigma^{2K-2}\right]^M}, \tag{4.5}$$

and the optimal ML detector of $\mathbf{v}$ is given by [13]:

$$\mathbf{v}_{\text{ML}} = \underset{\mathbf{v}\in\Omega_v}{\operatorname{argmax}} \left(\frac{\text{tr}\left(\mathbf{Y}^H\mathbf{Y}\ \mathbf{v}^*\mathbf{v}^T\right)}{\sigma^2(\sigma^2+\|\mathbf{v}\|^2)} - M\ln(\sigma^2+\|\mathbf{v}\|^2) \right). \tag{4.6}$$

As mentioned earlier, we focus on the design and detection of the unitary constellation Ω_v, where $\|\mathbf{v}\| = 1, \forall \mathbf{v} \in \Omega_v$; hence, the optimal ML detector in (4.6) can be simplified as follows:

$$\mathbf{v}_{\text{ML}} = \underset{\mathbf{v}\in\Omega_v}{\text{argmax}} \ \text{tr}\left(\mathbf{Y}^H\mathbf{Y}\ \mathbf{v}^*\mathbf{v}^T\right) = \underset{\mathbf{v}\in\Omega_v}{\text{argmax}} \|\mathbf{Y}^H\mathbf{v}\|^2. \tag{4.7}$$

The low complexity detection of the proposed structured unitary constellation is what will be discussed in Section 4.4.

4.3 Design of the Proposed Unitary Constellation

In this section, we propose a novel design of unitary constellations.

4.3.1 Proposed Unitary Constellation Design

One can represent a vector $\mathbf{v}$ of K symbols as a pair-wise product of amplitude vector $\mathbf{u}$ and phase vector $\mathbf{p}$ as:

$$\mathbf{v} = \mathbf{u} \circ \mathbf{p}, \tag{4.8}$$

where $\mathbf{u} = [u_0, \ldots, u_{K-1}]^T \in \mathbb{R}_+^{K\times 1}$ and $\mathbf{p} = \left[e^{j\phi_0}, \ldots, e^{j\phi_{K-1}}\right]^T \in \mathbb{C}^{K\times 1}$. The two design rules of our proposed unitary constellations Ω_v are mainly to reduce the construction and detection complexity as will be shown in Sections 4.3 and 4.4, respectively, and they can be explained as follows:

- *Design rule 1:* We assume that the amplitude vector $\mathbf{u}$ and phase vector $\mathbf{p}$ are independent of each other, i.e., they belong to independent constellation sets. Hence, the proposed unitary constellation Ω_v with the first design rule can be formally written as:

$$\Omega_v = \{\mathbf{v} \mid \mathbf{v} = \mathbf{u} \circ \mathbf{p}, \mathbf{u} \in \Omega_u, \mathbf{p} \in \Omega_p\}, \tag{4.9}$$

  where $\Omega_u = \{\mathbf{u}_0, \ldots, \mathbf{u}_{2^{l_u}-1}\}$ is the set of amplitude constellations and $\Omega_p = \{\mathbf{p}_0, \ldots, \mathbf{p}_{2^{l_p}-1}\}$ is the set of phase constellations, with l_u and l_p being the number of bits allocated to Ω_u and Ω_p, respectively. Please note that $l_u + l_p = l_v$.

- *Design rule 2:* We confine $\mathbf{p}$ such that its symbols belong to a set of PSK constellations

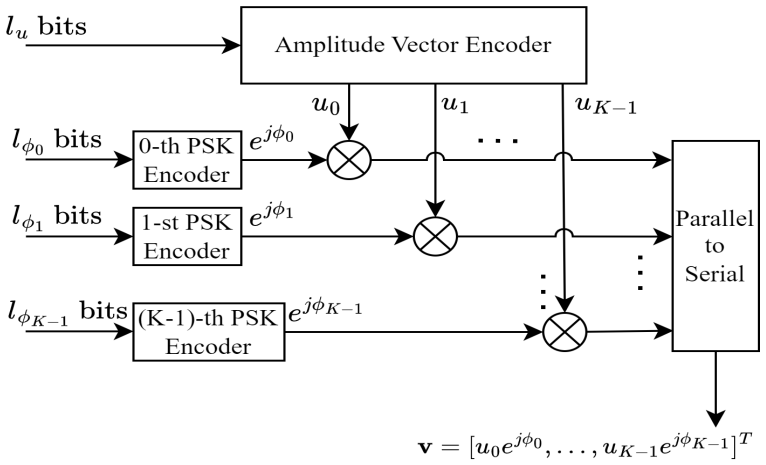

Figure 4.1: Encoder for the proposed unitary constellations.

defined as follows:

$$\mathbf{p} = [e^{j\phi_0}, \ldots, e^{j\phi_{K-1}}]^{\mathrm{T}}, \phi_k \in \Omega_{\phi_k}, \tag{4.10}$$

where Ω_{ϕ_k} is the set of $2^{l_{\phi_k}}$ PSK constellation for the k-th symbol, $k = 0, ..., K-1$, of the phase vector $\mathbf{p}$. Clearly, l_{ϕ_k} has to satisfy $l_p = \sum_{k=0}^{K-1} l_{\phi_k}$.

Fig. 4.1 depicts the encoder of our proposed unitary constellation. Fig. 4.2a and 4.2b provide examples of three-symbol constellation ($K = 3$) with ***equal modulation orders*** ($l_{\phi_1} = l_{\phi_2} = 2$) and ***unequal modulation orders*** ($l_{\phi_1} = 2$ and $l_{\phi_2} = 3$), respectively. In both examples, $l_u = 1$ corresponds to 1 bit encoded into the amplitude, while the remaining bits are used for encoding the PSK symbols in the phase vector $\mathbf{p}$. Please note that the first symbol in this three-symbol unitary constellation has a reference known phase, i.e., $l_{\phi_0} = 0$.

4.3.2 MCD Optimization of the Proposed Unitary Constellation

In this subsection, we formulate the MCD optimization problem of the proposed unitary constellation Ω_v under fixed bit allocation by considering the two design rules formally defined in (4.9) and (4.10). Let $\mathbf{l}_\phi = [l_{\phi_0}, \ldots, l_{\phi_{K-1}}]$ be a vector indicating the number of bits encoded into the K PSK symbols and $\Omega_p(\mathbf{l}_\phi)$ be the set of the PSK constellations of the phase vector $\mathbf{p}$ constructed from $\mathbf{l}_\phi$. Clearly, $\Omega_p(\mathbf{l}_\phi)$ is determined by knowing $\mathbf{l}_\phi$. The set of amplitude constellation Ω_u is unknown and has a size of 2^{l_u}. Hence, to construct the

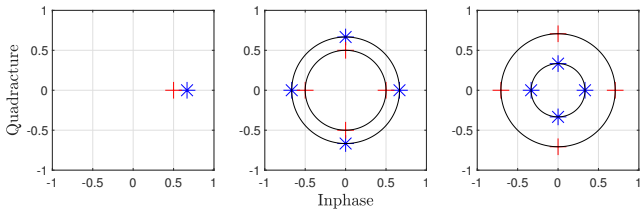

(a) Proposed design with ***equal modulation orders*** ($l_{\phi_1} = l_{\phi_2} = 2$).

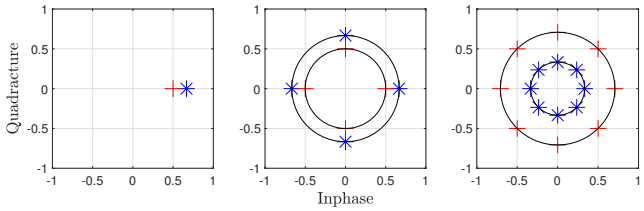

(b) Proposed design with ***unequal modulation orders*** ($l_{\phi_1} = 2$, $l_{\phi_2} = 3$).

Figure 4.2: Example of our proposed unitary constellations with $l_u = 1$. Blue: constellation points with $\mathbf{u}_0 = [\frac{2}{3}, \frac{2}{3}, \frac{1}{3}]$. Red: constellation points with $\mathbf{u}_1 = [\frac{1}{2}, \frac{1}{2}, \frac{\sqrt{2}}{2}]$.

proposed unitary constellation Ω_v, we need to optimize Ω_u for given $\mathbf{l}_\phi$ and l_u. Without loss of generality, we assume that $l_{\phi_0} \leq \cdots \leq l_{\phi_{K-1}}$, and since rotating all symbols of $\mathbf{v}$ by a constant phase does not affect the MCD in (4.3) or the ML detector in (4.7), we set the 0-th symbol phase as $\phi_0 = 0$, i.e., $l_{\phi_0} = 0$.

Under the design rules defined in (4.9) and (4.10), we reformulate the constellation design problem in (4.4) as follows:

$$\Omega_u(l_u, \mathbf{l}_\phi) = \underset{\Omega_u}{\operatorname{argmax}} \left\{ \min_{\substack{(\mathbf{u}_a, \mathbf{p}_a) \neq (\mathbf{u}_b, \mathbf{p}_b) \\ \mathbf{u}_a, \mathbf{u}_b \in \Omega_u \\ \mathbf{p}_a, \mathbf{p}_b \in \Omega_p(\mathbf{l}_\phi)}} D_v(\mathbf{u}_a \circ \mathbf{p}_a, \mathbf{u}_b \circ \mathbf{p}_b) \right\}, \tag{4.11a}$$

$$\text{s.t. } \Omega_u = \left\{ \mathbf{u} | \mathbf{u} \in \mathbb{R}_+^{K \times 1}, \|\mathbf{u}\| = 1 \right\}, \tag{4.11b}$$

$$\operatorname{card}\{\Omega_u\} = 2^{l_u}. \tag{4.11c}$$

The problem in (4.11) only involves the optimization of 2^{l_u} constellation points belonged to Ω_u. Thus, the complexity of solving (4.11) of our proposed design is significantly lower than the complexity of solving (4.4) of the general design, given that 2^{l_u} is chosen to be much smaller than 2^{l_v}.

In the following, we analyze the objective function in (4.11), which is the MCD of all the

constellation points. For any two different constellation points, i.e., $(\mathbf{u}_a, \mathbf{p}_a) \neq (\mathbf{u}_b, \mathbf{p}_b)$, the MCD only belongs to one of two possibilities. The first possibility is when the two points have different amplitude vectors, i.e., $\mathbf{u}_a \neq \mathbf{u}_b$, and in this case, we define $D_u(\mathbf{u}_a, \mathbf{u}_b)$ as the MCD between the two points with the amplitude vectors $\mathbf{u}_a$, $\mathbf{u}_b$ as follows:

$$\begin{aligned} D_u(\mathbf{u}_a, \mathbf{u}_b) &= \min_{\mathbf{p}_a, \mathbf{p}_b \in \Omega_p(\mathbf{l}_\phi)} D_v(\mathbf{u}_a \circ \mathbf{p}_a, \mathbf{u}_b \circ \mathbf{p}_b) \\ &= \sqrt{1 - \left| \sum_{i=0}^{K-1} u_{i,a} u_{i,b} \right|^2} = D_v(\mathbf{u}_a, \mathbf{u}_b). \end{aligned} \tag{4.12}$$

where $u_{i,a}$ and $u_{i,b}$ are the i-th elements of $\mathbf{u}_a$ and $\mathbf{u}_b$, respectively. As can be seen in (4.12), $D_u(\mathbf{u}_a, \mathbf{u}_b)$ does not depend on the phase vector $\mathbf{p}$. The second possibility is when the two points have the same amplitude vector but different phase vectors, i.e., $\mathbf{u}_a = \mathbf{u}_b = \mathbf{u}$ and $\mathbf{p}_a \neq \mathbf{p}_b$, and in this case, we define $D_p(\mathbf{u})$ as the MCD among all points with the same amplitude vector $\mathbf{u}$ as follows:

$$\begin{aligned} D_p(\mathbf{u}) &= \min_{\substack{\mathbf{p}_a \neq \mathbf{p}_b \\ \mathbf{p}_a, \mathbf{p}_b \in \Omega_p(\mathbf{l}_\phi)}} D_v\left(\mathbf{u} \circ \mathbf{p}_a, \mathbf{u} \circ \mathbf{p}_b\right) \\ &= \min_{\substack{\mathbf{p}_a \neq \mathbf{p}_b \\ \mathbf{p}_a, \mathbf{p}_b \in \Omega_p(\mathbf{l}_\phi)}} \sqrt{1 - \left| \sum_{i=0}^{K-1} u_i^2 e^{j(\phi_{i,b} - \phi_{i,a})} \right|^2}. \end{aligned} \tag{4.13}$$

A closed-form expression of $D_p(\mathbf{u})$ can be written as

$$D_p(\mathbf{u}) = \min \left[\min_{k \in \mathcal{K}} D_{p,1}^{(k)}(\mathbf{u}),\ \min_{l \in \mathcal{L}} D_{p,2}^{(l)}(\mathbf{u}) \right], \tag{4.14}$$

where $\mathcal{K} = \{k_1, k_2, \ldots, k_{Q_1}\}$ is a set of the non-zero indices of $\mathbf{l}_\phi$, $\mathcal{L} = \{l_1, l_2, \ldots, l_{Q_2}\}$ is a set of the non-zeros indices in ascending order of $\mathbf{l}_\phi$ without repetition, $D_{p,1}^{(k)}(\mathbf{u})$ is the MCD of the k-th PSK symbol and given by:

$$D_{p,1}^{(k)}(\mathbf{u}) = \sqrt{4u_k^2 \left(1 - u_k^2\right) \sin\left(\frac{\pi}{2^{l_{\phi_k}}}\right)^2}, \tag{4.15}$$

and $D_{p,2}^{(l)}(\mathbf{u})$ is the MCD of the reference symbols of the 2^l-PSK symbols and given by:

$$D_{p,2}^{(l)}(\mathbf{u}) = \sqrt{4 \left(\sum_{\{i | l_{\phi_i} < l\}} u_i^2 \right) \left(1 - \sum_{\{i | l_{\phi_i} < l\}} u_i^2 \right) \sin\left(\frac{\pi}{2^l}\right)^2}. \tag{4.16}$$

The proof is provided in Appendix 4.7.1 and Appendix 4.7.2.

We rewrite the proposed unitary constellation design problem in (4.11) with the help of $D_u(\mathbf{u}_a, \mathbf{u}_b)$ and $D_p(\mathbf{u})$ as follows:

$$\begin{aligned}
&\Omega_u(l_u, \mathbf{l}_\phi) \\
&= \underset{\Omega_u}{\operatorname{argmax}} \left\{ \min \left[\min_{\substack{\mathbf{u}_a \neq \mathbf{u}_b \\ \mathbf{u}_a, \mathbf{u}_b \in \Omega_u}} D_u(\mathbf{u}_a, \mathbf{u}_b), \min_{\mathbf{u} \in \Omega_u} D_p(\mathbf{u}) \right] \right\}, \qquad (4.17a) \\
&\text{s.t. } (4.11b), (4.11c).
\end{aligned}$$

To facilitate obtaining the solution of the unitary constellation design problem in (4.17), we make the following two reformulations. Firstly, we re-write the constraint $\|\mathbf{u}\|^2 = 1$ as $1 - \epsilon_v \leq \|\mathbf{u}\| \leq 1$, where ϵ_v is positive number tends to zero. Secondly, we use the epigraph representation [36] to simplify the objective function of the max-min optimization problem in (4.17). Thus, we rewrite the problem in (4.17) as follows:

$$\begin{aligned}
&\Omega_u(l_u, \mathbf{l}_\phi) = \underset{\Omega_u}{\operatorname{argmax}} \ t, && (4.18a) \\
&\text{s.t. } D_u^2(\mathbf{u}_a, \mathbf{u}_b) \geq t, \ \forall \mathbf{u}_a, \mathbf{u}_b \in \Omega_u, && (4.18b) \\
&\left(D_{p,1}^{(k)}(\mathbf{u}) \right)^2 \geq t, \ \forall \mathbf{u} \in \Omega_u, \ k \in \mathcal{K}, && (4.18c) \\
&\left(D_{p,2}^{(l)}(\mathbf{u}) \right)^2 \geq t, \ \forall \mathbf{u} \in \Omega_u, \ l \in \mathcal{L}, && (4.18d) \\
&\|\mathbf{u}\|^2 \geq 1 - \epsilon_v, \forall \mathbf{u} \in \Omega_u, && (4.18e) \\
&\|\mathbf{u}\|^2 \leq 1, \forall \mathbf{u} \in \Omega_u, && (4.18f) \\
&(4.11c).
\end{aligned}$$

Please note that the problem in (4.18) is a non-convex optimization problem due to the non-convex constraints (4.18b), (4.18c), (4.18d), and (4.18e). In the following, we address these non-convex constraints as follows. Firstly, one can see that the constraints in (4.18c) or (4.18d) can be rewritten as a quadratic inequality, i.e., $4x(1-x) \geq y$. This inequality can be reformulated as $1 - x \leq (\sqrt{1-y}+1)/2$ and $x \leq (\sqrt{1-y}+1)/2$. By setting $x = u_k^2$ and noting that $\sum_{i=0}^{K-1} u_i^2 = 1$, the constraints (4.18c) are reformulated to following convex

constraints:

$$\sum_{i=0,i\neq k}^{K-1} u_i^2 \leq \frac{\sqrt{1-t/\sin(\frac{\pi}{2^{l_{\phi_k}}})^2}+1}{2},$$
$$u_k^2 \leq \frac{\sqrt{1-t/\sin(\frac{\pi}{2^{l_{\phi_k}}})^2}+1}{2},\ \forall \mathbf{u}\in\Omega_u, k\in\mathcal{K}. \tag{4.19}$$

Similarly, by setting $x=\sum_{\{i|l_{\phi_i}<l\}} u_i^2$, the constraints (4.18d) are reformulated to following convex constraints:

$$\sum_{\{i|l_{\phi_i}<l\}} u_i^2 \leq \frac{\sqrt{1-t/\sin(\frac{\pi}{2^{l}})^2}+1}{2},$$
$$\sum_{\{i|l_{\phi_i}\geq l\}} u_i^2 \leq \frac{\sqrt{1-t/\sin(\frac{\pi}{2^{l}})^2}+1}{2},\ \forall \mathbf{u}\in\Omega_u, l\in\mathcal{L}. \tag{4.20}$$

Additionally, we employ Successive Convex Approximation (SCA) algorithm, which use the first-order Taylor series to approximate the non-convex constraints in (4.18b) and (4.18e), respectively, to the following convex constraints:

$$D_u^2(\bar{\mathbf{u}}_a,\bar{\mathbf{u}}_b)+\nabla_{\mathbf{u}_a}D_u^2(\bar{\mathbf{u}}_a)(\mathbf{u}_a-\bar{\mathbf{u}}_a)+\nabla_{\mathbf{u}_b}D_u^2(\bar{\mathbf{u}}_b)(\mathbf{u}_b-\bar{\mathbf{u}}_b)$$
$$\leq 1-t,\ \forall \mathbf{u}_a,\mathbf{u}_b\in\Omega_u,\ \forall \bar{\mathbf{u}}_a,\bar{\mathbf{u}}_b\in\bar{\Omega}_u(l_u,\mathbf{l}_\phi), \tag{4.21}$$

$$\|\bar{\mathbf{u}}\|^2+2\bar{\mathbf{u}}^T(\mathbf{u}-\bar{\mathbf{u}})\geq 1-\epsilon_v,\ \forall \mathbf{u}\in\Omega_u,\ \forall \bar{\mathbf{u}}\in\bar{\Omega}_u(l_u,\mathbf{l}_\phi). \tag{4.22}$$

where $\bar{\Omega}_u(l_u,\mathbf{l}_\phi)$ is the solution obtained from the previous iteration of the SCA. Finally, we approximate (4.17) into the convex optimization problem as follows:

$$\tilde{\Omega}_u(l_u,\mathbf{l}_\phi)=\underset{\Omega_u}{\text{argmax}}\ t, \tag{4.23a}$$
$$\text{s.t. } (4.18\text{f}),\ (4.11\text{c}),(4.19),(4.20),(4.21),(4.22). \tag{4.23b}$$

Since, the problem in (4.23) is convex, it can be solved by standard optimization toolboxes such as the CVX toolbox [37]. Once $\tilde{\Omega}_u(l_u,\mathbf{l}_\phi)$ of (4.23) is obtained, we replace $\bar{\Omega}_u(l_u,\mathbf{l}_\phi)$ with $\tilde{\Omega}_u(l_u,\mathbf{l}_\phi)$ and repeat the process to iteratively approach a solution of the original non-convex design problem in (4.18).

4.3.3 Searching Good Bit Allocation

In this subsection, we find bit allocations that result in unitary constellations with the highest MCD. To find the optimal bit allocations, one can perform an exhaustive search over all possible bit allocations. In other words, for each possible bit allocation, one needs to solve the optimization problem in (4.23), and then choose the bit allocation with the highest MCD. However, such an exhaustive search is not practical because the number of combinations of bit allocations that satisfy $l_u + \sum_{k=0}^{K-1} l_{\phi_k} = l_v$ is very large for typical values K and l_v ($K \geq 3$ and l_v is tens of bits).

To reduce the search space, we propose an approach that eliminates bit allocations with low MCDs. This is achieved by finding and testing an upper bound of the MCD $D_{\text{upper}}(l_u, \mathbf{l}_\phi)$ which is given as follows:

$$\begin{aligned} &D_{\text{upper}}(l_u, \mathbf{l}_\phi) \\ &= \min \left[\left(\frac{\pi^{\frac{1}{2}} \Gamma(\frac{K+1}{2})}{\Gamma(\frac{K}{2})} \right)^{\frac{1}{K-1}} 2^{-\frac{l_u}{K-1}}, \sin\left(\frac{\pi}{2^{l_{\phi,\max}}} \right) \right], \end{aligned} \tag{4.24}$$

where $\Gamma(.)$ is the Gamma function. The proof of the expression of $D_{\text{upper}}(l_u, \mathbf{l}_\phi)$ is given in Appendix 4.7.3. If a given bit allocation has a small value of D_{upper}, its corresponding MCD also must be small. Thus, by testing the upper bound on the MCD in (4.24), we can eliminate bit allocations that result in lower MCDs, and hence, poor error rate performance without solving the optimization problem in (4.23). Please note that bit allocations with high values of D_{upper} are not guaranteed to have high MCD. Hence, the MCD must be obtained by solving (4.23) in order to find the bit allocation with the highest MCD.

In Table 4.1, we provide the bit allocations of $K = 3$ and 4 and l_v up to 15 only due to space limitations. We generate the best bit allocation up to $K = 8$ and $l_v = 24$[2]. Because of the high complexity and because a high value of K is not necessary for SPC, we do not generate bit allocation for $K > 8$.

[2]The best found bit allocations for other values of K and the codebook of Ω_u are available at https://github.com/duongthanhson97/UnitaryConstellationsCodebook.

Table 4.1: Bit allocation with the highest MCD ($K = 3$ and 4, respectively).

l_v	$\hat{l}_u$	$\hat{\mathbf{l}}_\phi$	l_v	$\hat{l}_u$	$\hat{\mathbf{l}}_\phi$	l_v	$\hat{l}_u$	$\hat{\mathbf{l}}_\phi$
1	0	$0,0,1$	5	1	$0,2,2$	9	3	$0,3,3$
2	0	$0,1,1$	6	2	$0,2,2$	10	4	$0,3,3$
3	0	$0,1,2$	7	2	$0,2,3$	11	4	$0,3,4$
4	0	$0,2,2$	8	3	$0,2,3$	12	5	$0,3,4$

l_v	$\hat{l}_u$	$\hat{\mathbf{l}}_\phi$	l_v	$\hat{l}_u$	$\hat{\mathbf{l}}_\phi$	l_v	$\hat{l}_u$	$\hat{\mathbf{l}}_\phi$
1	0	$0,0,0,1$	6	0	$0,2,2,2$	11	4	$0,2,2,3$
2	0	$0,0,1,1$	7	2	$0,1,2,2$	12	4	$0,2,2,3$
3	0	$0,1,1,1$	8	2	$0,2,2,2$	13	4	$0,3,3,3$
4	0	$0,1,1,2$	9	3	$0,2,2,2$	14	5	$0,3,3,3$
5	0	$0,1,2,2$	10	4	$0,2,2,2$	15	6	$0,3,3,3$

4.4 Detection of the Proposed Unitary Constellations

In this section, we propose to iteratively detect the amplitude and the phase vectors of the proposed unitary constellation using an iterative unitary amplitude-phase (IUAP) detector. For the detection of the phase vector with equal and unequal modulation orders, we propose two low-complexity detectors, namely, posteriori-based-reliability-sort-DFDD (PR-sort-DFDD) and improved-PR-sort-DFDD, respectively.

4.4.1 Iterative Unitary Amplitude-Phase Detection Algorithm

As mentioned in (4.8), the transmitted signal $\mathbf{v}$ can be represented as the pair-wise product of the amplitude vector $\mathbf{u}$ and the phase vector $\mathbf{p}$. Hence, to jointly find the optimal values of $\mathbf{u}$ and $\mathbf{p}$ by directly solving the ML detector in (4.7) with a complexity order of $\mathcal{O}(2^{l_v})$, i.e., exponential in the number of bits allocated to the vector $\mathbf{v}$, i.e., l_v. However, by exploiting the first design rule defined in (4.9), i.e., the amplitude vector $\mathbf{u}$ and the phase vector $\mathbf{p}$ belong to independent constellation sets, we can reduce the complexity of the ML detector.

With the help of (4.9), the ML detector in (4.7) can be rewritten as follows:

$$\begin{aligned}\{\mathbf{u}_{\mathrm{ML}}, \mathbf{p}_{\mathrm{ML}}\} &= \underset{\mathbf{u}\in\Omega_u, \mathbf{p}\in\Omega_p}{\operatorname{argmax}} \operatorname{tr}\left(\mathbf{Y}^H\mathbf{Y}(\mathbf{u}\circ\mathbf{p})^*(\mathbf{u}\circ\mathbf{p})^T\right) \\ &= \underset{\mathbf{u}\in\Omega_u, \mathbf{p}\in\Omega_p}{\operatorname{argmax}} \operatorname{tr}\left(\mathbf{Y}^H\mathbf{Y}\left[(\mathbf{u}\mathbf{u}^T)\circ(\mathbf{p}^*\mathbf{p}^T)\right]\right), \end{aligned} \tag{4.25}$$

which can be equivalently represented as either one of the two following detection problems:

$$\{\mathbf{u}_{\mathrm{ML}}, \mathbf{p}_{\mathrm{ML}}\} = \underset{\mathbf{u}\in\Omega_u, \mathbf{p}\in\Omega_p}{\operatorname{argmax}} \operatorname{tr}\left(\left[(\mathbf{Y}^H\mathbf{Y})\circ(\mathbf{u}\mathbf{u}^T)\right](\mathbf{p}^*\mathbf{p}^T)\right), \tag{4.26a}$$

$$\{\mathbf{u}_{\mathrm{ML}}, \mathbf{p}_{\mathrm{ML}}\} = \underset{\mathbf{u}\in\Omega_u, \mathbf{p}\in\Omega_p}{\operatorname{argmax}} \operatorname{tr}\left(\left[(\mathbf{Y}^H\mathbf{Y})\circ(\mathbf{p}\mathbf{p}^H)\right](\mathbf{u}\mathbf{u}^T)\right). \tag{4.26b}$$

The idea of the proposed IUAP algorithm is to iteratively find sub-optimal $\tilde{\mathbf{u}}$ and $\tilde{\mathbf{p}}$ until a certain stopping criterion is satisfied. The sub-optimal $\tilde{\mathbf{u}}$ is found by solving:

$$\tilde{\mathbf{u}} = \underset{\mathbf{u}\in\Omega_u}{\operatorname{argmax}} \operatorname{tr}\left(\mathbf{Z}^{(\tilde{\mathbf{p}})}(\mathbf{u}\mathbf{u}^T)\right), \tag{4.27}$$

where $\mathbf{Z}^{(\tilde{\mathbf{p}})} = \left[(\mathbf{Y}^H\mathbf{Y})\circ(\tilde{\mathbf{p}}\tilde{\mathbf{p}}^H)\right]$. Similarly, the sub-optimal $\tilde{\mathbf{p}}$ is found by solving:

$$\tilde{\mathbf{p}} = \underset{\mathbf{p}\in\Omega_p}{\operatorname{argmax}} \operatorname{tr}\left(\mathbf{Z}^{(\tilde{\mathbf{u}})}(\mathbf{p}^*\mathbf{p}^T)\right), \tag{4.28}$$

where $\mathbf{Z}^{(\tilde{\mathbf{u}})} = \left[(\mathbf{Y}^H\mathbf{Y})\circ(\tilde{\mathbf{u}}\tilde{\mathbf{u}}^T)\right]$. In other words, the proposed IUAP solves (4.27) and (4.28) iteratively with a complexity order of $\mathcal{O}(2^{l_u})$ and $\mathcal{O}(2^{l_p})$, respectively. This represents a total complexity order of $\mathcal{O}(2^{l_u}) + \mathcal{O}(2^{l_p})$ which is much smaller than the complexity order of $\mathcal{O}(2^{l_v}) = \mathcal{O}(2^{l_u+l_p})$ required to directly solve the ML detection problem in (4.7). However, it is shown in Table 4.1 that the number of bits l_p is generally much larger than l_u thus it is necessary to develop a low-complexity phase detector to replace the ML phase detector. This is what will be discussed in the following subsections.

4.4.2 Detection of Phase Vector with Equal Modulation Orders

In this subsection, we develop the PR-sort-DFDD algorithm to detect the PSK-structured phase vector $\mathbf{p}$ with equal modulation orders. Let us assume that at the beginning of the n-th iteration of the PR-sort-DFDD, n PSK symbols have been detected with the indices belong to the set $\bar{\mathcal{D}} = \{k_0, \ldots, k_{n-1}\}$ and their final decisions are $\{\bar{\phi}_{k_0}, ..., \bar{\phi}_{k_{n-1}}\}$. The remaining undetected PSK symbols have the indices in the set $\mathcal{D} = \{d_0, ..., d_{K-n-1}\}$. Then,

the PR-sorted-DFDD chooses the symbol with the highest reliability among $\mathcal{D}$ to be detected next.

To explain the detection of a d-th undetected PSK symbol given all the detected PSK symbols in $\bar{\mathcal{D}}$, let $\bar{\mathbf{v}}_d = [v_{k_0}, \ldots, v_{k_{n-1}}, v_d]^T$, $\tilde{\mathbf{u}}_d = [\tilde{u}_{k_0}, \ldots, \tilde{u}_{k_{n-1}}, \tilde{u}_d]^T$ and $\bar{\mathbf{Y}}_d = [\mathbf{y}_{k_0}, \ldots, \mathbf{y}_{k_{n-1}}, \mathbf{y}_d]$ be transmitted signal, amplitude vector of the transmitted signal and the received signal corresponding to all the detected symbols in $\bar{\mathcal{D}}$ and the d-th undetetected symbol. Please note that $\mathbf{y}_i \in \mathbb{C}^{M\times 1}$ be the i-th column of $\mathbf{Y}$, which corresponds to the received signal of the i-th symbol v_i. Then, one can write the PDF of $\bar{\mathbf{Y}}_d$ given $\bar{\mathbf{v}}_d$ [13]:

$$\begin{aligned} f(\bar{\mathbf{Y}}_d|\bar{\mathbf{v}}_d) &= f(\bar{\mathbf{Y}}_d|\tilde{\mathbf{u}}_d, \bar{\phi}_{k_0}, \ldots, \bar{\phi}_{k_{n-1}}, \phi_d) \\ &= \frac{\exp\left(-\frac{\mathrm{tr}(\bar{\mathbf{Y}}_d^H \bar{\mathbf{Y}}_d)}{\sigma^2} + \frac{\mathrm{tr}\left(\bar{\mathbf{Y}}_d^H \bar{\mathbf{Y}}_d \ \bar{\mathbf{v}}_d^* \bar{\mathbf{v}}_d^T\right)}{\sigma^2(\sigma^2 + \|\bar{\mathbf{v}}_d\|^2)}\right)}{\pi^{(n+1)M}\left[(\sigma^2 + \|\bar{\mathbf{v}}_d\|^2)\sigma^{2n}\right]^M}. \end{aligned} \tag{4.29}$$

Please note that $\bar{\mathbf{Y}}_d$, $\bar{\phi}_{k_0}, \ldots, \bar{\phi}_{k_{n-1}}$ are known to the receiver and $\tilde{\mathbf{u}}_d$ can be found by solving the amplitude detection in (4.27); hence, only ϕ_d is unknown to the receiver. Thus, we simplify (4.29) as a function of ϕ_d as follows:

$$f(\bar{\mathbf{Y}}_d|\tilde{\mathbf{u}}_d, \bar{\phi}_{k_0}, \ldots, \bar{\phi}_{k_{n-1}}, \phi_d) = \bar{c}_1 \exp\left(\bar{c}_2 \mathrm{Re}\left\{\mu_d e^{-j\phi_d}\right\}\right), \tag{4.30}$$

where $\bar{c}_1$, $\bar{c}_2$, and μ_d are constant and independent of ϕ_d. The value of μ_d is given as:

$$\mu_d = \sum_{k\in\bar{\mathcal{D}}} z_{k,d}^{(u)} e^{j\bar{\phi}_k}, \tag{4.31}$$

where $z_{i,j}^{(u)} = \mathbf{y}_i^H \mathbf{y}_j \tilde{u}_i \tilde{u}_j$ is the (i,j)-th entry of $\mathbf{Z}^{(u)} = (\mathbf{Y}^H\mathbf{Y})(\tilde{\mathbf{u}}\tilde{\mathbf{u}}^T)$. The proof of (4.30) and the formulas of $\bar{c}_1$ and $\bar{c}_2$ are provided in the Appendix 4.7.4. A temporary value of ϕ_d is obtained by solving the following ML detection as follows:

$$\begin{aligned} \tilde{\phi}_d &= \underset{\phi_d\in\Omega_{\phi_d}}{\mathrm{argmax}} \ f(\bar{\mathbf{Y}}_d|\tilde{\mathbf{u}}_d, \bar{\phi}_{k_0}, \ldots, \bar{\phi}_{k_{n-1}}, \phi_d) \\ &= \underset{\phi_d\in\Omega_{\phi_d}}{\mathrm{argmax}} \ \mathrm{Re}\left\{\mu_d e^{-j\phi_d}\right\} = \underset{\phi_d\in\Omega_{\phi_d}}{\mathrm{argmax}} \ |\mu_d|\cos(\angle\mu_d - \phi_d). \end{aligned} \tag{4.32}$$

Please note that $\angle\mu_d$ is considered to be the reference phase, and the solution $\tilde{\phi}_d$ of (4.32) is obtained by choosing the d-th PSK symbol that is closest to $\angle\mu_d$, as shown in Fig. 4.3.

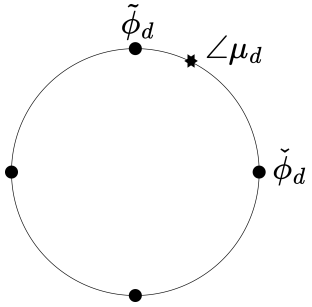

Figure 4.3: Closest PSK symbol $\tilde{\phi}_d$ and second closest PSK symbol $\check{\phi}_d$ to $\angle\mu_d$ of the d-th undetected symbol.

The ML detection of the phase in (4.32) can be obtained by an exhaustive search because the size of Ω_{ϕ_d} is typically small.

After the temporary decision of ϕ_d, i.e., $\tilde{\phi}_d$, is obtained, the reliability of the d-th symbol can be obtained. In [34], the sort-DFDD uses the LLR as the reliability criterion; however, it was limited only to multi-symbol 4-PSK modulations with equal amplitudes. Our proposed PR-sort-DFDD can detect multi-symbols 2^{l_ϕ}-ary PSK modulations with varying amplitudes. We define and use the posterior probability as the reliability criterion R_d of the d-th symbol as:

$$\begin{aligned} R_d &= P\left(\tilde{\phi}_d|\bar{\mathbf{Y}}_d, \tilde{\mathbf{u}}_d, \bar{\phi}_{k_0}, \ldots, \bar{\phi}_{k_{n-1}}\right), \\ &= \frac{f\left(\bar{\mathbf{Y}}_d|\tilde{\mathbf{u}}_d, \bar{\phi}_{k_0}, \ldots, \bar{\phi}_{k_{n-1}}, \tilde{\phi}_d\right)}{\sum_{\phi_d\in\Omega_{\phi_d}} f\left(\bar{\mathbf{Y}}_d|\tilde{\mathbf{u}}_d, \bar{\phi}_{k_0}, \ldots, \bar{\phi}_{k_{n-1}}, \phi_d\right)}, \\ &= \frac{\exp\left(\bar{c}_2\,|\mu_d|\cos(\angle\mu_d - \tilde{\phi}_d)\right)}{\sum_{\phi_d\in\Omega_{\phi_d}} \exp\left(\bar{c}_2\,|\mu_d|\cos(\angle\mu_d - \phi_d)\right)}. \end{aligned} \tag{4.33}$$

To simplify the calculation of R_d, we consider the two dominant terms in the denominator of (4.33), which correspond to the closest and second closest PSK symbols to $\angle\mu_d$, i.e., $\tilde{\phi}_d$ and $\check{\phi}_d$, respectively, as shown in Fig. 4.3. That said, the posterior probability in (4.33) is approximated as follows:

$$\begin{aligned} R_d &\approx \frac{e^{\bar{c}_2|\mu_d|\cos(\angle\mu_d-\tilde{\phi}_d)}}{e^{\bar{c}_2|\mu_d|\cos(\angle\mu_d-\tilde{\phi}_d)} + e^{\bar{c}_2|\mu_d|\cos(\angle\mu_d-\check{\phi}_d)}}, \\ &= \frac{1}{1 + e^{-\bar{c}_2|\mu_d|\left(\cos(\angle\mu_d-\tilde{\phi}_d)-\cos(\angle\mu_d-\check{\phi}_d)\right)}}. \end{aligned} \tag{4.34}$$

Since $1/(1+e^{-x})$ is an increasing function of x, we can further simplify R_d without affecting the solution of selecting the d-th PSK symbol with the highest R_d as follows:

$$\begin{aligned} R_d &= |\mu_d| \left(\cos(\angle \mu_d - \tilde{\phi}_d) - \cos(\angle \mu_d - \check{\phi}_d) \right) \\ &= \mathrm{Re}\left\{ \mu_d e^{-j\tilde{\phi}_d} \right\} - \mathrm{Re}\left\{ \mu_d e^{-j\check{\phi}_d} \right\}. \end{aligned} \tag{4.35}$$

The PR-sort-DFDD selects the most reliable symbol, $k_n = \mathrm{argmax}_{d \in \mathcal{D}} R_d$, and we detect the k_n-th symbol using (4.32) and obtain the final decision $\bar{\phi}_{k_n}$ of the k_n-symbol. The PR-sort-DFDD then updates the detected set $\bar{\mathcal{D}}$ and the undetected set $\mathcal{D}$ by adding k_n to $\bar{\mathcal{D}}$ and removing k_n from $\mathcal{D}$. The process continues until all the symbols are detected. The proposed PR-sort-DFDD algorithm is summarized in Algorithm 1.

Algorithm 1 PR-sort-DFDD algorithm

Input: $\mathbf{Z}^{(u)}$, $\bar{\mathcal{D}} = \{0\}$, $\bar{\phi}_0 = 0$, $\mathcal{D} = \{1, \ldots, K-1\}$.

Step 1: Calculate μ_d from (4.31) for each $d \in \mathcal{D}$.

Step 2: Find $\tilde{\phi}_d$ and $\check{\phi}_d$ from (4.32) for each $d \in \mathcal{D}$.

Step 3: Calculate reliability R_d as in (4.35) for each $d \in \mathcal{D}$.

Step 4: Select the undetected symbol with the highest R_d, i.e., k_n and obtain $\bar{\phi}_{k_n}$ as the final solution of (4.32).

Step 5: Remove k_n from $\mathcal{D}$ and add k_n to $\bar{\mathcal{D}}$.

Step 6: Repeat **Step 1** to **Step 5** until $\mathcal{D}$ is empty.

Output: $\bar{\phi}_0, \ldots, \bar{\phi}_{K-1}$.

4.4.3 Detection of Phase Vector with Unequal Modulation Orders

In this subsection, we propose the improved-PR-sort-DFDD algorithm, which improves the performance of the PR-sort-DFDD algorithm in the case of unequal modulation orders of the phase vector $\mathbf{p}$. The improvement in the performance is achieved by exploiting the information from undetected symbols with lower modulation order to enhance the detection of an undetected symbol with higher modulation order. For example, Fig. 4.4b shows that our proposed improved-PR-sort-DFDD uses information from undetected 2-PSK, 4-PSK symbols to detect the 8-PSK symbol. Meanwhile, the proposed PR-sort-DFDD (shown in

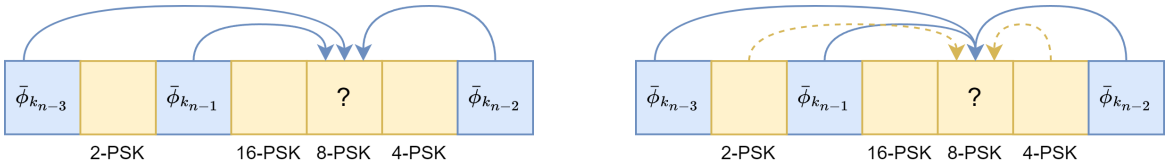

(a) Proposed PR-sort-DFDD (b) Proposed improved PR-sort-DFDD

Figure 4.4: Comparison between two proposed algorithms. Blue and yellow boxes indicate detected and undetected symbols, respectively. Blue solid arrows and yellow dashed arrows indicate information from the detected symbol and the undetected symbol, respectively.

Fig. 4.4a) as well as other DFDD algorithms only uses information from detected symbols to detect undetected symbols.

To explain the improved-PR-sort-DFDD, we first give an intuition on how the phase difference between undetected PSK symbols with unequal modulation orders can provide useful information. Fig. 4.5a shows the q-th undetected PSK symbol and d-th undetected PSK symbol with modulation orders of 2 and 8, respectively. Their phase difference can be estimated by calculating the phase between their corresponding received signal, i.e., $\angle \mathbf{y}_q^H \mathbf{y}_d$. For the sake of simplicity of explaining the concept, let us assume that $\angle \mathbf{y}_q^H \mathbf{y}_d = 0$. Given the phase difference $\angle \mathbf{y}_q^H \mathbf{y}_d = 0$, the d-th symbol is most likely to be $\pi/2$ if the q-th symbol is $\pi/2$; and the d-th symbol is most likely to be $-\pi/2$ if the q-th symbol is $-\pi/2$. Because we do not know the correct decision of the q-th PSK symbol, we do not know which phase value of the d-th PSK symbol is most likely to be. However, we can expect that the d-th PSK symbol phase is more likely to be $\pi/2$ or $-\pi/2$ when compared to other possible phase values. This information can be useful in enhancing the detection of the d-th symbol. Please note that if the undetected q-th and d-th PSK symbols have equal modulation orders as shown in Fig. 4.5b, then their phase difference only suggests the d-th symbol is more likely to be $\pi/2$ or $-\pi/2$. However, the d-th symbol is already likely to be $\pi/2$ or $-\pi/2$ without knowing the phase difference because there are only two possible choices of the d-th PSK symbol. As a result, the phase difference between two undetected symbols with equal modulation orders does not bring useful information.

In the following, we investigate the detection of the d-th undetected PSK symbol given the

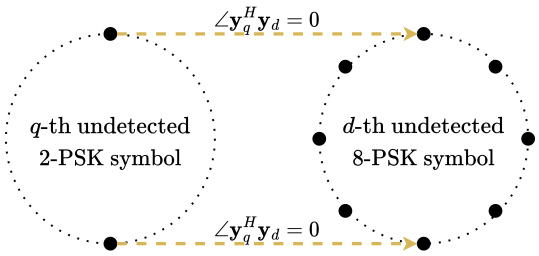

(a) Unequal modulation orders: The phase difference suggests that the d-th symbol is more likely to be $\pi/2$ or $-\pi/2$ than other values.

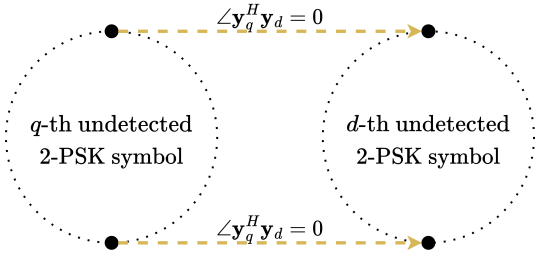

(b) Equal modulation orders: The phase difference suggests that the d-th symbol is more likely to be $\pi/2$ or $-\pi/2$. This information is not meaningful because d-th symbol has only two possible values.

Figure 4.5: Illustration of how the phase difference $\angle \mathbf{y}_q^H \mathbf{y}_d$ between two undetected PSK symbols can affect the detection of the d-th undetected PSK symbol. We assume that $\angle \mathbf{y}_q^H \mathbf{y}_d = 0$.

observations of the q-th and d-th undetected PSK symbols. Let $\mathbf{v}_{d,q} = [v_d, v_q]$, $\tilde{\mathbf{u}}_{d,q} = [\tilde{u}_d, \tilde{u}_q]$ and $\mathbf{Y}_{d,q} = [\mathbf{y}_d, \mathbf{y}_q]$ be transmitted signal, amplitude vector of transmitted signal and received signals corresponding to the d-th and q-th symbol, respectively. The PDF of $\mathbf{Y}_{d,q}$ given $\mathbf{v}_{d,q}$, is given as follows [13]:

$$f(\mathbf{Y}_{d,q}|\mathbf{v}_{d,q}) = f(\mathbf{Y}_{d,q}|\tilde{\mathbf{u}}_{d,q}, \phi_d, \phi_q). \tag{4.36}$$

Since $\mathbf{Y}_{d,q}$ is known to the receiver and $\tilde{\mathbf{u}}_{d,q}$ is obtained by the amplitude detection in (4.27), while ϕ_d and ϕ_q are unknown, we simplify (4.36) as a function of ϕ_d and ϕ_q as follows:

$$f(\mathbf{Y}_{d,q}|\tilde{\mathbf{u}}_{d,q}, \phi_d, \phi_q) = c_1 \exp\left(c_2 \mathrm{Re}\left\{z_{d,q}^{(u)} e^{j(\phi_d - \phi_q)}\right\}\right), \tag{4.37}$$

where c_1, c_2 and $z_{d,q}^{(u)}$ are constant and independent of ϕ_d and ϕ_q. The proof of (4.37) is similar to the proof of (4.30). Then, the log of the posterior probability of the d-th symbol

given all observations regarding the d-th symbol and q-th symbol, i.e., $\mathbf{Y}_{d,q}$, $\tilde{\mathbf{u}}_{d,q}$, is given by:

$$\begin{aligned}
&\log\left(P(\phi_d|\mathbf{Y}_{d,q},\tilde{\mathbf{u}}_{d,q})\right)\\
&\propto \log\left(\sum_{\phi_q\in\Omega_{\phi_q}} f(\mathbf{Y}_{d,q}|\tilde{\mathbf{u}}_{d,q},\phi_d,\phi_q)\right),\\
&\approx \log\left(\max_{\phi_q\in\Omega_{\phi_q}} c_1\exp\left(c_2\mathrm{Re}\left\{z_{d,q}^{(u)}e^{j(\phi_d-\phi_q)}\right\}\right)\right),\\
&\propto \eta_{d,q}(\phi_d), \qquad (4.38)
\end{aligned}$$

The approximation in (4.38) is achieved by the Max-Log approximation. The term $\eta_{d,q}(\phi_d)$ is defined as:

$$\eta_{d,q}(\phi_d) = \max_{\phi_q\in\Omega_{\phi_q}} \mathrm{Re}\left\{z_{d,q}^{(u)}e^{j(\phi_d-\phi_q)}\right\}. \qquad (4.39)$$

Since $\eta_{d,q}(\phi_d)$ in (4.39) represents the log-likelihood of the d-th PSK symbol given the observations of both the d-th and q-th PSK symbols, we include it as the selection criterion of the symbol to be detected in the PR-sort-DFDD; and this new algorithm is the improved-PR-sort-DFDD. The decision rule in (4.32) is modified as follows:

$$\tilde{\phi}_d = \underset{\phi_d\in\Omega_{\phi_d}}{\mathrm{argmax}} \underbrace{\mathrm{Re}\left\{\mu_d e^{-j\phi_d}\right\}}_{\substack{\text{log-likelihood given}\\ \text{all detected symbols}}} + \sum_{q\in\mathcal{D}/\{d\},l_{\phi_q}<l_{\phi_d}} \underbrace{\eta_{d,q}(\phi_d)}_{\substack{\text{log-likelihood given}\\ q\text{-th undetected symbol}}}. \qquad (4.40)$$

We follow a similar approach as PR-sort-DFDD in (4.35) by taking $\check{\phi}_{k_n}$ as a solution with the second-highest value of (4.40) and calculate the reliability criterion based on the difference of likelihood between $\tilde{\phi}_d$ and $\check{\phi}_{k_n}$, which is given by:

$$\begin{aligned}
R_d =& \mathrm{Re}\left\{\mu_d e^{-j\tilde{\phi}_d}\right\} - \mathrm{Re}\left\{\mu_d e^{-j\check{\phi}_d}\right\}\\
&+ \sum_{q\in\mathcal{D}/\{d\},l_{\phi_q}<l_{\phi_d}} \eta_{d,q}(\tilde{\phi}_d) - \eta_{d,q}(\check{\phi}_d). \qquad (4.41)
\end{aligned}$$

The improved-PR-sort-DFDD algorithm is similar to the PR-sort-DFDD in Alg. 1, except that $\tilde{\phi}_d$ and $\check{\phi}_d$ are calculated from (4.40) and R_d is calculated from (4.41) in the improved-PR-sort-DFDD algorithm. Please note that if we use the improved-PR-sort-DFDD for equal modulation orders, the decision rule (4.40) and reliability criterion (4.41) of the improved-PR-sort-DFDD algorithm is reduced to the decision rule (4.32) and reliability criterion (4.35) of the PR-sort-DFDD algorithm.

Table 4.2: Comparison of detection complexity for $M \geq K$.

Detectors	Detection complexity
ML detector	$\mathcal{O}\left(MK^2 + 2^{l_v}K^2\right)$
Exponential/cube-split	$\mathcal{O}(MK^2)$
Proposed detectors	$\mathcal{O}(MK^2 + 2^{l_u}K^2 + K^3 + 2^{l_{\phi,\max}}K^2)$

4.4.4 Detection Complexity Analysis

Overall, the detection process includes calculating $\mathbf{Y}^H\mathbf{Y}$, detecting the amplitude vector $\mathbf{u}$, and the phase vector $\mathbf{p}$.

The complexity of the amplitude vector detection in (4.27), is $\mathcal{O}(2^{l_u}K^2)$. This is as calculating the argument in (4.27) requires $\mathcal{O}(K^2)$ and solving the optimization problem in (4.27) for all possible 2^{l_u} amplitude vectors requires an exhaustive search of complexity order $\mathcal{O}(2^{l_u})$.

Regarding the complexity of the phase vector detection, the PR-sort-DFDD and the improved-PR-sort-DFDD include two nested loops with a maximum of K^2 iterations. In case of PR-sort-DFDD, each iteration includes the computation of (4.32) with complexity of $\mathcal{O}(K + 2^{l_{\phi_d}})$. Thus, the worst-case complexity of the PR-sort-DFDD is $\mathcal{O}(K^3 + 2^{l_{\phi\max}}K^2)$. Compared to PR-sort-DFDD, the improved-PR-sort-DFDD have higher complexity due to the calculation of $\eta_{d,q}(\phi_d)$ in (4.40). Please note that $\eta_{d,q}$ can be calculated and stored before starting the improved-PR-sort-DFDD, and the worst-case complexity of pre-calculating every possible values of $\eta_{d,q}(\phi_d)$ is $2^{l_{\phi\max}}K^2$. Hence, the complexity of improved-PR-sort-DFDD is still $\mathcal{O}(K^3 + 2^{l_{\phi\max}}K^2)$.

Given the complexity of calculating $\mathbf{Y}^H\mathbf{Y}$ is $\mathcal{O}(MK^2)$, the overall computational complexity order of the proposed IUAP is $\mathcal{O}\left(MK^2 + 2^{l_u}K^2 + K^3 + 2^{l_{\phi,\max}}K^2\right)$ excluding the number of iterations required for the IUAP algorithm to converge. As can be seen, the complexity of the proposed IUAP algorithm is polynomial in K and exponential in l_u.

In Table 4.2, we compare the complexity of our proposed detectors for proposed constellations with the detection complexity of other unitary constellations in the literature,

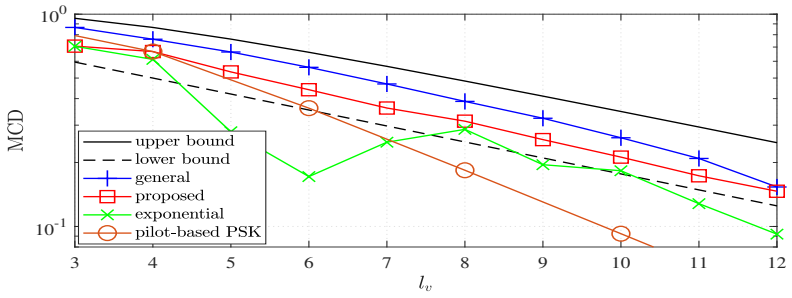

(a) $K = 3$

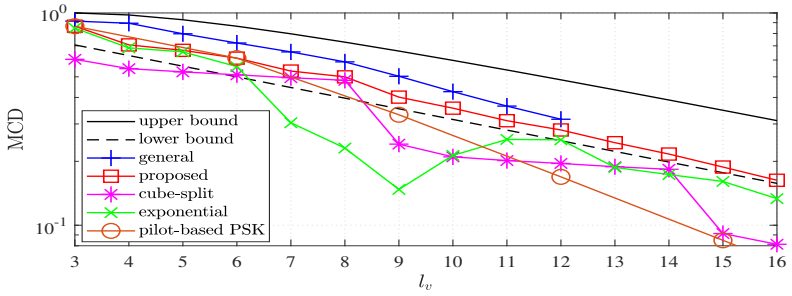

(b) $K = 4$

Figure 4.6: MCD comparison for different values of l_v and K.

assuming that M is large and K is small; hence, $M \geq K$. Since $2^{l_u} + 2^{l_{\phi_{\max}}} \ll 2^{l_v}$ as shown in Section 4.3.3, our proposed detectors have significantly lower complexity than the ML detector. However, our proposed detectors for our proposed constellations have higher detection complexity than the detectors of exponential or cube-split constellations.

4.5 Simulation Result

In this section, we evaluate the MCD and the error performance achieved by our proposed unitary constellation with proposed detectors and compare them with other schemes. Unless otherwise mentioned, the number of antennas is set to $M = 32$. Please note that we evaluate the performance for $K \geq 3$ since our proposed unitary constellation has the same structure as the one in [25] in the case of $K = 2$.

Fig. 4.6 depicts the MCD of the proposed unitary constellation with the following unitary constellations: general constellation [13], exponential constellation [22], cube-split constellation [24], and the pilot-based PSK constellations which include one pilot and $K - 1$ PSK symbols with equal amplitude and equal modulation orders. As can be seen from Fig. 4.6,

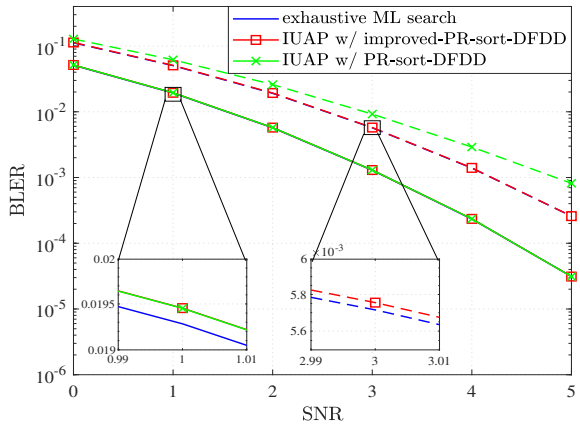

Figure 4.7: Performance comparisons with ML detector. Solid lines and dashed lines correspond to equal modulation orders ($\{l_{\phi_1}, l_{\phi_2}, l_{\phi_3}\} = \{2, 2, 2\}$) and unequal modulation orders ($\{l_{\phi_1}, l_{\phi_2}, l_{\phi_3}\} = \{2, 2, 3\}$), respectively.

the MCD of the proposed unitary constellation is higher, hence better, than its counterparts of the exponential, the cube-split, and the pilot-based PSK constellations, and it is close to the MCD of the general unitary constellation for $K = 3$, 4.

We compare the BLER of our proposed IUAP with PR-sort-DFDD and IUAP with improved-PR-sort-DFDD, with the optimal ML detector in (4.7), obtained through an exhaustive search. Please note that since the amplitude set Ω_u does not have a specific structure, the amplitude detection of the IUAP is carried out by an exhaustive search. As can be seen from Fig. 4.7, both proposed detectors achieve the performance of the ML detector for the case of equal modulation orders with negligible 0.01 dB SNR penalty; while only the performance of the IUAP with the PR-sort-DFDD deteriorates for the case of unequal modulation orders.

In the following, we compare the error performance of our proposed unitary constellations with general constellation [13], exponential constellation [22], cube-split constellation [24], and the pilot-based schemes for different values of K and l_v. The pilot-based schemes include one pilot and $K - 1$ QAM or PSK symbols. The optimal ML detector in (4.7) is required for the general constellations, while low-complexity detectors can be used for proposed unitary constellations (IUAP with improved-PR-sort-DFDD), cube-split constellations (greedy

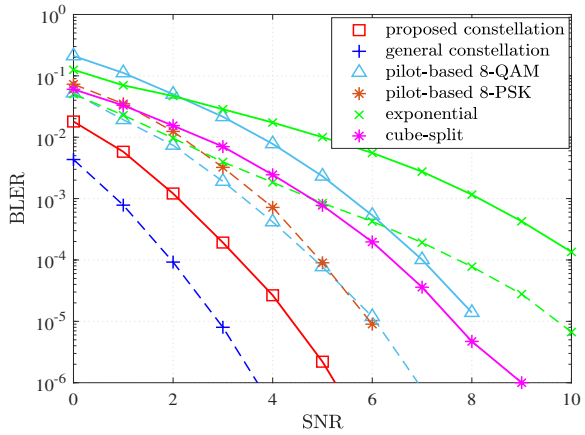

Figure 4.8: BLER comparisons of different schemes for $K = 4$, $l_v = 9$. Dashed lines and solid lines corresponds to high-complexity ML detectors and low-complexity detectors, respectively.

detector), exponential constellations (simplified detector), and the pilot-based QAM scheme (MMSE channel estimation and MMSE linear detector). Moreover, to show the best potential error performance of all the schemes, we simulate the ML detector for all the schemes except for the proposed unitary constellation and the cube-split constellations, as their low-complexity detectors already have near-optimal performance of the ML detector. Please note that the ML detector's performance does not necessarily reflect the actual performance in practical applications due to its prohibitive complexity.

Fig. 4.8 and Fig. 4.9 show that our proposed constellation outperforms all schemes with low-complexity detectors by a considerable margin. In specific, our proposed constellations outperform the pilot-based QAM and the cube-split constellations by at least 3 dB and outperforms the exponential constellation by almost 6 dB. Furthermore, our proposed constellation outperforms the pilot-based QAM, pilot-based PSK, and exponential constellations with their ML detector. As expected, the BLER of the general unitary constellation with the ML detector is better than its counterpart of our proposed constellation at different values of K and l_v. Please note that for the BER performance reported in Fig. 4.9b, the performance gap between our proposed constellation and the general constellation is slightly less than the BLER performance gap, because the general constellation does not have an efficient mapping criterion due to their random structure. In contrast, our proposed constellation can use Gray mapping to the PSK constellations, which improves its BER.

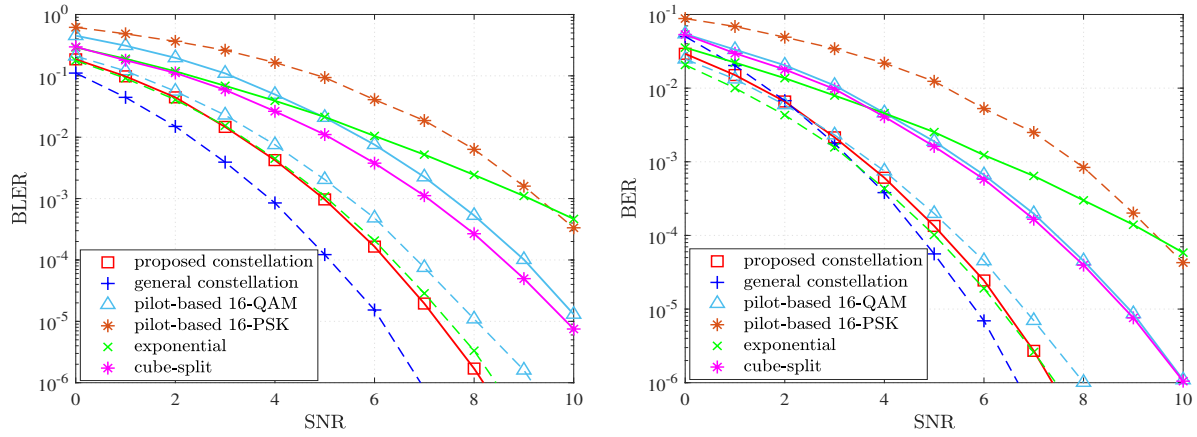

(a) BLER (b) BER

Figure 4.9: BLER and BER comparison of different schemes at $K = 4$, $l_v = 12$. Dashed lines and solid lines correspond to high-complexity ML detectors and low-complexity detectors, respectively.

In Fig. 4.10, we plot the BLER performance of the proposed unitary constellations and other competing unitary constellations as a function of M. As can be seen, the performance of our proposed unitary constellation improves when the value of M increases. This aligns with the fact that the PEP of unitary constellations decreases as M increases in (4.2). Furthermore, Fig. 4.10 also shows that for a sufficiently large number of antennas (typically $M \geq 8$) our proposed constellations also outperform other low-complexity constellations (exponential and cube-split) and pilot-based QAM with both coherent detectors and non-coherent ML detector.

4.6 Conclusion

In this paper, we proposed a novel design of unitary constellations, which is the Cartesian product of amplitude and phase vectors. The phase vector is confined to a generalized PSK structure where the PSK constellations can have unequal modulation orders and varying amplitude. By exploiting the Cartesian structure, we proposed a low-complexity algorithm that performs amplitude detection and phase detection iteratively. For the phase detection, we adopted the posterior probability as the reliability of the sort-DFDD algorithm, and proposed the PR-sort-DFDD algorithm, which approaches the optimal performance of ML detector in the case of PSK structure with equal modulation orders. For PSK structures with

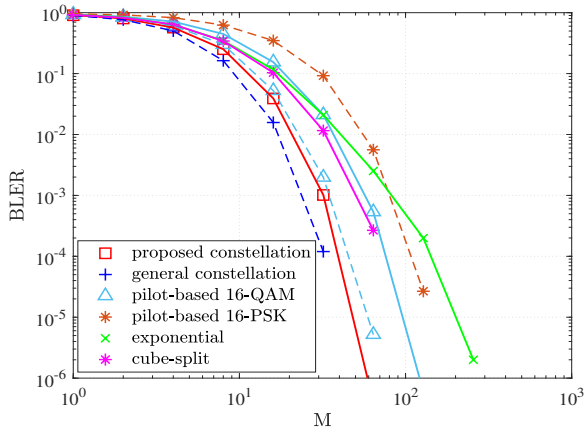

Figure 4.10: BLER as a function of M at $K = 4$, $l_v = 12$ and SNR $= 5$ dB. Dashed lines and solid lines correspond to high-complexity ML detectors and low-complexity detectors, respectively.

unequal modulation orders, we used feedback from undetected symbols with lower modulation order to enhance the detection of unknown symbols with higher modulation order and proposed the improved-PR-sort-DFDD algorithm. Both of the proposed phase detectors approach the ML detection performance, in their designated cases, with polynomial time complexity. Simulation results showed that the proposed constellations achieve better MCD when compared to other competing low-complexity unitary constellations, such as the exponential and cube-split constellations. For error performance, our proposed constellation with the proposed detectors outperforms conventional pilot-based QAM with coherent detection by 3 dB. Our proposed scheme also outperforms other low-complexity unitary constellations by up to 6 dB.

4.7 Appendix

4.7.1 Proof of the expression of $D_p(\mathbf{u})$ in (4.14)

First, let $\Delta\mathbf{p} = [e^{j\Delta\phi_0}, \ldots, e^{j\Delta\phi_{K-1}}]$ with $\Delta\phi_i = \phi_{i,a} - \phi_{i,b}$ being the phase difference between $\mathbf{p}_a$ and $\mathbf{p}_b$. Since the difference of two PSK values $\phi_{i,a}$ and $\phi_{i,b}$ is also a PSK value,

hence $\Delta\mathbf{p} \in \Omega_p(\mathbf{l}_\phi)$. Then, we rewrite $D_p(\mathbf{u})$ as follows:

$$D_p(\mathbf{u}) = \min_{\substack{\mathbf{p}_a \neq \mathbf{p}_b \\ \mathbf{p}_a, \mathbf{p}_b \in \Omega_p(\mathbf{l}_\phi)}} \sqrt{1 - \left| \sum_{i=0}^{K-1} u_i^2 e^{j(\phi_{i,b} - \phi_{i,a})} \right|^2}$$
$$= \min_{\Delta\mathbf{p} \in \Omega_p(\mathbf{l}_\phi) \backslash \mathbf{1}_K} \sqrt{1 - \left| \sum_{i=0}^{K-1} u_i^2 e^{j\Delta\phi_i} \right|^2}. \tag{4.42}$$

Let $\Delta\hat{\mathbf{p}}$ be the optimal argument of (4.42). If we can find $\Delta\hat{\mathbf{p}}$, we can easily obtain $D_p(\mathbf{u})$ by substituting $\Delta\hat{\mathbf{p}}$ into the objective function (4.42). One approach to find $\Delta\hat{\mathbf{p}}$ is to solve (4.42) using exhaustive search over the set $\Omega_p(\mathbf{l}_\phi)\backslash\mathbf{1}_K$. However, this approach is not practical because the size of the set $\Omega_p(\mathbf{l}_\phi)\backslash\mathbf{1}_K$ grows exponentially with l_p. To overcome this problem, we aim to find a subset of $\Omega_p(\mathbf{l}_\phi)\backslash\mathbf{1}_K$ (let us say $\Omega_p^\ddagger \in \Omega_p(\mathbf{l}_\phi)\backslash\mathbf{1}_K$) that guarantees to contain the optimal solution $\Delta\hat{\mathbf{p}}$. Thus, $D_p(\mathbf{u})$ can be rewritten as follows:

$$D_p(\mathbf{u}) = \min_{\Delta\mathbf{p} \in \Omega_p^\ddagger} \sqrt{1 - \left| \sum_{i=0}^{K-1} u_i^2 e^{j\Delta\phi_i} \right|^2}. \tag{4.43}$$

The subset $\Omega_p^\ddagger$ should have a sufficiently small size so an exhaustive search over $\Omega_p^\ddagger$ still has low complexity. Such subset $\Omega_p^\ddagger$ can be given in the Lemma 1.

Lemma 1. *Let $\Omega_{p,1}^\ddagger$ be a subset consisting of the Q_1 elements: $\left\{\Delta\mathbf{p}_{k_1}^\ddagger, \ldots, \Delta\mathbf{p}_{k_{Q_1}}^\ddagger\right\}$ corresponding to $\mathcal{K}$, where $\mathcal{K} = \{k_1, k_2, \ldots, k_{Q_1}\}$ is a set of the non-zero indices of $\mathbf{l}_\phi$. Each element $\Delta\mathbf{p}_k^\ddagger = \left[\Delta p_{0,k}^\ddagger, \ldots, \Delta p_{K-1,k}^\ddagger\right]^T$ is given by:*

$$\Delta p_{i,k}^\ddagger = \begin{cases} e^{j2\pi/2^{l_{\phi_k}}}, & \text{if } i = k \\ e^{j0}, & \text{if } i \neq k \end{cases}, \ i = 0, \ldots, K-1. \tag{4.44}$$

Let $\Omega_{p,2}^\ddagger$ be a subset consisting of Q_2 elements: $\left\{\Delta\mathbf{p}_{l_1}^\ddagger, \ldots, \Delta\mathbf{p}_{l_{Q_2}}^\ddagger\right\}$ corresponding to $\mathcal{L}$, where $\mathcal{L} = \{l_1, l_2, \ldots, l_{Q_2}\}$ is a set of the non-zeros indices in ascending order of $\mathbf{l}_\phi$ without repetition. Each element $\Delta\mathbf{p}_l^\ddagger = \left[\Delta p_{0,l}^\ddagger, \ldots, \Delta p_{K-1,l}^\ddagger\right]^T$ is given by:

$$\Delta p_{i,l}^\ddagger = \begin{cases} e^{j2\pi/2^l}, & \text{if } l_{\phi_i} \geq l \\ e^{j0}, & \text{if } l_{\phi_i} < l \end{cases}, \ i = 0, \ldots, K-1. \tag{4.45}$$

Then, a subset $\Omega_p^\ddagger$ given by $\Omega_p^\ddagger = \Omega_{p,1}^\ddagger(\mathbf{l}_\phi) \cup \Omega_{p,2}^\ddagger(\mathbf{l}_\phi)$ must contain the optimal argument $\Delta\hat{\mathbf{p}}$ of (4.42).

Proof: The proof is provided in the Appendix 4.7.2.

Please note that $D_{p,1}^{(k)}(\mathbf{u})$ in (4.15) is obtained by substituting $\Delta\mathbf{p}_k^{\ddagger}$ for $k \in \mathcal{K}$ into (4.42), and $D_{p,2}^{(l)}(\mathbf{u})$ in (4.16) is obtained by substituting $\Delta\mathbf{p}_l^{\ddagger}$ for $l \in \mathcal{L}$ into (4.42). Thus, we obtain $D_p(\mathbf{u})$ in (4.14) by substituting all elements of $\Omega_p^{\ddagger}$ into (4.42).

4.7.2 Proof of the Lemma 1

Let $[\hat{\phi}_0, \ldots, \hat{\phi}_{K-1}]$ be the angle of the optimal $\Delta\hat{\mathbf{p}}$, and $\Delta\hat{\phi}_{\text{avg}}$ be the average angle of $\Delta\hat{\mathbf{p}}$, i.e., $\Delta\hat{\phi}_{\text{avg}} = \angle\left(\sum_{i=0}^{K-1} u_i^2 e^{j\Delta\hat{\phi}_i}\right)$. Since $\left|\sum_{i=0}^{K-1} u_i^2 e^{j\Delta\phi_i}\right| = \left|\sum_{i=0}^{K-1} u_i^2 e^{-j\Delta\phi_i}\right|$, there always exists a pair of $\Delta\hat{\mathbf{p}}$. Thus, for simplicity, we only consider $\Delta\hat{\mathbf{p}}$ with $\Delta\hat{\phi}_{\text{avg}} \in [0, \pi]$.

We prove Lemma 1 by contradiction. In specific, if $\Delta\hat{\mathbf{p}}$ lies outside of $\Omega_p^{\ddagger}$, we can find an counter example, i.e., $\Delta\check{\mathbf{p}}$, whose objective value in (4.42) is lower than that of $\hat{u}_{\text{avg}}^2$ of $\Delta\hat{\mathbf{p}}$. Throughout the proof, we denote the complementary subset of $\Omega_p^{\ddagger}$ as $\Omega_p^{\S}$, and denote the angle and average angle of $\Delta\check{\mathbf{p}}$ as $[\check{\phi}_0, \ldots, \check{\phi}_{K-1}]$ and $\Delta\check{\phi}_{\text{avg}}$, respectively.

Then, we have the following lemma:

Lemma 2. *If there exists an optimal* $\Delta\hat{\mathbf{p}} \in \Omega_p^{\S}$*, then*

$$\Delta\hat{\phi}_i = \min_{\Delta\phi_i \in \Omega_{\phi_i}} |\Delta\phi_i - \Delta\hat{\phi}_{avg}|. \tag{4.46}$$

Proof: We prove Lemma 2 by contradiction. Assume that there exists symbol k that satisfies $\Delta\hat{\phi}_k \neq \min_{\Delta\phi_k \in \Omega_{\phi_k}} |\Delta\phi_k - \Delta\hat{\phi}_{\text{avg}}|$. Given $\Delta\hat{\mathbf{p}}$, we choose the counter example $\Delta\check{\mathbf{p}}$ as follows:

$$\Delta\check{\phi}_i = \begin{cases} \Delta\hat{\phi}_k - \text{sgn}\left(\Delta\hat{\phi}_k - \Delta\hat{\phi}_{\text{avg}}\right)\frac{2\pi}{2^{l_{\phi_k}}}, & \text{if } i = k, \\ \Delta\hat{\phi}_i, & \text{if } i \neq k. \end{cases} \tag{4.47}$$

Let $\{l_0, \ldots, l_{Q_2}\}$ contain values of $\mathbf{l}_\phi$ in an ascending order. This set is similar to $\mathcal{L}$ defined in (4.14), except that $\mathcal{L}$ does not contain $l_0 = 0$. Then, we have the following lemmas:

Lemma 3. *There does not exist an optimal* $\Delta\hat{\mathbf{p}} \in \Omega_p^{\S}$ *with its average phase* $\Delta\hat{\phi}_{avg} \in \left[2\pi/2^{l_{q+1}},\ \pi/2^{l_q}\right)$ *with* $0 \leq q < Q_2$.

Proof: We prove Lemma 3 by contradiction. Assume that $\Delta\hat{\mathbf{p}} \in \Omega_p^{\S}$ with $\Delta\hat{\phi}_{\text{avg}} \in \left[2\pi/2^{l_{q+1}},\ \pi/2^{l_q}\right)$. Clearly, we only need to prove the case of $l_{q+1} > l_q+1$, since $\left[2\pi/2^{l_{q+1}},\ \pi/2^{l_q}\right) = \varnothing$ when $l_{q+1} = l_q + 1$. Given the range of $\Delta\hat{\phi}_{\text{avg}}$ and using Lemma 2, we obtain $\Delta\hat{\mathbf{p}}$ where $\Delta\hat{\phi}_i = 0$ if $l_{\phi_i} \leq l_q$. Then, we choose the counter example $\Delta\check{\mathbf{p}}$ as follows:

$$\Delta\check{\phi}_i = \begin{cases} \Delta\hat{\phi}_i = 0, & \text{if } l_{\phi_i} \leq l_q, \\ \Delta\hat{\phi}_i - \left(\frac{2\pi}{2^{l_{q+1}}}\right), & \text{if } l_{\phi_i} \geq l_{q+1}. \end{cases} \tag{4.48}$$

Lemma 4. *There does not exist an optimal $\Delta\hat{\mathbf{p}} \in \Omega_p^{\S}$ with its average phase $\Delta\hat{\phi}_{avg} \in \left(\pi/2^{l_q}, 2\pi/2^{l_q}\right)$ with $0 \leq q \leq Q_2$.*

Proof: We prove Lemma 4 by contradiction. Assume that there exists $\Delta\hat{\mathbf{p}} \in \Omega_p^{\S}$ with $\Delta\hat{\phi}_{\text{avg}} \in \left(\pi/2^{l_q}, 2\pi/2^{l_q}\right)$. Lemma 4 is true for $q = 0$, since $\left(\pi/2^{l_q}, 2\pi/2^{l_q}\right) = (\pi, 2\pi)$ contradicts $\Delta\hat{\phi}_{\text{avg}} \in [0, \pi]$. Thus, we only need to prove Lemma 4 in case of $q \geq 1$. Given the range of $\Delta\hat{\phi}_{\text{avg}}$ and using Lemma 2, we obtain $\Delta\hat{\mathbf{p}}$ where $\Delta\hat{\phi}_i = 0$ if $l_{\phi_i} \leq l_{q-1}$. Given $\Delta\hat{\mathbf{p}}$, we choose the counter example $\Delta\check{\mathbf{p}}$ as follows:

$$\Delta\check{\phi}_i = \begin{cases} \Delta\hat{\phi}_i = 0, & \text{if } l_{\phi_i} \leq l_{q-1} \\ \frac{2\pi}{2^{l_q}} - \Delta\hat{\phi}_i, & \text{if } l_{\phi_i} \geq l_q. \end{cases} \tag{4.49}$$

Lemma 5. *There does not exist an optimal $\Delta\hat{\mathbf{p}} \in \Omega_p^{\S}$ with its average phase $\Delta\hat{\phi}_{avg} = \pi/2^{l_q}$ with $0 \leq q \leq Q_2$.*

Proof: We prove Lemma 5 by contradiction. Assume that $\Delta\hat{\mathbf{p}} \in \Omega_p^{\S}$ with $\Delta\hat{\phi}_{\text{avg}} = \pi/2^{l_q}$. We have two possibilities:

1) $q = 0$. Thus, $l_q = l_0 = 0$ and $\Delta\hat{\phi}_{\text{avg}} = 0$. Given $\Delta\hat{\phi}_{\text{avg}} = 0$, we use Lemma 2 to obtain $\Delta\hat{\mathbf{p}}$ with $\Delta\hat{\phi}_i = 0$ if $l_{\phi_i} = l_q = 0$ and $\Delta\hat{\phi}_i = \pi$ if $l_{\phi_i} \neq l_q = 0$. We have two cases:

- If $l_1 = 1$, then the obtained $\Delta\hat{\mathbf{p}}$ is equivalent to:

$$\Delta\hat{\phi}_i = \begin{cases} 0, & \text{if } l_{\phi_i} < l_1, \\ \frac{2\pi}{2^{l_1}}, & \text{if } l_{\phi_i} \geq l_1. \end{cases} \tag{4.50}$$

  Thus, $\Delta\hat{\mathbf{p}} \in \Omega_{p,2}^{\ddagger}$, contradicting with $\Delta\hat{\mathbf{p}} \in \Omega_p^{\S}$.

- If $l_1 \geq 2$, we choose the counter example $\Delta\check{\mathbf{p}}$ as follows:

$$\Delta\check{\phi}_i = \begin{cases} 0, & \text{if } l_{\phi_i} = l_q \\ \frac{2\pi}{2^{l_1}}, & \text{if } l_{\phi_i} \neq l_q. \end{cases} \tag{4.51}$$

2) $q \geq 1$. Given $\Delta\hat{\phi}_{\text{avg}} = \pi/2^{l_q}$, we use Lemma 2 to obtain $\Delta\hat{\mathbf{p}}$ as follows:

$$\Delta\hat{\phi}_i = \begin{cases} 0, & \text{if } l_{\phi_i} = 0, \\ 0 \text{ or } \frac{2\pi}{2^{l_q}}, & \text{if } l_{\phi_i} = l_q, \\ \frac{\pi}{2^{l_q}}, & \text{if } l_{\phi_i} \neq l_q. \end{cases} \tag{4.52}$$

We choose only one index k where $l_{\phi_k} = l_q$, and choose the counter example $\Delta\check{\mathbf{p}}$ as follows:

$$\Delta\check{\phi}_i = \begin{cases} \Delta\hat{\phi}_i, & \text{if } i \neq k \\ \frac{2\pi}{2^{l_{\phi_k}}} - \Delta\hat{\phi}_k, & \text{if } i = k. \end{cases} \tag{4.53}$$

Lemma 6. *There does not exist an optimal $\Delta\hat{\mathbf{p}} \in \Omega_p^{\S}$ with its average phase $\Delta\hat{\phi}_{avg} \in [0, \pi/2^{l_{Q_2}})$.*

Proof: We prove Lemma 6 by contradiction. Assume that there exists $\Delta\hat{\mathbf{p}} \in \Omega_p^{\S}$ with $\Delta\hat{\phi}_{\text{avg}} \in [0, \pi/2^{l_{Q_2}})$. Given the range of $\Delta\hat{\phi}_{\text{avg}}$, we use Lemma 2 to obtain $\Delta\hat{\mathbf{p}}$ as follows:

$$\Delta\hat{\phi}_i = \min_{\Delta\phi_i \in \Omega_{\phi_i}} |\Delta\phi_i - \Delta\hat{\phi}_{\text{avg}}| = 0. \tag{4.54}$$

Thus, $\Delta\hat{\mathbf{p}} = \mathbf{1}_K$, which is not valid.

Combining Lemma 3, Lemma 4 and Lemma 5, we obtain two corollaries:

Corollary 1. *There does not exist an optimal $\Delta\hat{\mathbf{p}} \in \Omega_p^{\S}$ with its average phase $\Delta\hat{\phi}_{avg} \in \left[2\pi/2^{l_{q+1}}, 2\pi/2^{l_q}\right)$ for $0 \leq q < Q_2$.*

Corollary 2. *There does not exist an optimal $\Delta\hat{\mathbf{p}} \in \Omega_p^{\S}$ with its average phase $\Delta\hat{\phi}_{avg} \in \left[\pi/2^{l_{Q_2}}, 2\pi/2^{l_{Q_2}}\right)$ for $0 \leq q \leq Q_2$*

Finally, using Corollary 1, Corollary 2, and Lemma 6, we list all possible range of $\Delta\hat{\phi}_{\text{avg}}$, for which an optimal $\Delta\hat{\mathbf{p}} \in \Omega_p^{\S}$ does not exist:

$$\bigcup_{q=0}^{Q_2-1} \left[\frac{2\pi}{2^{l_{q+1}}}, \frac{2\pi}{2^{l_q}}\right) \cup \left[\frac{2\pi}{2^{l_{Q_2}}}, \frac{2\pi}{2^{l_{Q_2}}}\right) \cup \left[0, \frac{\pi}{2^{l_{Q_2}}}\right) = [0, 2\pi)\,. \tag{4.55}$$

Hence, there does not exist an optimal $\Delta\hat{\mathbf{p}} \in \Omega_p^{\S}$. ■

4.7.3 Proof of Closed-form Expression of $D_{u,\text{upper}}$

To find $D_{\text{upper}}(l_u, \mathbf{l}_\phi)$, we can find the upper bound of each component, i.e., $D_{u,\text{upper}}(l_u)$ as an upper bound of minimum $D_u(\mathbf{u}_a, \mathbf{u}_b)$ given $\text{card}\{\Omega_u\} = 2^{l_u}$, and $D_{p,\text{upper}}(\mathbf{l}_\phi)$ as the upper bound of minimum $D_p(\mathbf{u})$ given $\mathbf{l}_\phi$. Since the MCD is the minimum value among $D_u(\mathbf{u}_a, \mathbf{u}_b)$ and $D_p(\mathbf{u})$, $D_{\text{upper}}(l_u, \mathbf{l}_\phi)$ can be given by:

$$D_{\text{upper}}(l_u, \mathbf{l}_\phi) = \min\left[D_{u,\text{upper}}(l_u), D_{p,\text{upper}}(\mathbf{l}_\phi)\right]. \tag{4.56}$$

Let us $l_{\phi,\max}$ be the highest value of $\mathbf{l}_\phi$, then $D_{p,\text{upper}}(\mathbf{l}_\phi)$ can be easily obtained from (4.14), (4.15), and (4.16) as follows:

$$D_{p,\text{upper}}(\mathbf{l}_\phi) = \sin\left(\frac{\pi}{2^{l_{\phi,\max}}}\right). \tag{4.57}$$

Since amplitude vectors are real positive values, finding $D_{u,\text{upper}}(l_u)$ is equivalent to packing 2^{l_u} metric balls into a surface of positive-valued K-dimensional unit sphere with an area of $S_K = 2(\frac{\pi}{4})^{\frac{K}{2}}/\Gamma(\frac{K}{2})$. Following [38], the volume of a metric ball with chordal distance D_u, i.e., $S(D_u)$, is equal to the area of a spherical cap whose chordal distance between its center and its boundary is D_u. It is easy to verify that the colatitude angle Φ of that spherical cap is $D_u = \sin(\Phi)$. Then, the volume of the metric ball is given by [39]:

$$S(D_u) = \frac{\pi^{\frac{K-1}{2}}\mathcal{B}\left(\sin^2(\Phi), \frac{K-1}{2}, \frac{1}{2}\right)}{\Gamma(\frac{K-1}{2})} = \frac{\pi^{\frac{K-1}{2}}\mathcal{B}(D_u^2, \frac{K-1}{2}, \frac{1}{2})}{\Gamma(\frac{K-1}{2})}, \tag{4.58}$$

where $\mathcal{B}(x, y, z)$ is the incomplete Beta function. For sufficiently small D_u^2, it is easy to prove that $\mathcal{B}\left(D_u^2, \frac{K-1}{2}, \frac{1}{2}\right) \approx 2D_u^{K-1}/(K-1)$. Thus, the Hamming bound is given by [40]:

$$2^{l_u} \leq \frac{S_K}{S(\frac{D_u}{2})} \approx \frac{\pi^{\frac{1}{2}}\Gamma(\frac{K+1}{2})}{\Gamma(\frac{K}{2})D_u^{K-1}}. \tag{4.59}$$

Thus, $D_{u,\text{upper}}(l_u)$ can be given as:

$$D_{u,\text{upper}}(l_u) = \left(\frac{\pi^{\frac{1}{2}}\Gamma(\frac{K+1}{2})}{\Gamma(\frac{K}{2})}\right)^{\frac{1}{K-1}} 2^{-\frac{l_u}{K-1}}. \tag{4.60}$$

4.7.4 Proof of the probability density function in (4.30)

The term $\text{tr}\left(\bar{\mathbf{Y}}_d^H \bar{\mathbf{Y}}_d \ \bar{\mathbf{v}}_d^* \bar{\mathbf{v}}_d^T\right)$ in (4.30) can be formulated as a function of ϕ_d and given by:

$$\text{tr}\left(\bar{\mathbf{Y}}_d^H \bar{\mathbf{Y}}_d \bar{\mathbf{v}}_d^* \bar{\mathbf{v}}_d^T\right) = \sum_{k_1,k_2 \in \bar{\mathcal{D}}} \mathbf{y}_{k_1}^H \mathbf{y}_{k_2} v_{k_1} v_{k_2}^* + \sum_{k_1 \in \bar{\mathcal{D}}} \mathbf{y}_{k_1}^H \mathbf{y}_d v_{k_1} v_d^*$$
$$+ \sum_{k_2 \in \bar{\mathcal{D}}} \mathbf{y}_d^H \mathbf{y}_{k_2} v_d v_{k_2}^* + \mathbf{y}_d^H \mathbf{y}_d v_d v_d^*. \tag{4.61}$$

The first and fourth terms in (4.61) are independent of ϕ_d. Thus, we reformulate the second and third terms of (4.61) as follows:

$$\sum_{k_1 \in \bar{\mathbf{D}}} \mathbf{y}_{k_1}^H \mathbf{y}_d v_{k_1} v_d^* + \sum_{k_2 \in \bar{\mathcal{D}}} \mathbf{y}_d^H \mathbf{y}_{k_2} v_d v_{k_2}^* = 2\text{Re}\left\{\mu_d e^{-j\phi_d}\right\}, \tag{4.62}$$

where μ_d is given by:

$$\mu_d = \sum_{k \in \bar{\mathcal{D}}} \mathbf{y}_k^H \mathbf{y}_d \tilde{u}_k \tilde{u}_d e^{j\bar{\phi}_k} = \sum_{k \in \bar{\mathcal{D}}} z_{k,d}^{(u)} e^{j\bar{\phi}_k}. \tag{4.63}$$

The remaining terms in (4.30) are independent of ϕ_d, thus can be grouped into two constant values $\bar{c}_1$ and $\bar{c}_2$ given by:

$$\bar{c}_1 = \frac{\exp\left(-\frac{\text{tr}(\bar{\mathbf{Y}}_d^H \bar{\mathbf{Y}}_d)}{\sigma^2} + \frac{\sum_{k_1,k_2 \in \mathcal{D}} \mathbf{y}_{k_1}^H \mathbf{y}_{k_2} v_{k_1} v_{k_2}^* + \mathbf{y}_d^H \mathbf{y}_d v_d v_d^*}{\sigma^2(\sigma^2 + \|\bar{\mathbf{v}}_d\|^2)}\right)}{\pi^{(n+1)M}\left[(\sigma^2 + \|\bar{\mathbf{v}}_d\|^2)\sigma^{2n}\right]^M}, \tag{4.64}$$

$$\bar{c}_2 = \frac{2}{\sigma^2(\sigma^2 + \|\bar{\mathbf{v}}_d\|^2)}. \tag{4.65}$$

Finally, the PDF in (4.29) can be simplified as follows:

$$f(\bar{\mathbf{Y}}_d|\bar{\mathbf{v}}_d) = \bar{c}_1 \exp\left(\bar{c}_2 \text{Re}\left\{\mu_d e^{-j\phi_d}\right\}\right). \tag{4.66}$$

References

[1] H. Chen *et al.*, "Ultra-reliable low latency cellular networks: Use cases, challenges and approaches," *IEEE Commun. Mag.*, vol. 56, no. 12, pp. 119–125, Sep. 2018.

[2] Z. Li, M. A. Uusitalo, H. Shariatmadari, and B. Singh, "5G URLLC: Design challenges and system concepts," in *Proc. IEEE Int. Symp. Wireless Commun. Syst. (ISWCS)*, Aug. 2018, pp. 1–6.

[3] A. A. Nasir, H. D. Tuan, H. Q. Ngo, T. Q. Duong, and H. V. Poor, "Cell-free massive MIMO in the short blocklength regime for URLLC," *IEEE Trans. Wireless Commun.*, vol. 20, no. 9, pp. 5861–5871, Apr. 2021.

[4] J. Östman, A. Lancho, G. Durisi, and L. Sanguinetti, "URLLC with massive MIMO: Analysis and design at finite blocklength," *IEEE Trans. Wireless Commun.*, vol. 20, no. 10, pp. 6387–6401, Apr. 2021.

[5] H. Ren, C. Pan, Y. Deng, M. Elkashlan, and A. Nallanathan, "Joint pilot and payload power allocation for massive-MIMO-enabled URLLC IIoT networks," *IEEE J. Sel. Areas Commun.*, vol. 38, no. 5, pp. 816–830, Mar. 2020.

[6] J. Zhang *et al.*, "Pilot contamination elimination for large-scale multiple-antenna aided OFDM systems," *IEEE J. Sel. Top. Signal Process.*, vol. 8, no. 5, pp. 759–772, Mar. 2014.

[7] C. Xu *et al.*, "Sixty years of coherent versus non-coherent tradeoffs and the road from 5G to wireless futures," *IEEE Access*, vol. 7, pp. 178 246–178 299, 2019.

[8] A. Manolakos, M. Chowdhury, and A. Goldsmith, "Energy-based modulation for non-coherent massive SIMO systems," *IEEE Trans. Wireless Commun.*, vol. 15, no. 11, pp. 7831–7846, Sep. 2016.

[9] M. Chowdhury, A. Manolakos, and A. Goldsmith, "Scaling laws for noncoherent energy-based communications in the SIMO MAC," *IEEE Trans. Inf. Theory*, vol. 62, no. 4, pp. 1980–1992, Feb. 2016.

[10] L. Jing, E. De Carvalho, P. Popovski, and A. O. Martinez, "Design and performance analysis of noncoherent detection systems with massive receiver arrays," *IEEE Trans. Signal Process.*, vol. 64, no. 19, pp. 5000–5010, Jul. 2016.

[11] H. Xie, W. Xu, H. Q. Ngo, and B. Li, "Non-coherent massive MIMO systems: A constellation design approach," *IEEE Trans. Wireless Commun.*, vol. 19, no. 6, pp. 3812–3825, Mar. 2020.

[12] V. M. Baeza and A. G. Armada, "Analysis of the performance of a non-coherent large scale SIMO system based on M-DPSK under rician fading," in *Proc. IEEE Eur. Signal Process. Conf. (EUSIPCO)*, Aug. 2017, pp. 618–622.

[13] B. M. Hochwald and T. L. Marzetta, "Unitary space-time modulation for multiple-antenna communications in Rayleigh flat fading," *IEEE Trans. Inf. Theory*, vol. 46, no. 2, pp. 543–564, Mar. 2000.

[14] M. J. Borran, A. Sabharwal, and B. Aazhang, "On design criteria and construction of noncoherent space-time constellations," *IEEE Trans. Inf. Theory*, vol. 49, no. 10, pp. 2332–2351, Oct. 2003.

[15] S. T. Duong, H. H. Nguyen, and E. Bedeer, "Multi-level Design for Multiple-Symbol Non-Coherent Unitary Constellations for Massive SIMO Systems," *IEEE Wireless Commun. Lett.*, 2023.

[16] L. Zheng and D. N. C. Tse, "Communication on the Grassmann manifold: A geometric approach to the noncoherent multiple-antenna channel," *IEEE Trans. Inf. Theory*, vol. 48, no. 2, pp. 359–383, Feb. 2002.

[17] D. Cuevas, J. Álvarez-Vizoso, C. Beltrán, I. Santamaria, V. Tuček, and G. Peters, "Union bound minimization approach for designing Grassmannian constellations," *IEEE Trans. Commun.*, vol. 71, no. 4, pp. 1940–1952, Feb. 2023.

[18] Y. Wu, K. Ruotsalainen, and M. Juntti, "Unitary space–time constellation design based on the Chernoff bound of the pairwise error probability," *IEEE Trans. Inf. Theory*, vol. 54, no. 8, pp. 3842–3850, Jul. 2008.

[19] B. M. Hochwald, T. L. Marzetta, T. J. Richardson, W. Sweldens, and R. Urbanke, "Systematic design of unitary space-time constellations," *IEEE Trans. Inf. Theory*, vol. 46, no. 6, pp. 1962–1973, Sep. 2000.

[20] K. M. Attiah, K. Seddik, R. H. Gohary, and H. Yanikomeroglu, "A systematic design approach for non-coherent grassmannian constellations," in *Proc. IEEE Int. Symp. Inf. Theory (ISIT)*, Jul. 2016, pp. 2948–2952.

[21] J.-K. Zhang, F. Huang, and S. Ma, "Full diversity blind space-time block codes," *IEEE Trans. Inf. Theory*, vol. 57, no. 9, pp. 6109–6133, Aug. 2011.

[22] I. Kammoun, A. M. Cipriano, and J.-C. Belfiore, "Non-coherent codes over the Grassmannian," *IEEE Trans. Wireless Commun.*, vol. 6, no. 10, pp. 3657–3667, Oct. 2007.

[23] J. Kim, K. Cheun, and S. Choi, "Unitary space-time constellations based on quasi-orthogonal sequences," *IEEE Trans. Commun.*, vol. 58, no. 1, pp. 35–39, Jan. 2010.

[24] K.-H. Ngo, A. Decurninge, M. Guillaud, and S. Yang, "Cube-split: A structured Grassmannian constellation for non-coherent SIMO communications," *IEEE Trans. Wireless Commun.*, vol. 19, no. 3, pp. 1948–1964, Dec. 2019.

[25] S. Li, J.-K. Zhang, and X. Mu, "Design of optimal noncoherent constellations for SIMO systems," *IEEE Trans. Commun.*, vol. 67, no. 8, pp. 5706–5720, Apr. 2019.

[26] R. H. Gohary and T. N. Davidson, "Noncoherent MIMO communication: Grassmannian constellations and efficient detection," *IEEE Trans. Inf. Theory*, vol. 55, no. 3, pp. 1176–1205, Feb. 2009.

[27] P. Ho and D. Fung, "Error performance of multiple-symbol differential detection of PSK signals transmitted over correlated Rayleigh fading channels," *IEEE Trans. Commun.*, vol. 40, no. 10, pp. 1566–1569, Oct. 1992.

[28] D. Divsalar and M. K. Simon, "Maximum-likelihood differential detection of uncoded and trellis coded amplitude phase modulation over AWGN and fading channels-metrics and performance," *IEEE Trans. Commun.*, vol. 42, no. 1, pp. 76–89, Jan. 1994.

[29] D. S. Papailiopoulos, G. Abou Elkheir, and G. N. Karystinos, "Maximum-likelihood noncoherent PAM detection," *IEEE Trans. Commun.*, vol. 61, no. 3, pp. 1152–1159, Jan. 2013.

[30] F. Adachi and M. Sawahashi, "Decision feedback differential phase detection of M-ary DPSK signals," *IEEE Trans. Veh. Technol.*, vol. 44, no. 2, pp. 203–210, May. 1995.

[31] ——, "Decision feedback differential detection of differentially encoded 16APSK signals," *IEEE Trans. Commun.*, vol. 44, no. 4, pp. 416–418, Apr. 1996.

[32] R. Schober, W. H. Gerstacker, and J. B. Huber, "Decision-feedback differential detection of MDPSK for flat Rayleigh fading channels," *IEEE Trans. Commun.*, vol. 47, no. 7, pp. 1025–1035, Jul. 1999.

[33] A. Schenk and R. F. Fischer, "Noncoherent detection in massive MIMO systems," in *Proc. VDE Int. ITG Workshop Smart Antennas (WSA)*, Mar. 2013, pp. 1–8.

[34] R. F. Fischer, M. Bense, and C. Stierstorfer, "Noncoherent joint decision-feedback detection in multi-user massive MIMO systems," in *Proc. VDE Int. ITG Workshop Smart Antennas (WSA)*, Mar. 2014, pp. 1–8.

[35] S. T. Duong, H. H. Nguyen, E. Bedeer, and R. Barton, "Low-Complexity Design of Unitary Constellations in Non-Coherent SIMO Systems for 5G NR URLLC Applications," in *to appear in Proc. IEEE Global Communications Conference 2023 (GLOBECOM)*, Dec. 2023.

[36] S. Boyd, S. P. Boyd, and L. Vandenberghe, *Convex optimization*. Cambridge university press, 2004.

[37] M. Grant and S. Boyd, "CVX: Matlab software for disciplined convex programming, version 2.1," 2014.

[38] K. K. Mukkavilli, A. Sabharwal, E. Erkip, and B. Aazhang, "On beamforming with finite rate feedback in multiple-antenna systems," *IEEE Trans. Inf. Theory*, vol. 49, no. 10, pp. 2562–2579, Oct. 2003.

[39] S. Li, "Concise formulas for the area and volume of a hyperspherical cap," *Asian Journal of Mathematics and Statistics*, vol. 4, no. 1, pp. 66–70, Jan. 2011.

[40] W. Dai, Y. Liu, and B. Rider, "Quantization bounds on Grassmann manifolds and applications to MIMO communications," *IEEE Trans. Inf. Theory*, vol. 54, no. 3, pp. 1108–1123, Feb. 2008.

5. Conclusion and Suggested Future Studies

5.1 Conclusion

This thesis has studied two types of non-coherent multi-symbol constellations in block Rayleigh fading channels in SIMO systems, i.e., the multi-level unitary constellations and unitary constellations. The main objective of these studies is to improve the error performance of the non-coherent multi-symbol constellations while still achieving low complexity in the design and detection. The main contributions of this thesis are given as follows:

- In Chapter 3, we investigated the multi-level design for the multi-level unitary constellations. Based on the reformulation of the KL divergence as the design criterion, we proposed a structure of multi-level unitary constellations, i.e., the Cartesian product of magnitude levels and unitary vectors. We formulated and solved an optimization problem to improve the error performance of the proposed constellations based on the KL divergence. This method has lower complexity compared to the relevant multi-level design in the literature. The numerical results showed the merits of our proposed multi-level unitary constellations compared to other schemes in the literature in terms of error performance.

- In Chapter 4, we proposed a novel structure of unitary constellations based on the Cartesian product of amplitude and PSK vectors. We formulated and solved an optimization method to maximize the chordal distance as the design criterion of our proposed unitary constellations, hence improving the error performance. The proposed structure of unitary constellations was exploited to reduce the complexity of the design when compared to unstructured unitary constellations. Furthermore, we exploited the

proposed structures to propose novel detectors. The first one is an iterative unitary amplitude-phase (IUAP) detector to detect the amplitude and phase iteratively. For the phase detection, we adopted the posterior probability as the reliability of the sort-DFDD algorithm and proposed the PR-sort-DFDD algorithm, which approaches the optimal performance of the ML detector in the case of PSK structure with equal modulation orders. For PSK structures with unequal modulation orders, we used feedback from undetected symbols with lower modulation order to enhance the detection of unknown symbols with higher modulation order and proposed the improved-PR-sort-DFDD algorithm. Both of the proposed phase detectors approach the ML detection performance, in their designated cases, with polynomial time complexity. The simulation results show that our proposed unitary constellations have better chordal distance than other low-complexity unitary constellations, and outperform the low-complexity unitary constellations and pilot-based scheme with coherent detection in terms of error performance.

5.2 Future Research Topics

Based on the results from the thesis, several future research directions can be explored:

Further improvement of unitary constellations: In our proposed unitary constellations in Chapter 4, the whole constellations are confined to only one set of PSK constellations. While this method helps reduce the complexity of designing the unitary constellations, it also acts as a constraint that reduces the performance of our proposed unitary constellations. Hence, we can improve the performance of unitary constellations further by relaxing the constraints of PSK constellations and allowing the constellations to have many possible subsets of PSK constellations. For example, we can use three subsets of PSK constellations as shown in Fig. 5.1. The first subset includes the sequence of 1-PSK, 4-PSK, 4-PSK, and 4-PSK symbols and contains 64 constellation points. The second subset includes the sequence of 1-PSK, 2-PSK, 4-PSK, and 4-PSK symbols and contains 32 constellation points. The third subset includes the sequence of 4-PSK, 4-PSK, 1-PSK, and 2-PSK symbols and contains 32 constellation points. Hence, the total number of constellation points is 128 points, which is

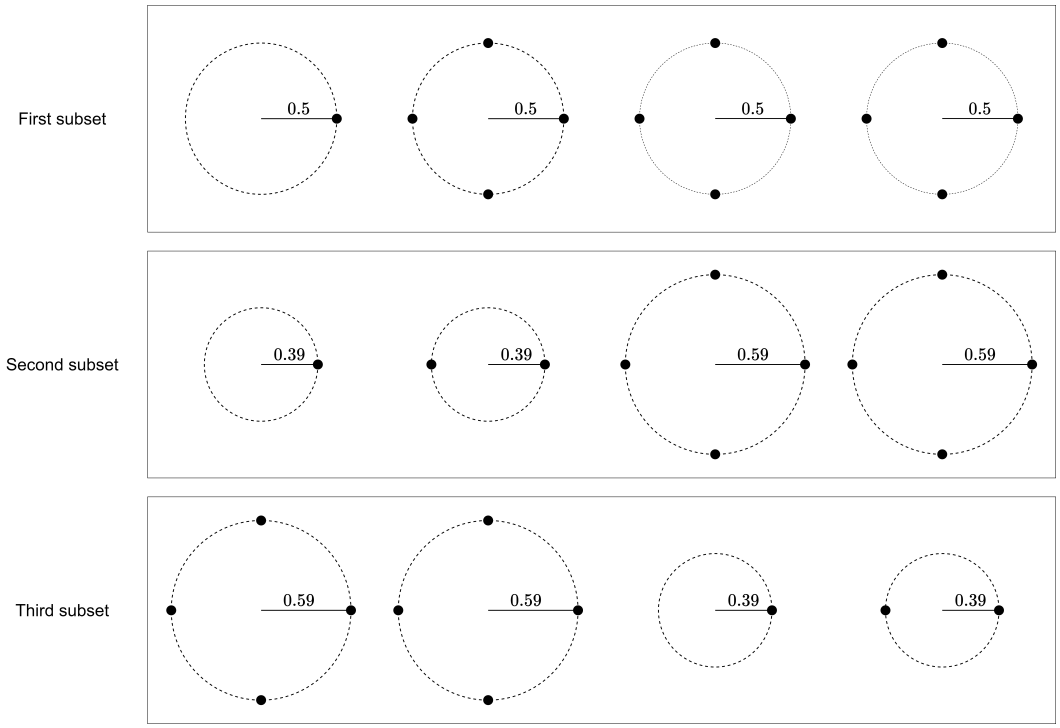

Figure 5.1: Example of a more generalized version of the proposed multi-symbol unitary constellations

equivalent to 7 bits.

Non-coherent multi-symbol detection of QAM and APSK constellations: To the best of our knowledge, the non-coherent multi-symbol detection of QAM and APSK constellations has not been investigated. Please note that if the amplitude of the QAM and APSK is somehow perfectly detected in the receiver, then the sequence of QAM or APSK symbols can become the sequence of PSK symbols with unequal modulation order and unequal amplitude, as shown in Fig. 5.2. Hence, it is possible to use our proposed improved PR-sort-DFDD for non-coherent multi-symbol detection of any symbols with PSK structure, such as QAM or APSK.

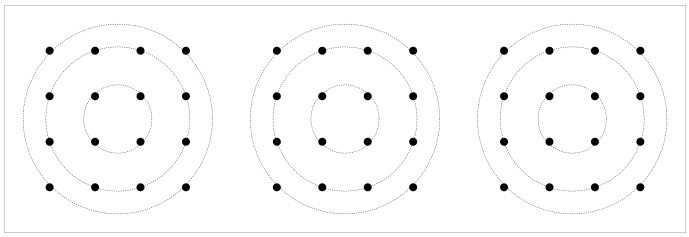

(a) Sequence of QAM symbols.

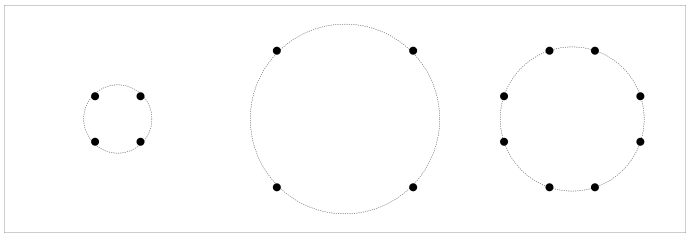

(b) Given known amplitude, the sequence of QAM symbols is equivalent to the sequence of PSK symbols with unequal modulation orders and amplitude.

Figure 5.2: Sequence of QAM symbols without and with knowing amplitude.